Effect of Water Salinity on the Hydro-Mechanical Behaviour of Light Backfill Material

by

Hamid Batenipour

A Thesis
Submitted to the Faculty of Graduate Studies
in Partial Fulfillment of the Requirements
for the Degree of

Masters of Science in Environmental Engineering

Engineering Department
Lakehead University
Thunder Bay, Ontario
July, 2007

Your file Votre référence
ISBN: 978-0-494-31846-1
Our file Notre référence
ISBN: 978-0-494-31846-1

ABSTRACT

A series of one-dimensional compression tests was conducted to examine and compare the hydro-mechanical behaviour of light backfill (LBF) material, composed of 50% bentonite and 50% sand, in the presence of distilled water and 100 g/l $CaCl_2$ and 200 g/l $CaCl_2$ solutions. In addition, the hydro-mechanical parameters of LBF required for compliance modelling of the deep geologic repository (DGR) emplacement room sealing system were determined. The tests were conducted on 50-mm-diameter by 10-mm-thick LBF samples, using standard lever arm consolidation equipment. Several different loading and wetting paths were examined, including allowing the LBF to swell up to 20% vertical strain on distilled water or solution uptake and constraining the LBF from swelling on distilled water or solution uptake. The samples were loaded in increments following initial distilled water or solution uptake, and then unloaded in increments.

The results of individual test loading and unloading increments were used to compute void ratio (e), hydraulic conductivity (k), effective montmorillonite dry density (EMDD), bulk modulus (K) and water activity (a_w). The hydraulic conductivity versus EMDD and vertical applied pressure versus EMDD results were compared to results compiled by Dixon et al. (2002a). The bulk modulus versus vertical strain results were used to simulate the interaction between highly

compacted bentonite (HCB) (inner material) and LBF (outer material) in a hypothetical emplacement room sealing system, using a two-material axisymmetric linear elastic analytical model.

The test results show that the compression, swelling and hydraulic behaviour of LBF with 100 g/l or 200 g/l $CaCl_2$ cell reservoir solution is distinctly different than the behaviour of LBF with distilled water in the cell reservoir. All of the test results show significant hysteresis between the loading/compression and unloading/swelling paths. The results of the simulations show that the water activity values in HCB and LBF in the hypothetical emplacement room sealing system are greater than the 0.96 threshold value.

ACKNOWLEDGEMENTS

I would like to express my gratitude to my supervisor Dr. Bruce Kjartanson for his unending patience, encouragement, and mentorship during this research. Dr. Kjartanson made time for all my questions and provided support to me both personally and professionally. I thoroughly enjoyed being his grad student and look forward to working with him in the future.

Thank you to the environmental engineering professors including Dr. Lionel Catalan and Dr. Baoqiang Liao for their friendship, advice and encouragement.

Thanks to Conrad Hagstrom for his helps in the laboratory as well as guidance and support. Thanks to environmental graduate students and civil undergraduate students for their friendship, discussions and assistance during this research. I would like to specifically acknowledge Danny Carlos, Salvatore Rustico, Matthew Stack and Neil Mullin for their assistance during this research.

Financial support is acknowledged from National Science and Engineering Research Council of Canada, Atomic Energy of Canada Limited and Faculty of Graduate Studies at Lakehead University.

A big thanks to my family: Mansoureh Pourghadiri, Amir and Soheila Batenipour for their love and support during my studies.

TABLE OF CONTENTS

LIST OF TABLES

LIST OF FIGURES

Chapter 1 : INTRODUCTION

1.1 General Overview of Management of Canada's Used Nuclear Fuel

Nuclear power plants account for approximately 15% of Canada's power generation. Currently Canada has 22 operating nuclear reactors and they have produced over 2 million used fuel bundles (36,000 metric tones of radioactive waste) which, according to estimates by the Nuclear Waste Management Organization (NWMO), will double in the next 40 years. The used fuel bundles contain highly radioactive material, primarily uranium-235 and uranium-238, and will remain radioactive for 4.5 billion years (NWMO 2005). The management of the waste generated from nuclear power must be addressed and a long term solution has to be implemented for the safe storage, security and management of this material.

The Government of Canada passed a law called the Nuclear Fuel Waste Act (NFWA) in 2002 requiring the owners of spent nuclear fuel to create the Nuclear Waste Management Organization. Following an extensive study of management options and with significant public input, the NWMO is recommending an adaptive phased management approach which is comprised of three phases of implementation. The first two phases involve interim stage. The first phase involves storing the used fuel bundles at the nuclear reactor sites for about thirty years. The second phase requires the used fuel bundles to be placed in a shallow storage facility for about thirty years. The final phase would involve placement of the used fuel bundles in a deep geologic repository (DGR) (NWMO 2005).

Atomic Energy of Canada Limited (AECL) developed DGR concepts for the disposal of used nuclear fuel waste between 1978 and 1996. Since 1996, Ontario Power Generation (OPG) has been leading the research and development for a DGR that would be constructed in the stable plutonic rock of the Canadian Shield. More recently, sedimentary rock formations in Southern Ontario are also being considered as host rocks for a DGR (NWMO 2005). Figure 1.1 shows a conceptual layout of a DGR.

The proposed depth of a repository would be between 500 to 1000 m below the ground surface and would consist of a series of horizontal tunnels and emplacement rooms as shown conceptually on Figure 1.1 (Maak and Simmons

2005). The design and construction of the DGR would have to be adapted to the specific rock and groundwater conditions (i.e. permeability and geochemistry) and other subsurface conditions at the particular site. A location with low permeablity rock with sparse fracturing would be favoured for a DGR (Maak and Simmons 2005).

1.2 Background

The used-fuel container (Fig. 1.2) proposed for use in OPG's concept will have a design life of not less than 100,000 years under in situ conditions (Maak and Simmons 2005). The outer shell of the container will be constructed of oxygen-free phosphorusdoped copper (OFP-Cu) which will perform as the primary corrosion barrier material. It has been predicted that a container made from OFP-Cu will have a corrosion service life of more than 1,000,000 years in the conditions found in the Canadian Shield. This container has an outer diameter of about 1.2 m, length of about 3.9 m, a copper shell thickness of 25 mm and is designed to hold 324 used fuel bundles (Maak and Simmons 2005).

Dixon et al. (2001) state the function and performance of the repository backfill as the follows:

- Fill the space in waste emplacement rooms in order to keep the buffer and used-fuel containers securely in place

- Fill the space in tunnels and shafts in order to make the repository intrusion resistant
- Retard the movement of contaminants by slowing any movement of groundwater by enhancing sorption of contaminants, and by chemically conditioning the groundwater

The sealing system preliminary design requirements state that backfills should have a swelling potential to give a self-healing/self-sealing capability to fill the gaps and to provide an interface contact pressure greater than 100 kPa to close interfaces and promote rock stability. Moreover, backfills should maintain a hydraulic conductivity less than 10^{-10} m/s to give a diffusion-dominated contaminant transport system (Kjartanson et al. 2003a, c). The requirements of the sealing system entail that swelling clays should be used in the backfill.

The sealing system design also needs to limit the viability and activity of microbes on and near the container. Microbe activity can enhance container corrosion (Kjartanson et al. 2003a, c). This microbially influenced corrosion (MIC) occurs either as a direct effect of microbes on the container surface (under biofilms) or as a result of corrosive microbial metabolites coming in contact with the container surface (Stores-Gascoyne and King 2002). Using backfill sealing materials that would limit the viability and activity of microbes in the sealing system and MIC of the containers is important because the 100,000 year

container design life is a principal safety feature of the DGR concept (Kjartanson et al. 2003c).

Water activity (a_w) describes the amount of water that is thermodynamically available in a solution. Water activity of a solution is defined as the ratio of the vapour pressure of the solution to that of pure water at a given temperature and is equal to the relative humidity. Experimental studies have shown that an a_w of 0.96 is a threshold for the culturability, and possibly the viability of bacteria in clay-based materials. Significant microbial activity is likely severly limited and largely ceases below an a_w of 0.96 (Kjartanson et al. 2003a, c).

Effective Montmorillonite Dry Density (EMDD) is a parameter that has been used to normalize the hydraulic and swelling behaviour of clay-based barriers containing varying quantities of bentonite and aggregates. EMDD is calculated by dividing the dry mass of montmorillonite by the volume occupied by the montmorillonite and the volume of voids present in the system (Baumgartner and Snider 2002).

Kjartanson et al. (2003a ,c) proposed a model that related a_w to total suction of an unsaturated soil and swelling pressure of a saturated soil using the thermodynamic relationships between total suction and relative humidity (i.e. a_w) and swelling pressure and relative humidity (i.e. a_w). As total suction or swelling pressure increases, the availability of water for microbial metabolism decreases

and a_w decreases. For the saturated case, therefore, clay barriers with high EMDD and high swelling pressures will tend to minimize microbe viability and activity. Expansion of highly compacted bentonite (HCB), therefore, would result in a lower EMDD, lower swelling pressure and a high a_w.

OPG's DGR concept has three container emplacement options (Fig. 1.3). All options would use clay-based sealing materials to surround the containers and separate them from the host rock. The in-floor borehole method (Fig. 1.3a) involves the containers being carefully lowered into excavated boreholes and separated from the rock by highly compacted (dense) bentonite (composed primarily of the clay mineral montmorillonite). The horizontal borehole method (Fig. 1.3b) requires the containers to be placed in large diameter boreholes that are excavated horizontally into the rock. The containers would be separated from the host rock by highly compacted (dense) bentonite (Maak and Simmons 2005).

The in-room method (Fig. 1.3c) has the most complex pattern of sealing materials. The containers are placed horizontally within the emplacement room and are surrounded by five different clay-based sealing materials (Fig. 1.4). The materials considered as the Engineered Barriers System (EBS) components are listed in Table 1.1.

Referring to Figure 1.4, the clay sealing material directly in contact with the container is Highly Compacted 100% Bentonite (HCB). A compacted 50/50 bentonite/sand buffer (BSB) will surround the HCB, followed by dense backfill (DBF). In this concept these three layers would be placed as large precompacted blocks. Gap Fills (GF) would be used to fill the remaining construction voids around and between the placed blocks and the containers.

The layer closest to the emplacement room wall is the Light Backfill (LBF) Material. The LBF will fill all the construction voids between the dense backfill blocks and the emplacement room wall. It is presently a 50% bentonite/50% sand mix placed at a water content of 15%. Note in Table 1.1 that the as-placed dry density for this material is low compared with the machine compacted materials, such as HCB, BSB and DBF. Thus the term "Light" is used for this material. This lower dry density represents what is achievable using current remote placement technologies. One proposed method of placement for the LBF is by a shot-crete style procedure (Fig. 1.5).

Because of the remote placement procedure, maintaining a high content of montmorillonite clay is essential to achieving a relatively high EMDD. The highest EMDD can be achieved by near dry placement of the LBF (Kjartanson et al. 2003b, Kjartanson et al. 2005). Self-healing/self-sealing capability, low hydraulic conductivity, sorption capacity and plastic behaviour under load are all characteristics of the bentonite used in the LBF. The addition of non-

montmorillonite material such as the sand is used to increase the thermal conductivity of the LBF and facilitate the placement procedure. Using sand or any non-montmorillonite material in the LBF inhibits achieving a high EMDD (Kjartanson et al. 2003b).

Gascoyne et al. (1987) and Mazurek (2004) have collated data on the salinity of groundwater within the crystalline rock of the Canadian Shield and the sedimentary rock in southern Ontario, respectively. Salt concentration tends to be low near the ground surface and increases with depth. Salinities, in terms of Total Dissolved Solids (TDS) at the proposed repository depths of 500 to 1000 m can vary from 8 to >100 g/l in the Canadian Shield and >200 g/l in Ordovician-age sedimentary rocks. Salt speciation is often Na-Ca-Cl at shallow depth trending to Ca-Na-Cl at greater depth (Baumgartner et al. 2007). The effect that Ca-rich goundwaters may have on the mechanical and hydraulic performance of bentonite clay-based barriers is an important aspect of DGR performance.

Immediately following container and sealing system emplacement, moisture will tend to be thermally driven from the sealing materials closest to the container (HCB and Compacted Buffer) to the LBF and the LBF will be taking up moisture from the surrounding rock. The HCB and Compacted Buffer will therefore tend to undergo thermal drying and shrinkage and the LBF will tend to swell in the early stages after emplacement. In the longer term, on water uptake and saturation of the sealing system components, there will be a tendency for the components with

high EMDD and high swelling pressure, such as the HCB adjacent to the container, to expand and those with lower EMDD, such as the LBF, to compress. Significant expansion of the HCB could impact its ability to limit MIC of the container. The stress-strain properties of the sealing materials play an important role in this "compliance effect" (Batenipour and Kjartanson 2007).

Based on the in-room emplacement geometry presented in Figure 1.4, Chandler (2005) developed a numerical model to address this relative compliance of the in-room sealing system components on full saturation. Chandler examined the hydro-mechanical response of the sealing system components and also the effect of sealing system component volume change on EMDD and water activity. The FLAC[1] analysis software code was used, and non-linear elastic properties were input into the model using a user-defined subroutine. An assumption was also made that the final saturated densities and stresses are dependent on only the initial as-placed densities and that they are independent of stress or strain history. The results of the preliminary FLAC modelling indicated that the LBF will be compressed approximately 15% and the HCB will expand up to about 40%. These results along with the assumption that the LBF could swell up to about 20% in the early stages before saturation of the HCB and BSB were used to define testing protocols that would make the tests representative of repository conditions as defined below (Baumgartner et al. 2007).

[1] Fast Lagrangian Analysis of Continua. A stress, displacement, temperature and pore pressure analysis software code commercially available from Itasca Consulting Group Inc. 111 Third Avenue South, Suite 450 Minneapolis, MN 55401.

A series of one-dimensional compression tests have been carried out to determine the hydro-mechanical parameters of LBF required for compliance modelling of the emplacement room sealing system. Tests were carried out to determine the 1-D swelling, compression and hydraulic behaviour of the LBF under different loading/wetting paths and different reservoir and mixing solutions (using distilled water and $CaCl_2$ as reservoir solutions, and using LBF mixed with $CaCl_2$ instead of distilled water as used in the other tests). Other institutions are investigating the behaviour of the DBF and HCB under similar conditions.

1.3 Objectives

In the light of the requirements for the in room sealing system compliance modelling, the objectives of this thesis are as follows:

- Examine and compare the 1-D swelling/compression response of the light backfill (LBF) under different loading/wetting paths. Three loading/wetting paths were examined:
    - compression/swelling behaviour of the LBF after 20% initial swelling during water uptake.
    - compression/swelling behaviour of the LBF after water uptake under confined conditions followed by 20% swelling.

- compression/swelling behaviour of the LBF after water uptake under confined conditions.

- Examine and compare the 1-D swelling/compression response of the LBF with distilled reservoir water, 100 g/l $CaCl_2$ and 200 g/l $CaCl_2$ reservoir solutions.

- Examine and compare the 1-D swelling/compression response of LBF mixed with distilled water and LBF mixed with 100 g/l $CaCl_2$.

- Compare the results with previously published results on swelling, compression and hydraulic behaviour of bentonite-based materials by Dixon et al. (2002a).

- Evaluate and compare the bulk modulus and water activity values of LBF determined from 1-D compression tests with distilled reservoir water, 100 g/l $CaCl_2$ and 200 g/l $CaCl_2$ reservoir solutions and with LBF mixed with 100 g/l $CaCl_2$.

- Examine the interaction between HCB and LBF using an analytical solution for a two-material linear-elastic model in an axisymmetric configuration. Using the results of the modelling, calculate the water

activity of the HCB and LBF to assess microbial viability in these materials.

1.4 Organization of This Thesis

This thesis is organized as follows. Chapter 2 provides a literature review pertaining to this study. It describes the swelling and compression behaviour of high plastic clays including the effect of saline pore fluids. The materials and methods used in this study are presented in Chapter 3. Chapter 4 contains the results of the tests and analysis. Chapter 5 summarizes the conclusions and recommendations of this research. The appendices contain all the data and details of the analysis calculations performed for this project.

	HCB	BSB	GF	DBF	LBF
Clay % of total mass (f_c)	100	50	100	30	50
% of clay that is montmorillonite (f_m)	75	75	75	12.5	80
Sand or granite aggregate % by mass	0	50	0	70	50
Initial Gravimetric Water Content (%)	17	18.5	2	8.5	15
As-placed dry density (Mg/m^3)	1.61	1.69	1.4	2.12	1.24
EMDD (Mg/m^3)*	1.41	1.05	1.2	0.34	0.66
Swelling pressure (MPa)$^+$	6.09	0.92	2.04	0.024	0.12

*EMDD - Effective Montmorillonite Dry Density = (mass of bentonite *montmorillonite fraction) / (volume of voids + volume of montmorillonite minerals)
– Assumes that bentonite is 75% montmorillonite content
$^+$ Swelling pressures calculated from an empirical relationship between EMDD and swelling pressure developed by Dixon et al. (2002) for fresh water

Table 1.1: Compositions, Placement Densities and Swelling Pressures of Emplacement Room Clay-Based Materials (Revised from Chandler 2005 and Maak and Simmons 2005)

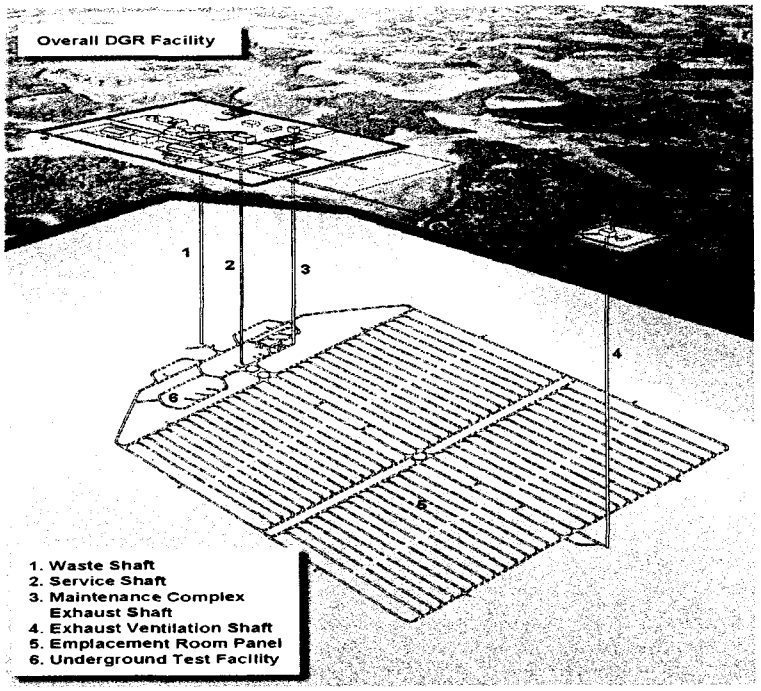

Figure 1.1: Illustration of the Updated Canadian DGR Conceptual Design (Maak and Simmons 2005)

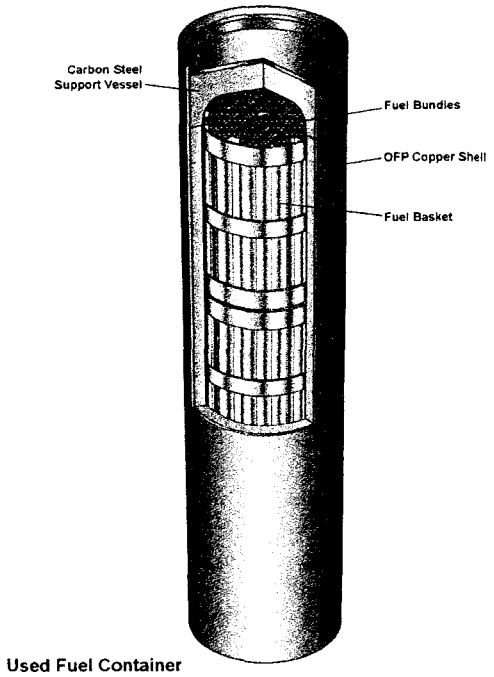

Figure 1.2: Cut – away View of the Reference Used-fuel Container (Maak and Simmons 2005)

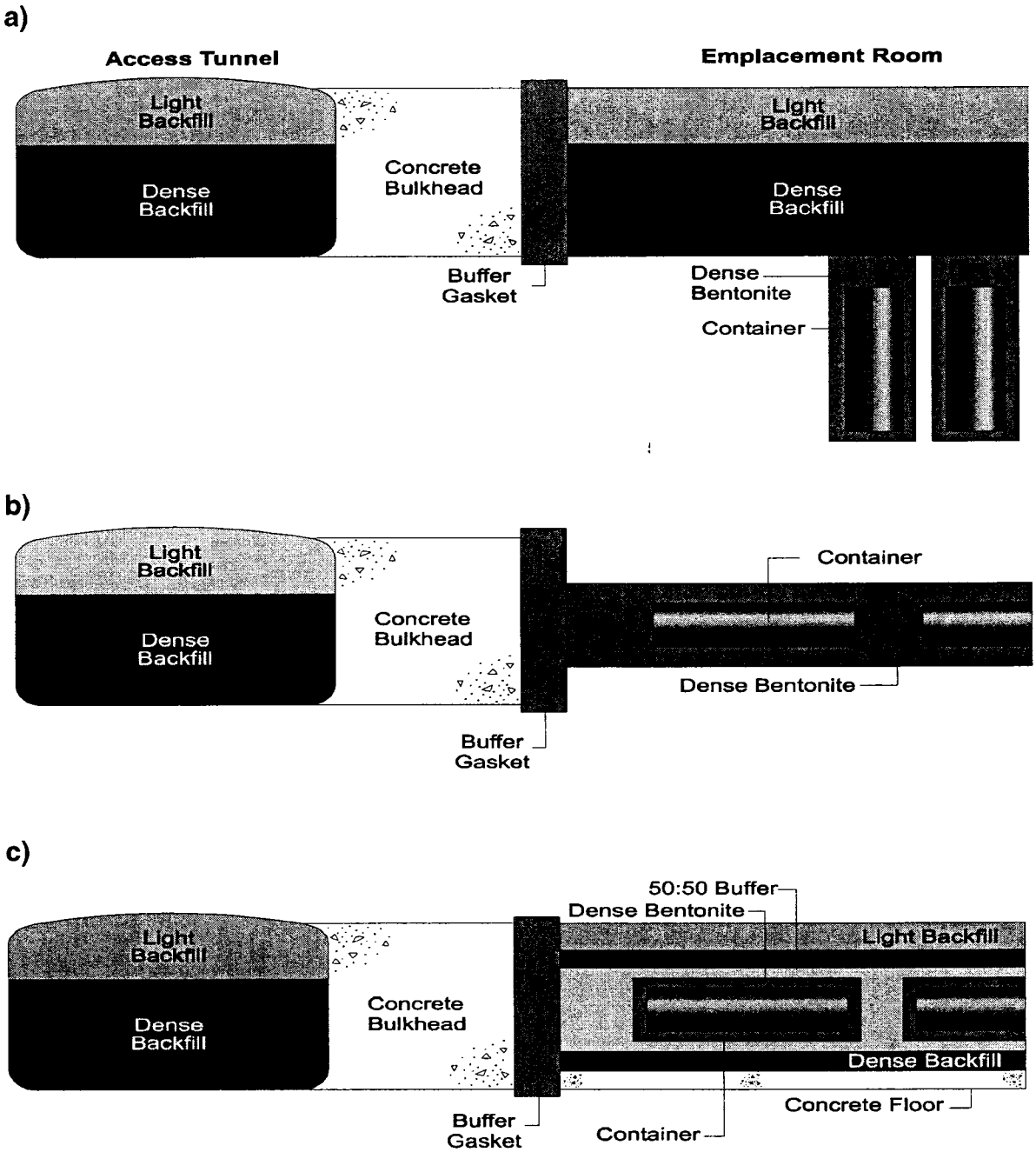

Figure 1.3: Schematic Representation of Container Emplacement Options (not to scale): a) in-floor borehole, b) horizontal borehole and c) in-room (Maak and Simmons 2005)

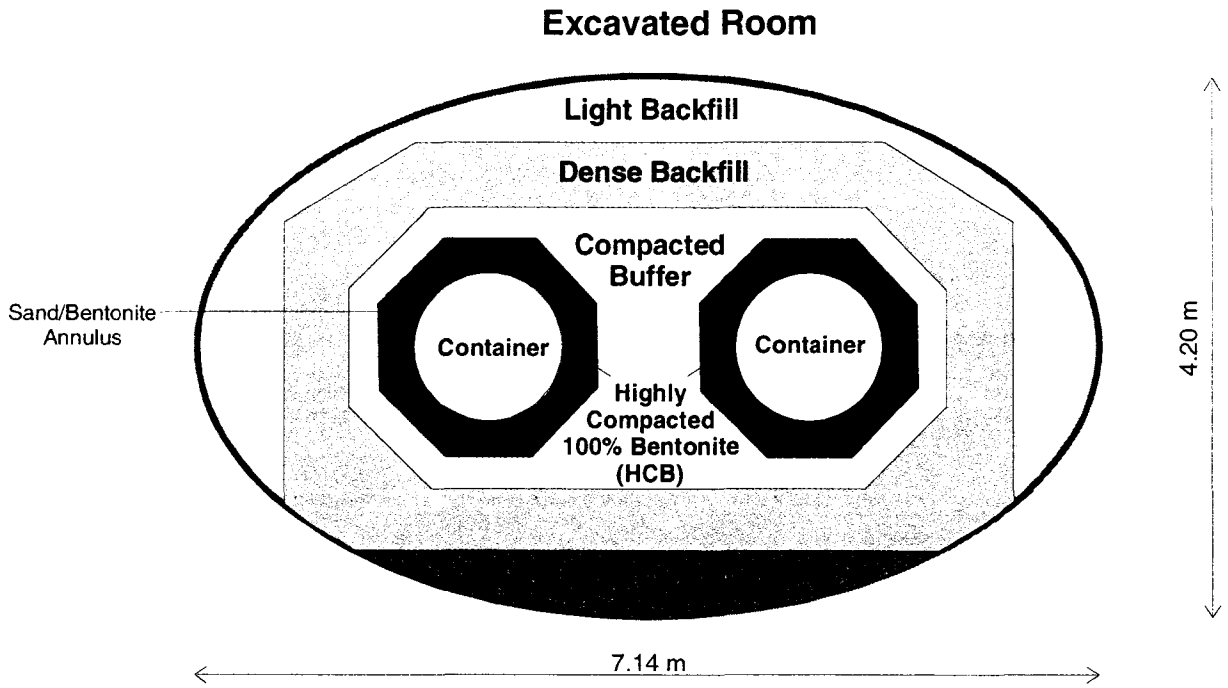

Figure 1.4: Third Case Study In-room Emplacement Geometry (after Gierszewski et al. 2004)

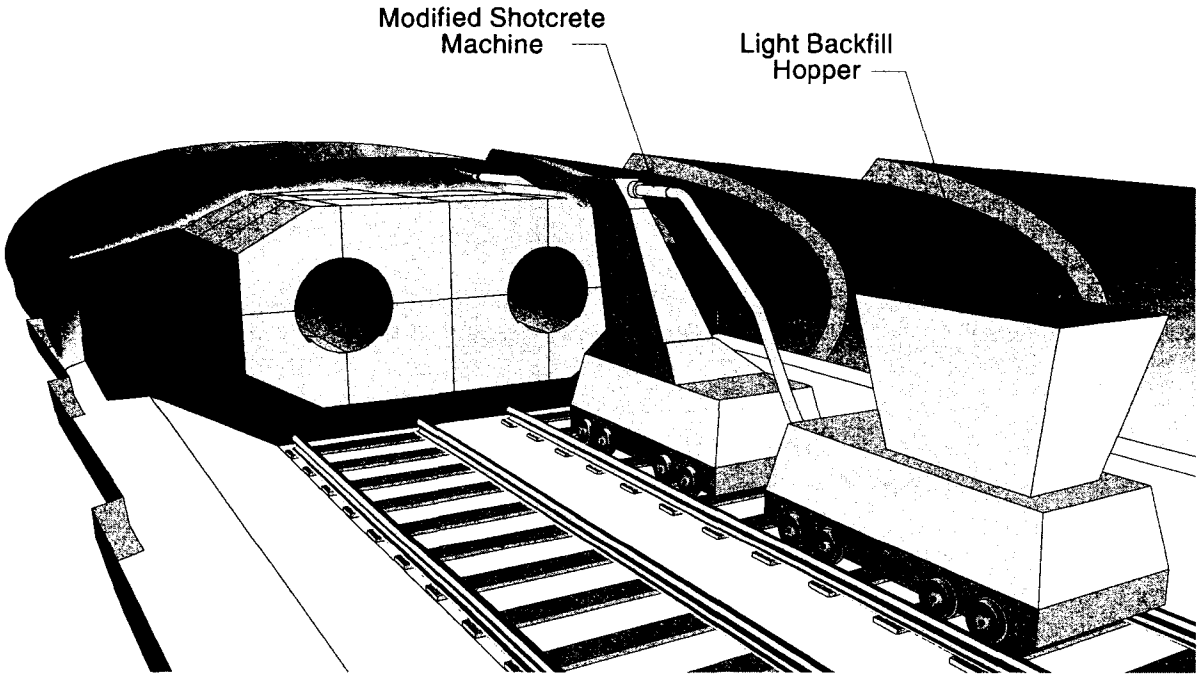

Figure 1.5: Light Upper Backfill Placement (In-Room Emplacement Method) (Kjartanson et al. 2003b)

Chapter 2 : LITERATURE REVIEW

2.1 Introduction

The focus of this research is to evaluate the one-dimensional compression and swelling properties of the Light Backfill (LBF) Material which is a 50/50 bentonite/sand mix. An important goal is to describe the effect of pore fluid salinity on the compression and swelling behaviour of LBF. This chapter provides a review and background information on clay mineralogy and swelling and compression behaviour of bentonite. In addition, the review examines the effect of different pore fluid compositions and salinities on the compression and swelling behaviour of bentonite.

2.1 Clay Mineralogy

Bentonite is composed principally of the clay mineral montmorillonite with other minerals such as feldspar and quartz. Swelling of bentonite is mainly caused by the swelling of montmorillonite, which is a swelling clay mineral (Komine 2004). This section presents an overview of the mineralogy of clays, with a focus on the clay mineral montmorillonite which is a member of the smectite group of clay minerals.

The most prevalent minerals in the clay fraction of temperate region soils are the silicate clays, whereas in tropical regions hydrated oxides of iron and aluminium may be more prevalent. The typical clay minerals appear as laminated microcrystals, composed primarily of two basic structural units, a tetrahedron of four oxygen atoms surrounding a central cation, usually Si^{4+}, and an octahedron of six oxygen atoms or hydroxyls surrounding a larger cation of lesser valency, usually Al^{3+} or Mg^{2+} (Hillel 1980).

The tetrahedra are joined together at their basal corners by means of shared oxygen atoms, in a hexagonal network which forms a flat sheet 0.493 nm thick. The octahedra are joined along their edges to form a flat sheet also. These sheets are about 0.505 nm thick (Hillel 1980).

The layered clay minerals are of two principal types, either 1:1 or 2:1 depending upon the ratios of tetrahedral to octahedral sheets. A clay particle is composed of multiple stacked composite layers, called *lamellae*. The 2:1 clay minerals are further divided into expanding and nonexpanding types (Hillel 1980).

2.2.1 Kaolinite Mineralogy

In 1:1 minerals an octahedral sheet is attached to a single tetrahedral sheet by the sharing of oxygens. *Kaolinite* is the most common mineral of the 1:1 type (Fig. 2.1). The basic layer in the crystal structure is a pair of silica-alumnia sheets, and these are stacked in alternating fashion and held together by hydrogen bonding in a rigid, multilayered lattice. These basic layers can not ordinarily be split or separated so water and ions can not enter between them. Kaolinite crystals generally range in planar size from 0.1 to 2 μm with a variable thickness in the range of about 0.02 to 0.05 μm. Kaolinite exhibits less plasticity, cohesion, and swelling than most other clay minerals because of its relatively large particle sizes, low specific surface and low charge. The unit layer formula of kaolinite is $Al_4Si_4O_{10}(OH)_8$ (Hillel 1980).

2.2.2 Illite Mineralogy

Illie is the most commonly found clay mineral in soils. It is a non-expanding, clay-sized, micaceous 2:1 clay mineral. Illite is intermediate in expanding properties between kaolinite and montmorillonite. The structure of illite is shown on Figure 2.2. The basic layer in the crystal structure is composed of two inward-pointing silica tetragonal sheets with a central octahedral sheet. The layers held together by a very strong potassium bond so their separation, and hence expansion of the entire lattice, are effectively prevented. Illite is formed by weathering or hydrothermal alteration of other aluminum-rich minerals. The unit layer formula of illite is $Al_4Si_7AlO_{20}(OH)_4K_{0.8}$ (Hillel 1980, Mitchell and Soga 2005 and Rowe et al. 1995).

2.2.3 Montmorillonite Mineralogy

Montmorillonite is an expansive clay mineral which undergoes large volumetric changes (swelling) as a result of increases in its water content. It is a 2:1 clay (Fig. 2.3), which means that it has 2 tetrahedral sheets sandwiching 1 central octahedral sheet (Rowe et al. 1995). The tetrahedral and octahedral sheets are combined so that the tips of the tetrahedrons of each silica sheet and one of the hydroxyl layers of the octahedral sheet form a common layer as shown schematically in Figure 2.3. In the stacking of the silica-alumina-silica units, O

layers of each unit are adjacent to O layers of the neighboring units (Grim 1962). Bonding between successive layers is by van der Waals forces and by cations that balance charge deficiencies in the structure. These bonds are weak and easily separated by adsorption of water or other polar liquids (Mitchell and Soga 2005). Water and ions are drawn into the cleavage planes between the lamellae, and as the crystal expands, it can readily be separated into flakelike thinner units and, ultimately, into individual lamellae, which are 1 nm thick (Fig. 2.4). Montmorillonite exhibits pronounced swelling-shrinkage behaviour, as well as high plasticity and cohesion because of its tendency to expand (Hillel 1980). Montmorillonite consists of very tiny particles which produce a specific surface of up to 800 m^2/g. Montmorillonite also has a very low hydraulic conductivity (hydraulic conductivity$\approx 10^{-11}$ to 10^{-15} m/s) even at high void ratios (Rowe et al. 1995). For these reasons, montmorillonite is marketed (as bentonite) for use in clayey liners. The unit layer formula of montmorillonite is $Al_{3.5}Mg_{0.5}Si_8O_{20}(OH)_4$ (Hillel 1980).

Bentonite is a very highly plastic, swelling clay deposit which is very widely used as a backfill during the construction of slurry trench walls, as a soil admixture for construction of seepage barriers, as a grout material, as a sealant for piezometer installations, and for other special applications. Bentonite is a highly colloidal, expansive alteration product of volcanic ash deposited into shallow marine basins. Bentonite deposits are normally exploited by quarrying. Extracted bentonite is distinctly solid. It is subsequently dried and either sieved (granular

form) or milled (into powder and super fine powder form). It has a liquid limit of 500 percent or more (Mitchel and Soga 2005 and Dixon 1994). Canada is rich in bentonite, particularly in the Prairie Provinces (Manitoba, Saskatchewan and Alberta) (Pusch 2001).

2.3 Clay Water Interaction

Swelling soils are found throughout the world and can have both positive and negative effects associated with their swelling properties. The swelling behaviour of expansive soils often causes problems, such as differential settlement and ground heaving. On the positive side, the self healing abilities of swelling soils are used to advantage in the development and design of waste repositories. Recently, expansive soils are attracting greater attention as back-filling (buffer) materials for high-level nuclear waste repositories (Maak and Simmons 2005).

This section discusses the background on diffuse double layer theory. In addition, the factors contributing to the swelling and compression behaviour of bentonite have been reviewed.

2.3.1 Diffuse Double Layer Theory

Clay particles carry negative charges on their surfaces due to isomorphous substitution in the crystal lattice. Exchangeable cations (e.g. K^+, Na^+ and Ca^{2+}) are attracted to these negatively charged surfaces. In a clay–water electrolyte system, the adsorbed cations near the surface of the clay particles have a much higher concentration as compared with the cation concentration in solution away from the surfaces. Because of the difference in cation concentration in solution near the surfaces and away from the surfaces of the clay particles, the cations near the surfaces of the particles tend to diffuse away to equalize the concentration throughout. Their tendency to do so is opposed by the negative electric field originating in the particle surfaces. The tendency of the cations to diffuse away and the opposing electrostatic attraction lead to a cation distribution adjacent to a clay particle in suspension as shown in Figure 2.5. Because of their negative charge, anions are excluded from the region adjacent to the clay surface, with the distribution as shown in Figure 2.5. The charged clay surface and the distributed ions in the adjacent phase are together termed the *diffuse double layer* (Bolt 1956, Van Olphen 1963, Mitchell and Soga 2005 and Tripathy et al. 2004).

The diffuse double layer occupies the space between the clay surface and the soil solution and has a thickness less than 10^{-5} mm. The thickness of the diffuse double layers decreases with an increase in the electrolyte concentration, with an

increase in cation valency and with a decrease in dielectric constant of the solution. In this case, the double layer is said to be compressed (Mitchell and Soga 2005).

2.3.2 Factors Contributing to Clay Swelling and Compression

For a compacted clay with a reasonable amount of water but still unsaturated, the swelling upon wetting is a result of the repulsive forces developed between adjacent clay particles (Yong and Mohammad 1992). The actual amount of volume change of a soil in response to a change in applied stress depends on the environmental factors such as the cation type, electrolyte type, concentration and pore fluid dielectric constant (Mitchell and Soga 2005). From the structure and interlayer bonding of clays, it can be expected that montmorillonite should undergo greater volume changes on wetting than kaolinite. In general, the swelling properties of the clay minerals follow the same pattern as their plasticity properties, that is, the more plastic the mineral, the more potential swell (Mitchell and Soga 2005).

When a confined body of swelling clay is allowed to adsorb water, swelling pressures develop. The swelling pressures are related to the osmotic pressure difference between the double layer and the external solution. In a partially hydrated micelle, the thickness of the absorbed water is less than the potential

thickness of the diffuse double layer. The double layer will tend to expand to its full potential thickness by the osmotic absorption of additional water, if available. As each micelle expands, its swarm of hydrated cations repels those of the adjacent micelle, and thus the micelles tend to push each other apart. This has the internal effect of closing the large pores and the external effect of causing the system as a whole to swell (Hillel 1980).

The concentration of cations between two associated clay particles is greater than in the external solution as shown in Figure 2.6. The actual concentration difference depends on the interparticle distance (i.e. on the degree of hydration) and on the potential extent of the diffuse double layer (which, in turn, depends upon the valence and concentration of the adsorbed cations). The osmotic attraction for external water is generally twice as high with monovalent than with divalent cations. Hence swelling and repulsion will be greatest with monovalent cations such as sodium, and with distilled water as the external solution. With calcium as the predominant cation in the exchange complex, swelling is greatly reduced. High salinity of the soil solution will also suppress swelling.

The time-dependent volume increase of clays in the process of hydration is illustrated in Figure 2.7. This time dependence is due to the low permeability of clay systems. The eventual swelling is seen to depend on the amount and the nature of the clay present. In general, swelling increases with increasing specific surface area (Hillel 1980).

The mineral composition has the most important role in the compressibility and swelling behaviour of clay soils. The influence of mineral composition is particularly strong when the pore liquid is distilled water, as shown by Figure 2.8 in which the compression and swelling curves of Ponza bentonite (mainly Na-montmorillonite, liquid limit = 390%), commercial kaolin (80% Kaolinite, liquid limit = 50%) and sand prepared with and immersed in distilled water are compared. The specimens were loaded and subsequently unloaded in steps. Figure 2.8 shows the compression and swelling curves plotted as void ratio versus the logarithm of the vertical effective stress. Void ratio (e) is defined as the ratio of the volume of voids to the volume of solids. As expected, the behaviour of the two pure clays is very different. In particular, kaolin behaves more similarly to the sand than to the bentonite, in terms of compression and swelling behaviour (Maio 2004). Significant hysteresis in the loading and unloading paths of the bentonite is evident in Figure 2.8.

An even stronger influence of the montmorillonite content can be observed with respect to time evolution of volume change. Figure 2.9 illustrates swelling and consolidation deformations versus time for artificial bentonite-kaoline mixtures for a decrease in axial stress from 40 to 20 kPa and for an increase from 20 to 40 kPa, respectively. The bentonite and kaolinite are the same clays used in the tests shown in Figure 2.8. The artificial bentonite-kaoline mixtures were prepared by mixing the air-dried powders with distilled water. The specimens were loaded and subsequently unloaded in steps and immersed in distilled water.

The figure shows that by adding 10% or more bentonite to the mixture, the time trend of the deformations changed dramatically (Miao 2004).

2.3.3 Summary

The diffuse double layer occurs at the interface between the clay surface and the soil solution. The cations in the soil solution are influenced by two opposing forces – the electrical force attracting the positive ions to the negative clay mineral particle surface, and the diffusive or thermal forces which tend to drive the cations away from the surface. The balance of these two forces gives rise to a distribution of cations in the solution adjacent to the clay surface. This distribution, described as a diffuse double layer, is made up of the negative clay surface and the diffuse distribution of hydrated cations and adsorbed water.

Unsaturated swelling clay experiences swelling upon wetting. The total amount of swelling of a soil is determined by the amount of swelling clay that it contains. When a body of clay is allowed to adsorb water, then the double layer expands followed by the expansion of micelles. Thus the micelles push each other apart and cause the whole system to swell. The eventual swelling depends on the amount and the nature (mineral composition) of the clay present and increases with increasing specific surface area of clay particles. When a swelling clay is

rigidly confined and given access to water, the tendency for expansion of the diffuse double layer will produce a swelling pressure against the confinement.

2.4 Case Studies of Swelling and Compression of High Plastic Clays

Volume changes in clays are the result of complex interactions between the solid skeleton and the pore fluid. Bentonite behaviour is greatly controlled by pore fluid composition. In particular, compressibility and swelling (which depend also on the type of exchangeable cations) decrease with increasing pore fluid ionic strength. The compressibility and swelling of clays saturated with salt solutions are explained in terms of diffuse double layer properties. This section discusses the effect of varying pore fluid salinity on compression and swelling behaviour of bentonite.

2.4.1 The Effect of Pore Fluid Salinity on Compression and Swelling Behaviour of Bentonite

Miao (2004) reported the 1-D compressibility and swelling results for specimens of Ponza bentonite (mainly Na-montmorillonite, liquid limit = 390%) reconstituted at about the liquid limit with NaCl solutions at various concentrations and immersed in the same solutions (Fig. 2.10). The specimens were loaded and

subsequently unloaded in steps. The curves of the specimens reconstituted with the concentrated solutions are distinctly different from those of the distilled water-saturated bentonite. The different compression curves tend to converge towards a narrow range of void ratio at stresses higher than 1000 kPa. A similar effect can be observed in the case of the Bisaccia clay (30% Ca-montmorillonite, liquid limit = 110%) (Fig. 2.11) (Miao 2004). Also of particular interest is the flattening of the shape of the void ratio versus log of effective stress curve in the higher stress ranges. This behaviour is particularly evident for the bentonite specimens in the presence of distilled water.

The swelling behaviour of air dried Wyoming bentonite powder (mainly Na-montmorillonite, liquid limit = 354%, plastic limit = 27%) was investigated over a range of vertical effective stresses by Studds et al. (1998). Samples of air dried bentonite powder were subjected to a vertical stress and the samples were given access to distilled water from a reservoir. The sample height was monitored until swelling ceased, at which point the final void ratio was calculated. Figure 2.12 shows swelling data, plotted as void ratio versus the logarithm of the vertical effective stress. It can be clearly seen that at vertical effective stresses below ~200 kPa the void ratio of the clay is very sensitive to the vertical effective stress, decreasing approximately linearly with the logarithm of the stress. Above ~200 kPa the void ratio of the clay is less sensitive to changes in vertical effective stress, but still appears to decrease linearly with the logarithm of the stress.

Studds et al. (1998) also report similar tests where the same air-dried bentonite is allowed to swell in the presence of 0.01, 0.1 and 1.0 mol/l Na, K, Cs, Mg, Ca and Al chloride salt solutions (Fig. 2.13). Studds et al. (1998) did not differentiate the data for different chloride salts, as the different salts gave broadly similar trends (full details are given by Studds et al. 1996). The test results show that at vertical effective stresses less than 200 kPa, the amount of swelling decreased with increasing solution concentration, and for each concentration the void ratio decreases approximately linearly with increasing vertical stress (Studds et al. 1998).

Figure 2.14 shows the swelling data for bentonite-sand mixtures, plotted as clay-void ratio versus the logarithm of the vertical effective stress. Clay void ratio is not defined in the paper; it is likely the void ratio related to the clay component of the mixture. Samples of bentonite-sand mixtures were subjected to a vertical stress and the samples were given access to distilled water from a reservoir. The sample height was monitored until swelling ceased, at which point the final clay-void ratio was calculated. The trendline for the bentonite powder from Figure 2.12 has been superimposed on this figure. It can be observed that at low vertical effective stresses, the behaviour of the bentonite-sand mixtures is similar to that of the bentonite alone. However, as the vertical effective stress increases, there is a deviation from bentonite behaviour at a stress which depends on the bentonite content (10 and 90 kPa for the mixtures containing 10% and 20% of bentonite, respectively). Above these 'threshold stresses' the decrease in the

clay-void ratio is less sensitive to increases in vertical effective stress (Studds et al. 1998).

Studds et al. (1998) also report similar tests where the same bentonite-sand mixtures are allowed to swell in the presence of 0.01 mol/l Na, K, Cs, Mg, Ca and Al chloride salt solutions (Fig. 2.15). Studds et al. (1998) did not differentiate the data for different chloride salts, as the different salts gave broadly similar trends (full details are given by Studds et al., 1996). The response of a 20% bentonite-sand mixture in 0.01 mol/l salt solutions is similar to that observed for the same mixture in distilled water. At low vertical effective stresses the response of the mixture was similar to that of bentonite alone, deviating from that response at vertical effective stresses greater than ~70 kPa (Studds et al. 1998).

The influence of water chemistry on the swelling capacity of a statically compacted Ca-bentonite (92% montmorillonite, liquid limit = 102%, plastic limit = 49%) was investigated under oedometer conditions by Castellanos et al. (2006). The samples were statically compacted to a dry density of 1.65 Mg/m^3 at a water content of 13.7%. Specimens were soaked under constant stress (0.02, 0.5 and 2.0 MPa) using distilled water, and NaCl and $CaCl_2$ aqueous solutions with concentrations of 0.5, 2.0 and 5.5 mol/l. Figure 2.16 presents the time evolution of vertical strains during wetting of the compacted samples. Vertical strain is the ratio of change of the sample's height. Negative vertical strains correspond to swelling. For NaCl and $CaCl_2$ salt solutions, when high vertical stresses are

applied (2.0 MPa) all samples experienced an initial collapse followed by a swelling. In the same figure, it can be seen that an increase in salinity reduces the value of the final swelling strain.

The elapsed time from start to finish of the swelling process appears to be approximately the same for the samples loaded at 0.02 MPa and soaked with different NaCl solutions. However, the end of swelling time appears to increase with increasing concentration in samples flooded with $CaCl_2$ solutions at the same stress, despite an opposite trend of the sample soaked with 2.0 mol/l solution.

It can be observed from Figure 2.16 that the amount of collapse strains induced on highly loaded samples seems to be influenced by the type of cationic solution and not much by concentration. Specimens saturated with distilled water and $CaCl_2$ showed larger collapse than the samples soaked with NaCl solutions. Initial collapse is a consequence of the redistribution of soil aggregates due to reduced suctions whilst chemical swelling is a consequence of the increase in the repulsion forces acting inside the aggregates, and it emerges over longer times as smaller pores are inundated later (Castellanos et al. 2006).

The effects of the applied vertical stress and the concentration of the saline solution on the final swelling strains are shown on Figure 2.17. It can be seen that the swelling capacity decreases significantly with increased salinity at a

vertical stress of 0.02 MPa and that the differences in the swelling strains with increasing salinity tend to be smaller with increasing vertical stress. On the other hand, samples soaked with both $CaCl_2$ and NaCl solutions yielded similar swelling strains. "The reduction of the swelling strains at increasing concentrations of the flooding solution can be explained by the increase of the electrolyte concentration near the clay particle surfaces that reduces the thickness of the double layer. In addition, high saline concentrations may also induce cation exchange phenomena that also affect the thickness of the double layers" (Castellanos et al. 2006).

2.4.2 Summary

Swelling of clays is the effect of complex interactions between the solid skeleton and the pore fluid. Pore fluid salinity affects the swelling and compression behaviour of bentonite. In particular, compressibility and swelling reduce with increasing pore fluid concentration. This reduction can be explained by the increase of the electrolyte concentration near the clay particles and the decrease of the double layer thickness.

The compression and swelling behaviour of bentonite-sand mixtures is strongly influenced by clay content, in particular by the montmorillonite fraction, and by the pore fluid and applied vertical stress. With increasing vertical stress, the

compressibility and swelling reduce. In fact, at low stresses, the clay swells sufficiently in dilute solutions to separate the sand particles. At high stresses, or in strong solutions, the bentonite has insufficient swelling capacity to force the sand particles apart and swelling is limited by the sand pore volume.

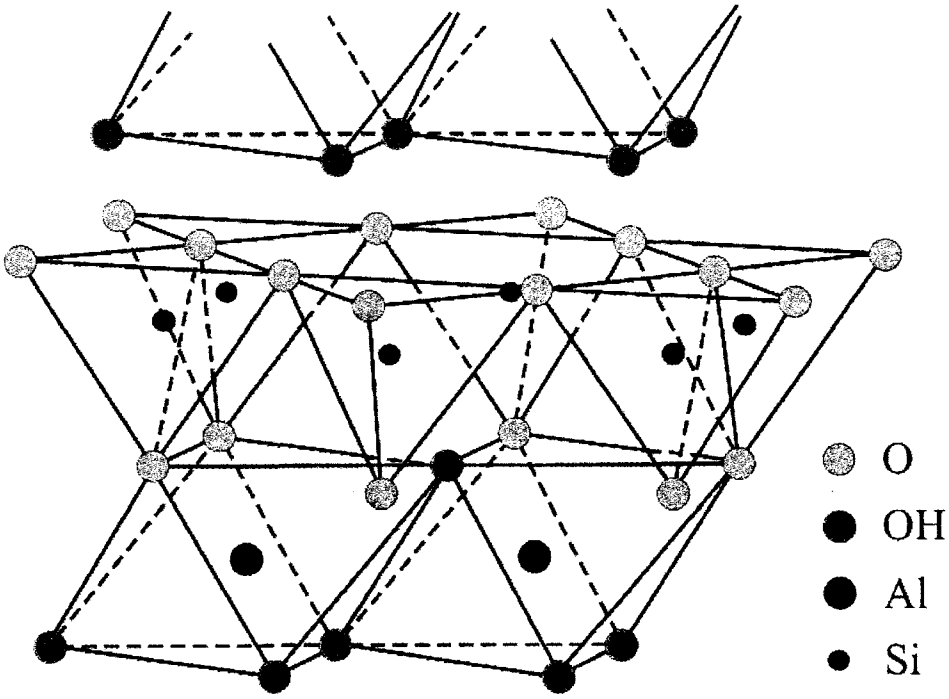

Figure 2.1: Structure of Kaolinite layer (Grim 1962)

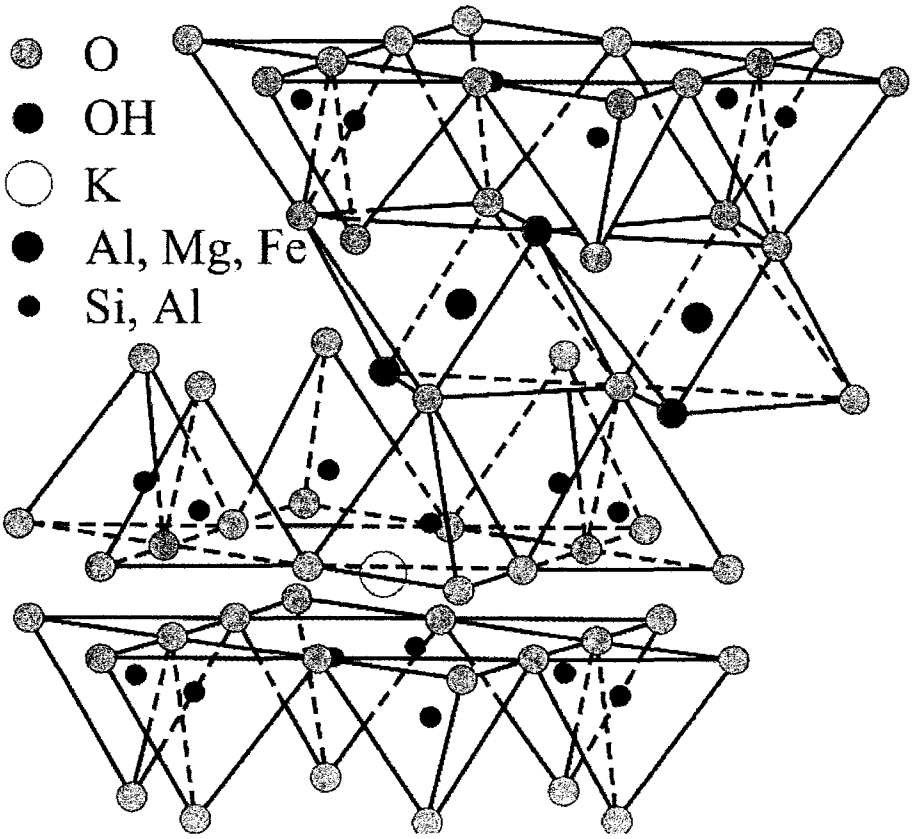

Figure 2.2: Structure of Illite layer (Grim 1962)

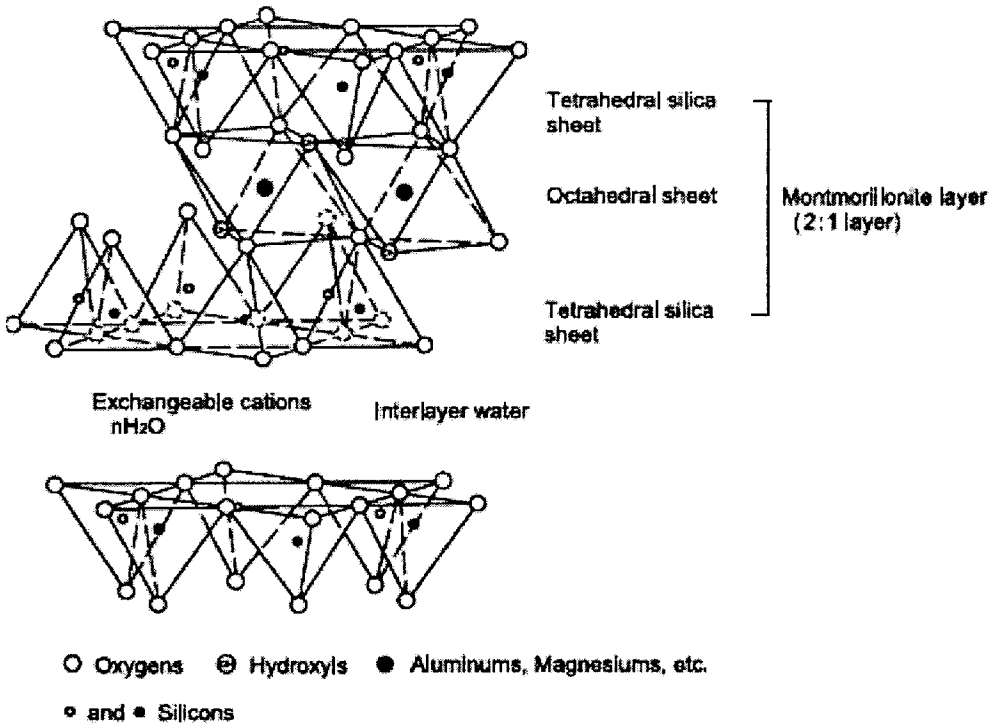

Figure 2.3: Structure of montmorillonite mineral (Komine 2004)

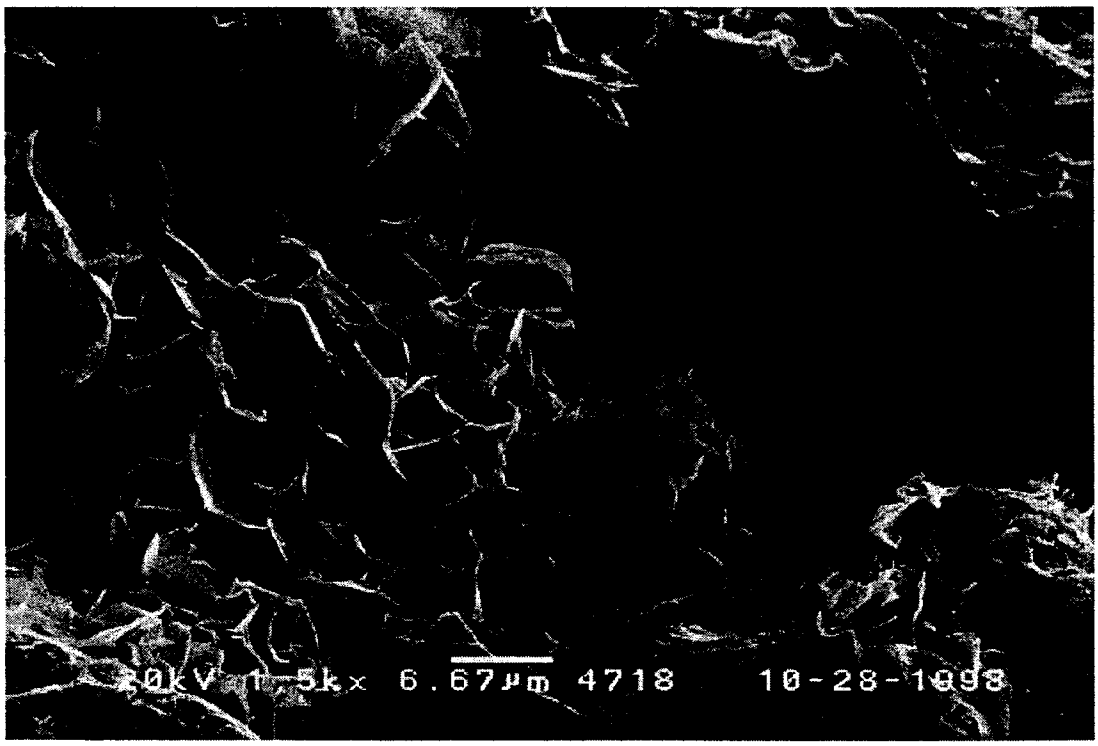

Figure 2.4: Montmorillonite magnified about 1,500 times (http://webmineral.com/specimens/picshow.php?id=1285)

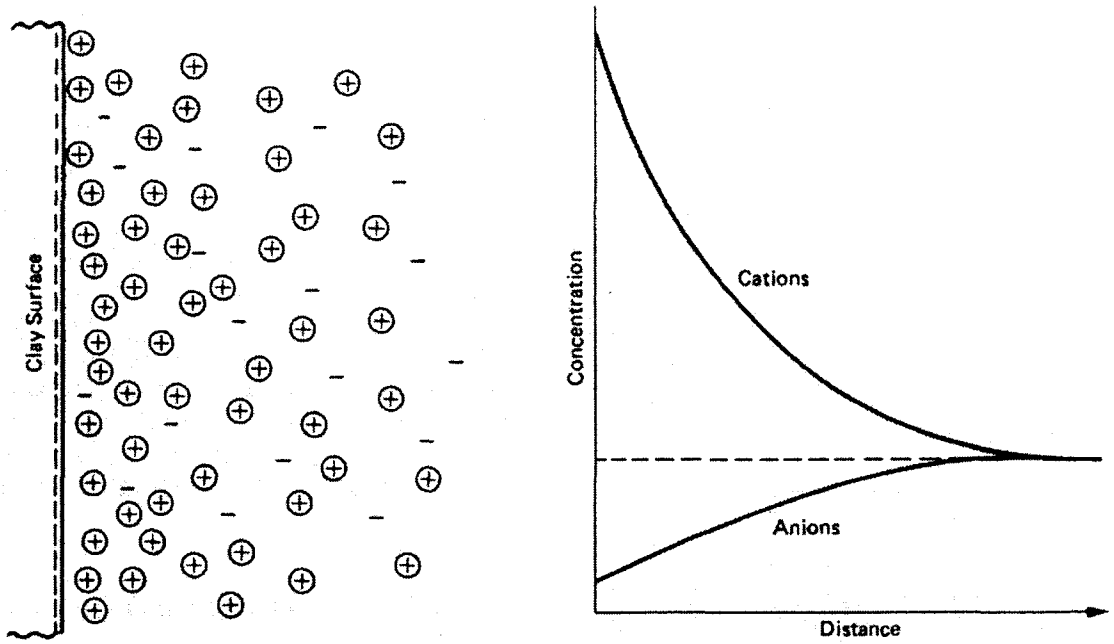

Figure 2.5: Distributions of ions adjacent to a clay surface according to the concept of diffuse double layer (Mitchell and Soga 2005)

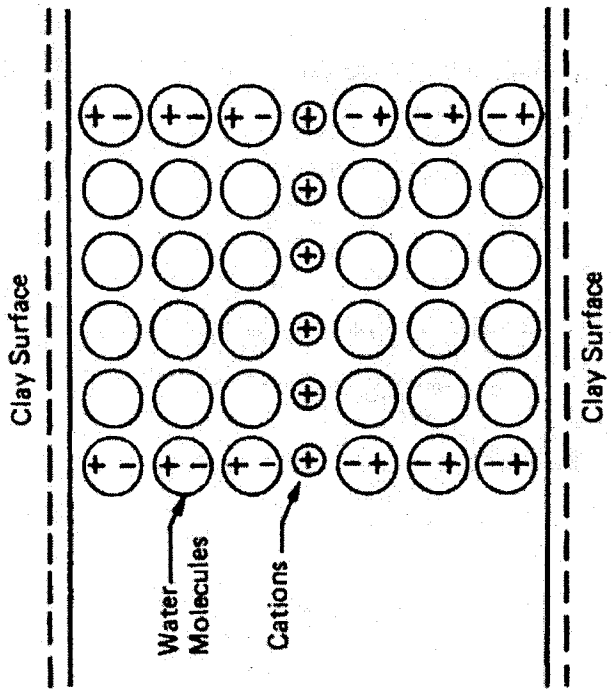

Figure 2.6: Water adsorption by clay surfaces (Mitchell and Soga 2005)

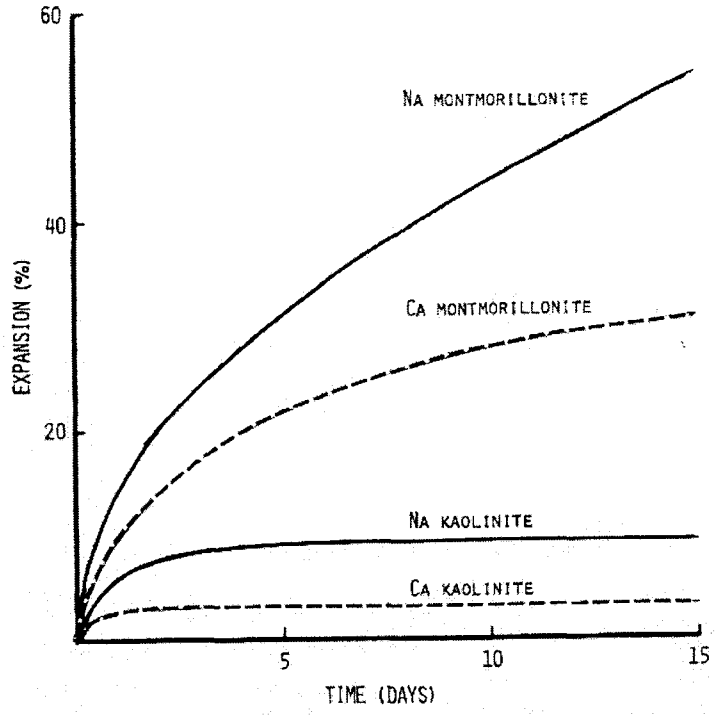

Figure 2.7: Volume changes of montmorillonite and kaolinite clays during the process of water adsorption (Hillel 1980)

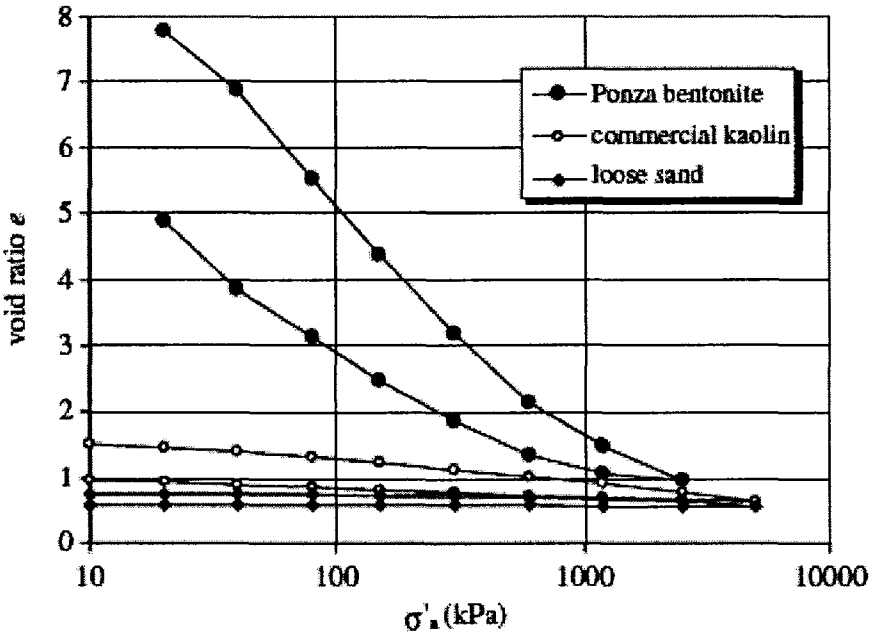

Figure 2.8: Oedometer curves of water saturated Ponza bentonite, commercial kaolin and sand (Maio 2004)

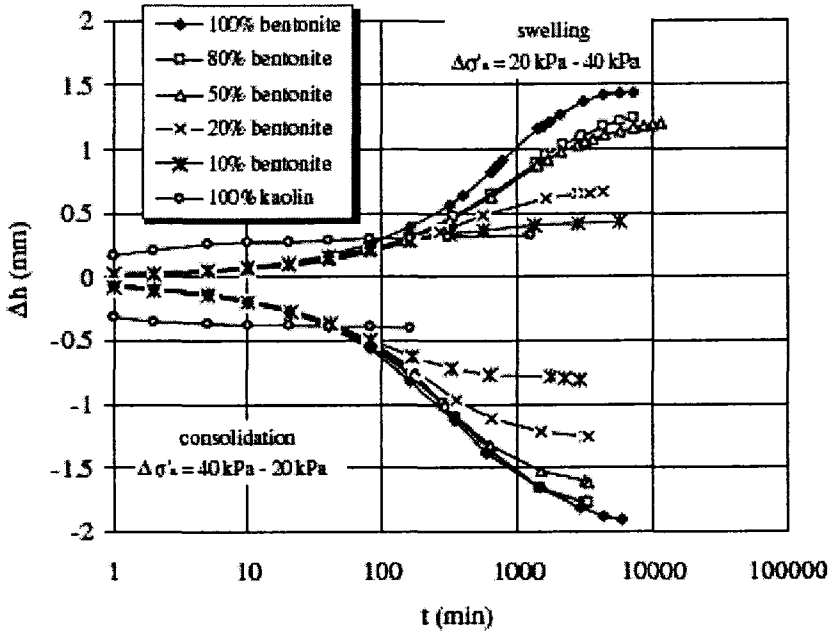

Figure 2.9: Consolidation and swelling curves of the bentonite–kaolin mixtures for an increment of axial stress from 20 to 40kPa and for a decrement from 40 to 20 kPa respectively (Miao 2004)

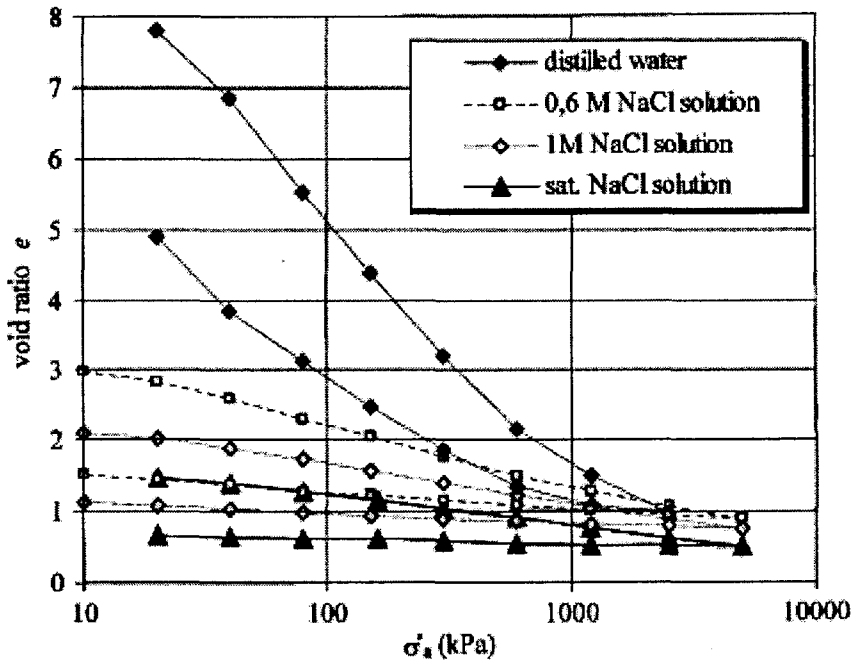

Figure 2.10: Oedometer curves for the Ponza bentonite reconstituted with and immersed in NaCl solutions at various concentrations (Miao 2004)

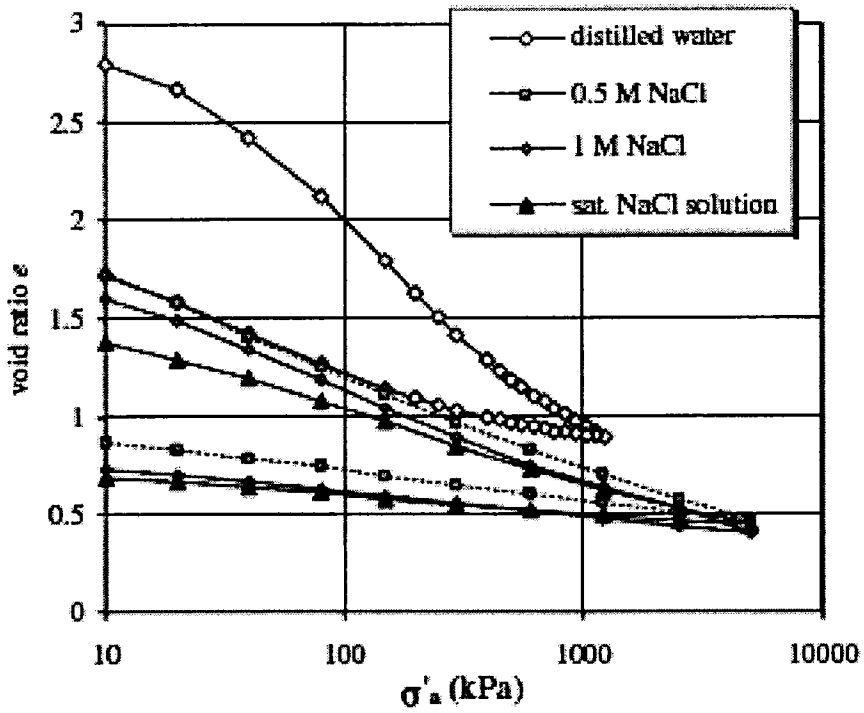

Figure 2.11: Oedometer curves for the Bisaccia clay reconstituted with and immersed in NaCl solutions at various concentrations (Miao 2004)

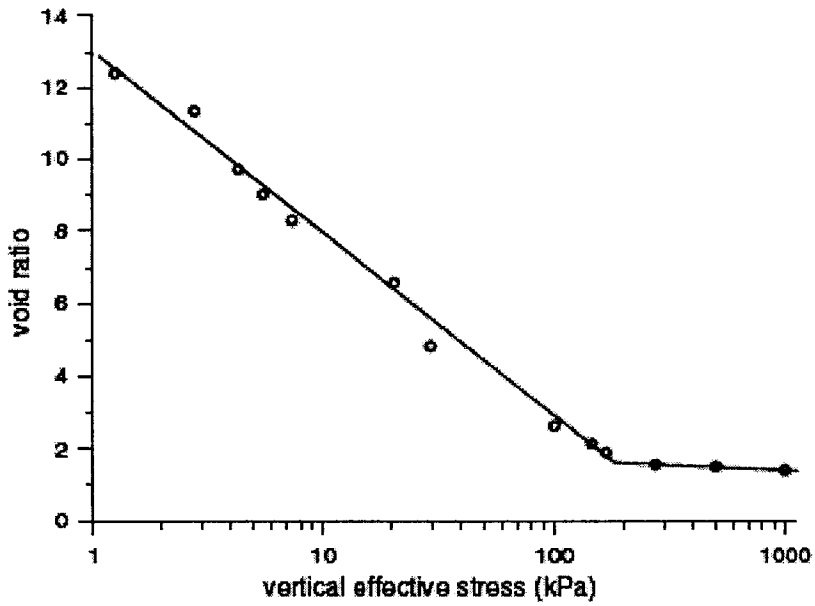

Figure 2.12: Swelling of bentonite powder with distilled water (Studds et al. 1998)

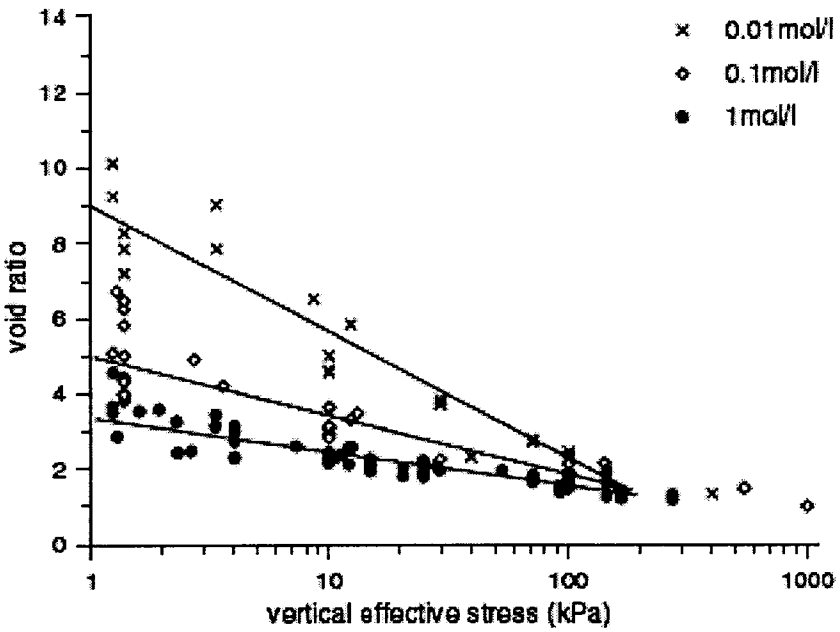

Figure 2.13: Swelling of bentonite powder with different strength chloride salt solutions (Studds et al. 1998)

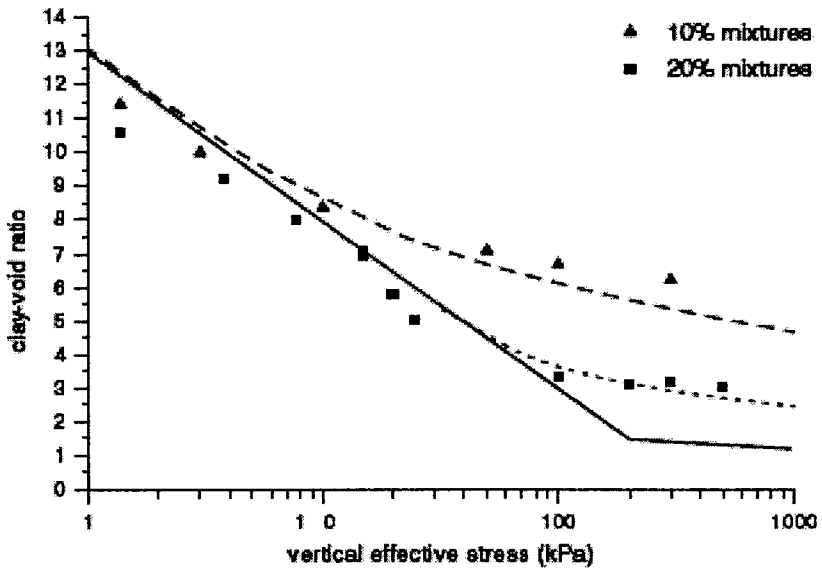

Figure 2.14: Swelling of bentonite-sand mixtures with distilled water (Studds et al. 1998)

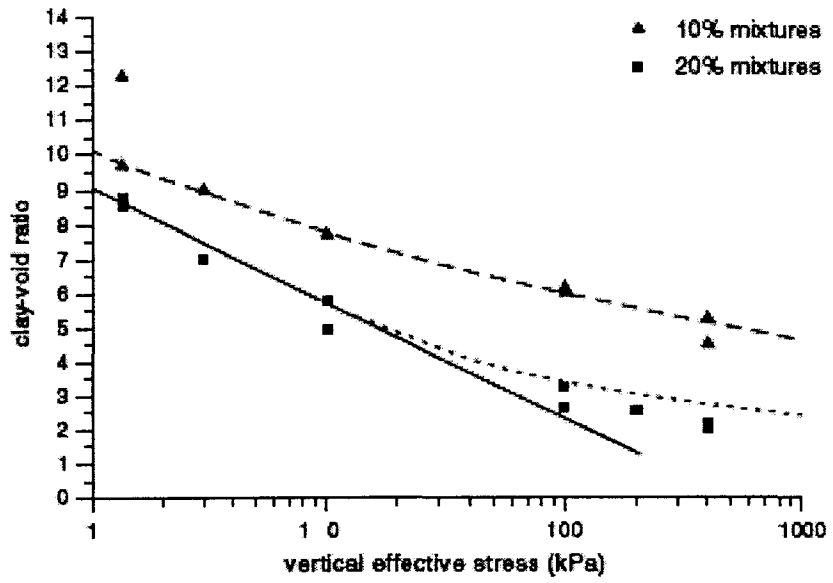

Figure 2.15: Swelling of bentonite-sand mixtures with various 0.01 mol/l salt solutions (Studds et al. 1998)

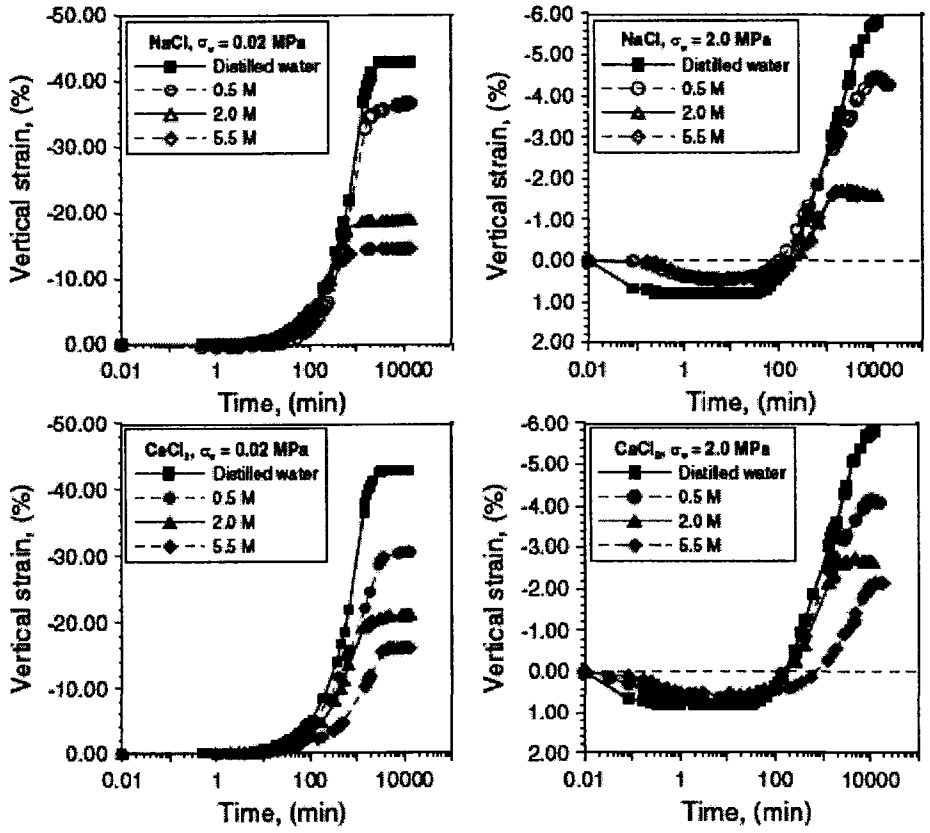

Figure 2.16: Time evolution of volumetric strains undergone by the compacted samples on soaking with different salt solutions and under different vertical stresses (Castellanos et al. 2006)

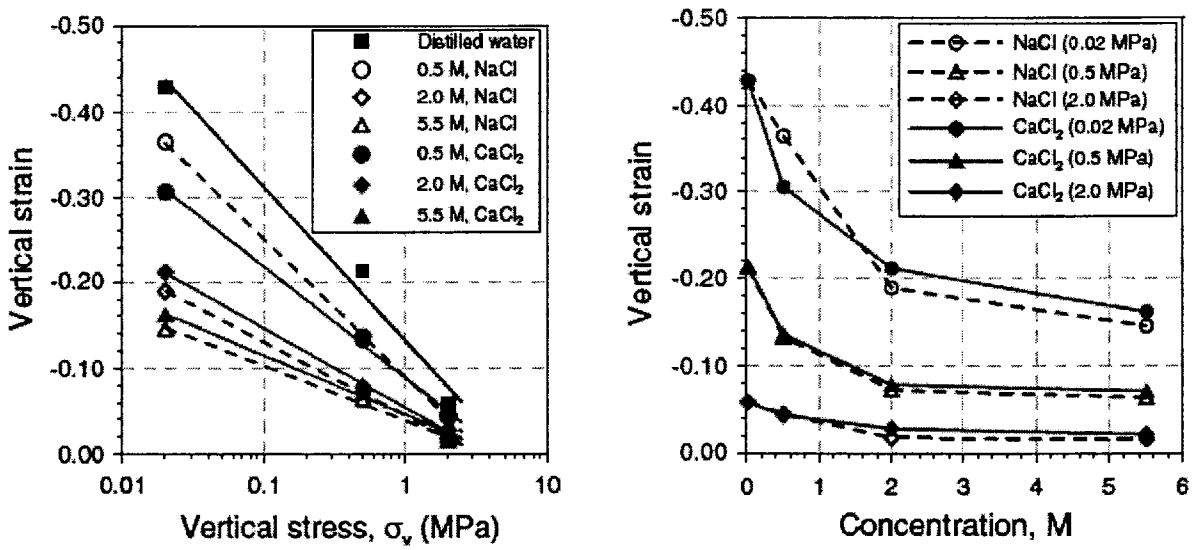

Figure 2.17: Swelling strains versus vertical stresses and concentration of NaCl and CaCl2 saline solutions for compacted samples in soaking under load tests (Castellanos et al. 2006)

Chapter 3 : MATERIALS AND METHODS [2]

3.1 Introduction

This chapter describes the materials and the testing procedures and equipment used in this research study. In addition, this chapter describes the test matrix and loading/unloading and wetting paths that were used in this test program.

3.2 Light Backfill Material Characteristics

The light backfill (LBF) used in this research study is composed of 50-dry wt% bentonite and 50-dry wt% silica sand and was obtained from a premixed stock of

[2] Significant portions of this chapter have been drawn from:
Baumgartner et al. (2007) – Appendix C, Kjartanson and Batenipour. Light BackFill (LBF), Preliminary Results Of One-Dimensional Consolidation Testing On Bentonite Clay-Based Sealing Components Subjected To Two Pore-Fluid Chemistry Conditions, Ontario Power Generation Report.

material prepared by AECL. The bentonite clay component was batched and reblended Saskatchewan bentonite with the properties listed in Table 3.1. The 50/50 bentonite/sand mix was prepared for the Buffer/Container and Isothermal Tests carried out in AECL's Underground Research Laboratory (URL) (Dixon et al. 2002b). It was mixed to a target gravimetric water content of 18% using relatively fresh groundwater from the URL.

Table 3.2 shows the results of wet sieve tests carried out to characterize the 50/50 bentonite/sand mixture used in this research study (Dixon et al. 1994). These sieve results indicate a maximum particle size of about 2 mm, with about 90% of the particles less than 0.85 mm in size.

Table 3.3 shows the initial water content, height, dry density, EMDD, void ratio and degree of saturation of the LBF samples prepared and tested in this research. These calculations use a specific gravity of soil solids of 2.70 for the LBF and an 80% montmorillonite content for the Saskatchewan bentonite used to make the 50/50 mix. The average initial water content, height, dry density and EMDD were 20.54%, 0.96 cm, 1.36 Mg/m^3 and 0.79 Mg/m^3, respectively. The average initial void ratio and degree of saturation were 0.99 and 57%, respectively. As Table 1.1 shows, the current OPG specification indicates that LBF should be placed at a water content of 15%. It was agreed to test the material at it as-delivered water content of about 20% to 21%. The increase in water content from the original target of 18% is likely due to some temperature-

gradient-driven water redistribution within the barrels during storage. All the samples were prepared using the delivered 50/50 bentonite/sand mix from AECL except the two samples tested using a 100 g/l $CaCl_2$ solution as the mixing water. These samples were first air-dried and then mixed to a water content of about 21% using 100 g/l $CaCl_2$ solution. The volume and weight of the $CaCl_2$ in the mixing solution was accounted for in the weight-volume calculations.

3.3 Consolidation Test Equipment

Two Wykeham Farrance model 24251 front loading and two Wykeham Farrance model 24001 rear loading consolidation frames were used in this test program. The frames were supplied by Lakehead University and AECL and all tests were performed in the Geotechnical Laboratory at Lakehead University (Figs. 3.1 and 3.2). The consolidation cell constrains the sample laterally and allows it to drain vertically. The WF24251 front loading and WF24001 rear loading consolidation frames use the same consolidation cells. Conventional 50-mm-diameter consolidation rings that allow 19-mm-high samples were used in all four consolidation cells. The fixed specimen ring and the cell is constructed of steel and Plexiglas. The cells also include two porous stones: a larger stone which is placed beneath the sample and a smaller stone that is screwed on to the loading cap. Filter paper is placed between the porous stones and the sample to ensure that no soil particles will infiltrate the stones.

The cell is mounted to the apparatus on the fixed machine plate. The cross beam can then be lowered bringing the yoke assembly into contact with the female seating of the cell loading cap. As the beam hanger is loaded it applies vertical force to the yoke assembly and the cell loading cap which in turn applies pressure to the sample. The dial gauge moves as the yoke assembly lowers or rises. The gauge can be adjusted to any height along the height of the bar. The rotations on the gauge are used to measure the consolidation of the sample. The load hangars for all four frames were positioned to a give lever arm (load) ratio of 11.04:1. Given this load ratio, the stress applied to the sample can be calculated with the following relationship:

$$[\text{Load on hangar (kg)}/0.0181] = \text{Applied Pressure (kPa)} \qquad (3.1)$$

This equation incorporates the lever arm ratio. The maximum load that can be suspended from the hanger on this particular model is 150 kg. The entire apparatus must be bolted down to a solid base to prevent overturning when a high load is applied to the sample.

3.4 Sample Preparation and Test Setup

An initial target sample thickness of 10 mm was selected for this program. The rationale for this selection is as follows. The consolidation time is proportional to

the length of the longest drainage path squared (i.e. half the sample thickness squared), so the thinner the sample, the shorter the testing time. On the other hand, the sample cannot be made too thin. As Table 3.2 shows, the LBF mixture contains about 4% sand sized particles coarser than 1.7 mm size. Consequently samples at least 10 mm thick are required to minimize the effect that the larger sand particles may have on the compression behaviour of the sample.

The steps in the sample preparation and test setup procedure used to carry out the tests are as follows:

- Soak two porous stones in distilled water 24 hours before setting up the test.
- Saturate two pieces of Whatman 40 Ashless filter paper just before placing the sample into the consolidation ring.
- Weigh 30.9 g of as-delivered LBF mixture and place it loosely into the consolidation ring, on top of the piece of saturated Whatman 40 Ashless filter paper (Fig. 3.3). Also weigh about the same amount of LBF from the same batch used to prepare the sample and place it into the oven for initial water content determination.
- Compress the sample to a height of about 10 mm using a suitably-sized steel ram, as shown in Figure 3.4. The compression could be carried out with hand pressure alone because of the relatively low density of LBF. Figure 3.5 shows the prepared sample.

- Using electronic callipers, take about 12 measurements from the top of consolidation ring to the top of sample to calculate an average initial height of sample.
- Place the piece of saturated Whatman 40 Ashless filter paper on the top of sample, install the consolidation ring and restraining ring into the consolidation cell, with the lower saturated porous stone in place, and place the load cap with porous stone on top of the upper filter paper.
- Place the assembled consolidation cell into the consolidation frame, set the dial gauge in place (see Fig. 3.6) and, at the start of the test, apply the appropriate cell fluid (either distilled water or $CaCl_2$ solution) and weights to the lever arm hangar system.

3.5 Test Matrix and Test Procedures

Fifteen tests were completed to meet the research objectives outlined in the Introduction. The matrix of tests is listed in Table 3.4. Six loading/wetting paths using the mixing and consolidation cell reservoir water as listed in Table 3.4 were followed.

For path 1, the LBF was allowed to swell to a target value of 20% of its initial height during initial distilled water uptake from the reservoir. Sample swelling was closely monitored after the cell reservoir was filled and the loads on the

hangar were adjusted accordingly to allow the sample to swell to the target value. It was not necessary to let the sample equilibrate under each of these loads as the 20% expansion was approached, but rather to get as close as possible to the target 20% expansion and then let the sample equilibrate under the final applied load in this sequence. Table 3.4 indicates that the actual initial swelling strains achieved for the tests carried out for path 1 range from 19.5% to 22.4%.

The sample would take 4 to 7 days on average to reach equilibrium between the applied stress and sample swelling (equilibrium condition is when the vertical deformation rate was less than about 0.02 mm/day). Once the equilibrium was achieved, the loads on the samples were increased using a load increment ratio of about 1 (i.e. doubling of the applied load with each increment). Following loading to the maximum stresses indicated in Table 3.4, the samples were unloaded in stages. The unloading increments were carried out in reverse of the loading increments. Each load and unload increment was generally applied until equilibrium was achieved. The tests were terminated at the completion of the final unloading increment of 55 kPa (i.e. 1 kg weight on the hanger).

Path 2a and 2b differ from path 1 in that the samples for path 2a were confined during water uptake and then loaded and the samples for path 2b were confined during water uptake, allowed to swell to about 20% strain and then loaded. The load and unload increments were applied in the same manner as for path 1 and

distilled water was used in the reservoir. The tests were terminated at the completion of the final unloading increment of 55 kPa.

Path 3 was intended to be the same as path 1 except that 100 g/l $CaCl_2$ solution was used as the reservoir water rather than distilled water. The intent was to allow the LBF to swell to a target value of 20% of its initial height during initial solution uptake from the reservoir followed by loading of the samples. As shown in Table 3.4, however, the samples only swelled to between about 6% and 10% strain, and this was under unloaded (unrestrained) conditions. For these samples, once the maximum amount of swelling was achieved and the samples came to equilibrium, they were loaded and unloaded in the same manner as the samples for the other paths. The tests were terminated at the completion of the final unloading increment of 55 kPa.

Path 4 was intended to be the same as path 2b except that 100 g/l $CaCl_2$ solution was used as the reservoir solution rather than distilled water. After initial solution uptake with the sample confined, the intent was to allow this sample to swell to a target value of 20% of its initial height during initial solution uptake from the reservoir followed by loading of the sample. As indicated in Table 3.4, however, the sample only swelled to 3.6% strain, and this was under essentially unloaded conditions. Once the maximum amount of swelling was achieved and the sample came to equilibrium, the sample was loaded and unloaded in the same

manner as the samples for the other paths. The tests were terminated at the completion of the final unloading increment of 55 kPa.

Path 5 was intended to be the same as path 3 except that 100 g/l $CaCl_2$ solution was used as the LBF mixing water. The LBF samples in this path were first air-dried and then mixed to a water content of about 21% using 100 g/l $CaCl_2$ solution. The 100 g/l $CaCl_2$ solution was used also as the reservoir water. The intent, as with path 3, was to allow these samples to swell to a target value of 20% of its initial height during initial solution uptake from the reservoir followed by loading of the samples. As indicated in Table 3.4, however, the samples only swelled to between about 6% and 7% strain, and this was under essentially unloaded conditions. For these samples, once the maximum amount of swelling was achieved and the samples came to equilibrium, they were loaded and unloaded in the same manner as the samples for the other paths. The tests were terminated at the completion of the final unloading increment of 55 kPa.

Path 6 was intended to be the same as path 3 except that 200 g/l $CaCl_2$ solution was used as the reservoir water rather 100 g/l $CaCl_2$ solution. The intent, as with path 3, was to allow these samples to swell to a target value of 20% of its initial height during initial solution uptake followed by loading of the samples. As shown in Table 3.4, however, the samples only swelled to about 6% strain, and this was under essentially unloaded conditions. For these samples, once the maximum amount of swelling was achieved and the samples came to

equilibrium, they were loaded and unloaded in the same manner as the samples for the other paths. The tests were terminated at the completion of the final unloading increment of 55 kPa.

3.6 Test Decommissioning and Sample Recovery

On test completion and decommissioning, the sample was recovered quickly and carefully in order to provide accurate data that were crucial for the analysis of results. Once equilibrium was achieved under the last unloading increment of the test (55 kPa), the consolidation cell was removed from the consolidation frame and quickly disassembled. The final height of the sample was measured using electronic calipers. As with the initial height, typically about 12 measurements were made and averaged to obtain the final sample height. Next, the consolidation ring containing the sample and the top and bottom filter papers was weighed and then placed in the oven for drying for 24 hours.

The consolidation ring containing the oven-dry sample and filter papers was carefully weighed. These weights were used to calculate the sample final water content, void ratio, degree of saturation and dry density. Also the dry and wet weights and dry and wet thicknesses of the filter papers used in these tests were measured. These weights and thicknesses were used in calculating the sample heights and weights for all stages of the tests.

Property	Value
Montmorillonite Content, %	80
Liquid Limit	214 ± 6
Plasticity Index	182 ± 5
Cation Exchange Capacity, meq/100g	88
Specific Surface area, m^2/g	520-630

Table 3.1: Properties of the Saskatchewan Bentonite Component of LBF (after Graham et al. 1997)

Sieve	Opening Size (mm)	% Passing
#8	2.36	100
#12	1.7	95.8-96.5
#20	0.85	89.5-90.5
#40	0.425	74.0-76.0
#70	0.212	64.3-66.0
#140	0.106	48.8-50.2
#200	0.075	48.2-49.8

Table 3.2: Particle Size Distribution of the 50/50 Bentonite/Sand LBF Mixture (Dixon et al. 1994)

Test	Water Content, %	Height, cm	Dry Density, Mg/m^3	EMDD, Mg/m^3	Void Ratio	Degree of Saturation, %
HB2	21.19	1.029	1.26	0.71	1.14	50
HB3	21.19	1.040	1.25	0.70	1.16	49
HB4	19.63	1.010	1.30	0.74	1.08	49
HB6	21.23	0.990	1.31	0.75	1.06	54
HB7	21.03	0.961	1.35	0.78	1.00	57
HB8	20.70	0.888	1.47	0.88	0.84	67
HB9	20.67	1.001	1.30	0.74	1.08	52
HB11	20.04	0.928	1.41	0.83	0.91	59
HB12	20.27	0.945	1.39	0.81	0.94	58
HB13	20.88	0.953	1.37	0.79	0.97	58
HB14	20.04	0.949	1.38	0.80	0.96	57
HB15	20.95	0.933	1.40	0.82	0.93	61
HB16	20.43	0.865	1.51	0.92	0.79	70
HB19	20.03	0.967	1.36	0.78	0.99	55
HB20	19.84	0.960	1.37	0.79	0.97	55
Averages	20.54	0.960	1.36	0.79	0.99	57

Table 3.3: Initial Properties of LBF Samples

Path	Test	Mixing Water	Reservoir Water	Swelling % on Initial Water Uptake	Loading Sequence
1	HB3	As supplied by AECL	distilled	19.5	Load to 1325.7 kPa after initial swelling
	HB5[1]				
	HB6			20.8	Load to 3986.5 kPa after initial swelling
	HB8			22.4	Load to 2651.8 kPa after initial swelling
2a	HB1[1]	As supplied by AECL	distilled		
	HB2			confined[3]	Load to 2651.4 kPa
	HB4				Load to 2653.8 kPa
2b	HB7	As supplied by AECL	distilled	confined[3]	Unload and let swell to 21.2%, reload to 3986.3 kPa
	HB9				Unload and let swell to 21.4%, reload to 2659.2 kPa
3	HB11	As supplied by AECL	100 g/L (0.90 mol/L) $CaCl_2$	10.4	Load to 3989.8 kPa after initial swelling
	HB12			7.5	Load to 2674.8 kPa after initial swelling
	HB17 & HB 18[1]				
	HB19			6.3	Load to 2659.8 kPa after initial swelling
4	HB10[2]	As supplied by AECL	100 g/L (0.90 mol/L) $CaCl_2$		
	HB14			confined[3]	Unload and let swell to 3.63%, reload to 4000.3 kPa
5	HB13	100 g/L (0.90 mol/L) $CaCl_2$	100 g/L (0.90 mol/L) $CaCl_2$	6.4	Load to 2650.2 kPa after initial swelling
	HB15			7.1	Load to 3985.4 kPa after initial swelling
6	HB16	As supplied by AECL	200 g/L (1.80 mol/L) $CaCl_2$	6.1	Load to 2650.4 kPa after initial swelling
	HB20	As supplied by AECL	200 g/L (1.80 mol/L) $CaCl_2$	6.0	Load to 3981.4 kPa after initial swelling

[1] Tests discontinued prematurely due to equipment problems
[2] HB10 - initial trial to test the unrestrained swelling ability of the LBF with 100 g/l $CaCl_2$ reservoir fluid
[3] Samples were prohibited from swelling by applying appropriate vertical pressure

Table 3.4: Test Matrix and Loading/Wetting Paths

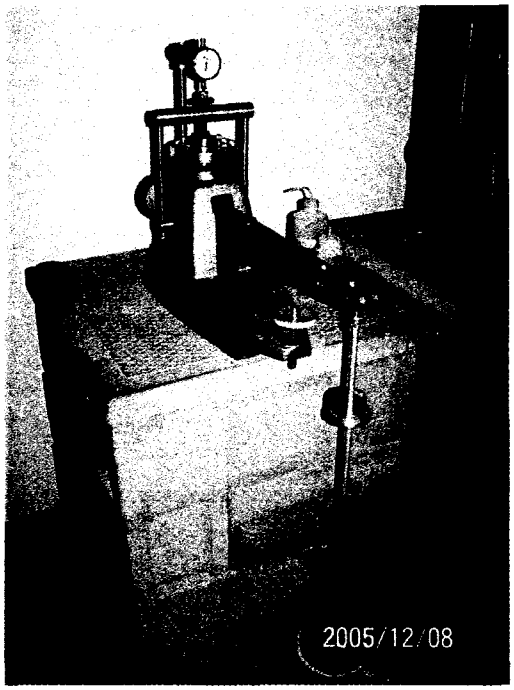

Figure 3.1: Front Loading Consolidation Frame

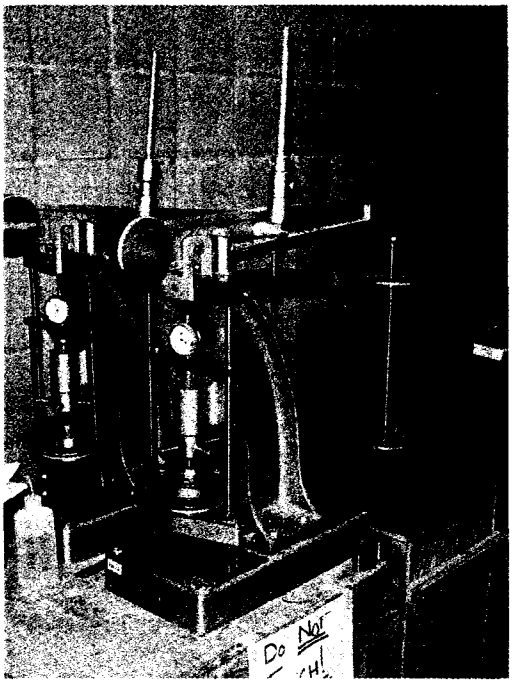

Figure 3.2: Rear Loading Consolidation Frame

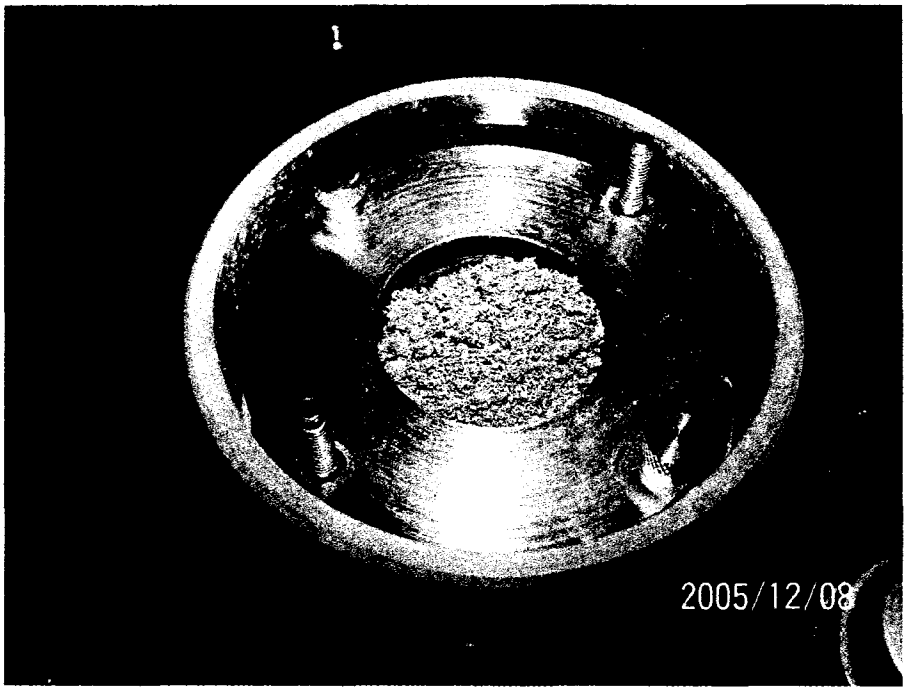

Figure 3.3: Preparation of LBF Samples: Loose LBF placed in the consolidation ring

Figure 3.4: Preparation of LBF Samples: Compression of the LBF sample to the target height with a steel ram

Figure 3.5: Preparation of LBF Samples: Final prepared sample before placement of the upper filter paper and loading cap

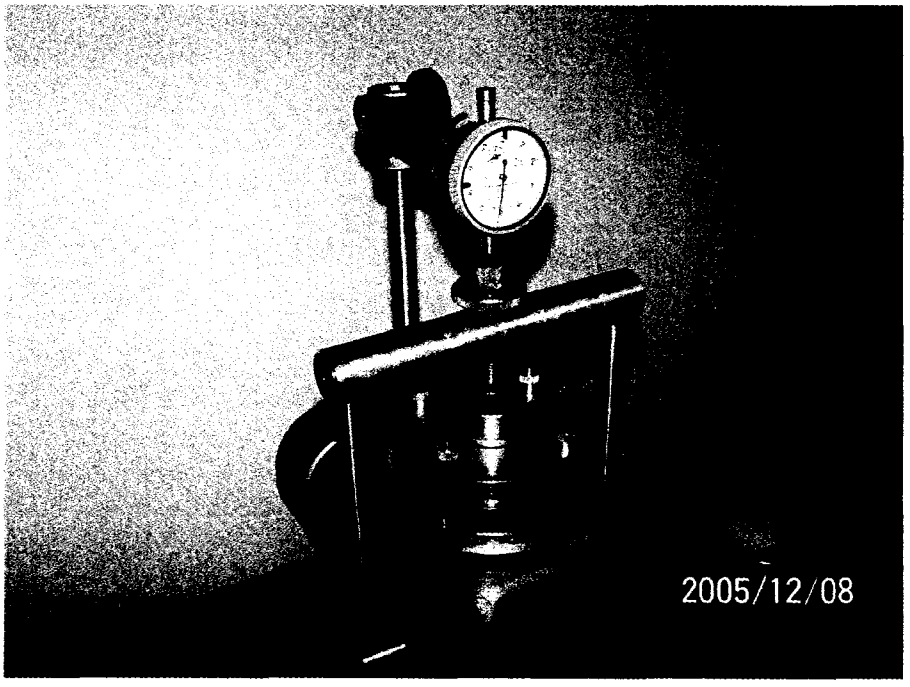

Figure 3.6: Preparation of LBF Samples : Loading Cell on the Front Loading Consolidation Frame

Chapter 4 : RESULTS AND ANALYSIS

4.1 Sample Height versus Time Results and Final Sample Conditions

Appendix A contains the sample height versus time graphs for all of the loading and unloading increments for the tests. Also the applied stress for each of the loading and unloading increments is indicated. As these graphs indicate, dial gauge readings were taken more frequently at the beginning of the increment (6-7 times a day) and then 1-2 times a day on days until the next increment. All dial gauge readings were converted to sample heights.

As the figures in Appendix A show, the loading/compression response for each test is distinctly different from the unloading/swelling response. For example, compare the response of loading/compression with unloading/swelling of test HB9 in Figure A.7. This indicates that there is significant hysteresis in the sample height between loading/compression and unloading/swelling. This

hysteresis is much more pronounced in the tests using $CaCl_2$ as the reservoir fluid as opposed to the tests using distilled water as the reservoir fluid. For example, compare the response of test HB9, which used distilled water (Fig. A.7), with the response of test HB11, which used 100 g/l $CaCl_2$ as the reservoir fluid (Fig. A.8).

Several loading and unloading increments were left on for extended time periods to examine the potential for longer term creep; for example the 663 kN/m^2 loading increment of test HB9 (Fig. A.7), the 2660 kN/m^2 loading increment of test HB11 (Fig. A.8), the 336 kN/m^2 loading increment of test HB12 (Fig. A.9), the 1326 kN/m^2 unloading increment of test HB13 (Fig. A.10) and the 165 kN/m^2 loading increment of test HB15 (Fig. A.12). As these figures show, long term creep is negligible for this material under these test conditions.

Figure 4.1 shows the vertical strain versus time for tests with distilled reservoir water (e.g. HB6 and HB9) and tests with 100 g/l $CaCl_2$ reservoir solution (e.g. HB11 and HB15) and test with 200 g/l $CaCl_2$ reservoir solution (e.g. HB16) during initial increments while samples were allowed to swell (see test matrix in Table 3.4) (Note that swelling corresponds to negative vertical strain). The figure shows that the samples with distilled water in the reservoir achieved swelling strains of about 20% under applied vertical stresses of about 55 kN/m^2 while the samples with 100 g/l or 200 g/l $CaCl_2$ solution in the reservoir achieved only about 6% to 10% swelling strain under essentially unrestrained conditions (Table

3.4 indicates that test HB20 with 200 g/l $CaCl_2$ solution in the reservoir achieved only about 6% strain, essentially the same as HB16). This indicates that swelling response of the LBF samples with distilled water in the reservoir is distinctly different from the LBF samples with 100 g/l or 200 g/l $CaCl_2$ solution in the reservoir. Also the swelling occurred rapidly in the samples with $CaCl_2$ solution in the reservoir as opposed to the samples with distilled water in the reservoir. Comparison of the HB11, HB15 and HB16 graphs shows that the samples with 200 g/l $CaCl_2$ solution in the reservoir achieved the lowest swelling strains (including HB20) at 6% while the sample with 100 g/l $CaCl_2$ solution in the reservoir achieved slightly higher swelling strains.

As described in section 3.6, the final height of the sample was measured and the oven-dry sample was weighted after the completion of each test. These values (i.e. final height and final dry weight of the test sample) have been used to calculate the key volume-mass parameters (i.e. Mass of Solid M_s (gr) and Dry Density ρ_d (Mg/m^3)) for the final conditions for each test. These parameters have been calculated for all of the test samples and are listed in Tables 4.1 and 4.2. The equations used for calculation of these parameters are provided in Appendix B.

4.2 Hydro-Mechanical Parameters for Loading and Unloading Increments

The values of vertical strain, void ratio (e), dry density (ρ_d), coefficient of volume compressibility (m_v), hydraulic conductivity (k), EMDD, bulk modulus (K) and water activity (a_w) for each loading and unloading increment of the tests have been calculated and are tabulated in Appendix C. The equilibrium height for each loading and unloading increment was used to calculate the vertical strain, dry density and EMDD for the increment. Hydraulic conductivity, bulk modulus and water activity values were not calculated for increments which did not reach an equilibrium height or a clearly identifiable t_{90} value. This section provides an evaluation of vertical strain, dry density, void ratio, hydraulic conductivity and EMDD. The equations used for calculation of bulk modulus and water activity are provided in Appendix D and these results are discussed in detail in section 4.4.

The equilibrium vertical strain for each increment is calculated as:

$$Vertical\ Strain = \frac{Initial\ sample\ height - Equilibrium\ sample\ height\ for\ each\ increment}{Initial\ sample\ height} \qquad (4.1)$$

Negative vertical strains correspond to swelling and positive vertical strain corresponds to compression.

By evaluating sample volume for each increment (based on equilibrium height), the dry density (ρ_d) for each increment can be calculated by using equation 4.2.

$$\rho_d = \frac{M_S}{V} \qquad (4.2)$$

where M_s = mass of solid (see Tables 4.1 and 4.2).

The void ratio (e) for each increment can be calculated as :

$$e = \frac{G_s \cdot \rho_w - \rho_d}{\rho_d} \qquad (4.3)$$

where G_s = specific gravity of bentonite-sand mixture (2.70);

ρ_d = dry density for each increment; and

ρ_w = density of water (1.0 Mg/m^3 used in these calculations);

The coefficient of volume compressibility (m_v) is calculated for an increment using the equation:

$$m_V = \frac{1}{1+e_0}\left(\frac{e_0 - e_1}{\sigma_1' - \sigma_0'}\right) \qquad (4.4)$$

where e_0 is the void ratio corresponding to σ_0', the initial effective stress for the increment, and e_1 is the void ratio corresponding to σ_1', the final effective stress for the increment (Craig 2004).

The t_{90} values (time to 90% consolidation) used for calculating the c_v values for the increments are determined using the square root of time graphical construction method (ASTM, 1998). For some of the square root of time versus sample height graphs t_{90} values could not be properly identified. As noted previously, the coefficient of consolidation and hydraulic conductivity values for those increments are not given in Appendix C. Figure 4.2 shows an example of a sample height versus square root of time graph.

The coefficient of consolidation c_v (m^2/yr) can be calculated using the equation (Craig 2004):

$$c_V = \frac{\left[0.848\left(d^2\right)\right]}{t_{90}} \qquad (4.5)$$

where d = length of the longest drainage path (m) (the average height of the sample during the increment divided by two); and

t_{90} = time to 90% consolidation (yrs).

Hydraulic conductivity k values (m/s) can be calculated for the increments using the equation (Craig 2004):

$$k = c_v \, m_v \, \gamma_w \qquad (4.6)$$

where c_v and m_v are as defined previously and γ_w is the unit weight of water (9.81 kN/m^3).

The EMDD is defined as the dry mass of montmorillonite divided by the volume occupied by the montmorillonite and the volume of voids present in the system (Kjartanson et al. 2005). The mass of the montmorillonite fraction per unit volume (m_m) is defined as (Kjartanson et al. 2005):

$$m_m = f_m \times f_c \times \rho_d \qquad (4.7)$$

The volume of the montmorillonite plus voids (V_m) per unit total volume is (Kjartanson et al 2005):

$$V_m = 1 - \left(\frac{(1 - f_c) \times \rho_d}{G_s \times \rho_w} \right) - \left(\frac{(1 - f_m) \times f_c \times \rho_d}{G_n \times \rho_w} \right) \qquad (4.8)$$

And so EMDD is:

$$EMDD = \frac{m_m}{V_m} \qquad (4.9)$$

where f_m = montmorillonite content of clay fraction (wt%/100) (0.8 in this research from Table 3.1);

f_c = clay content of sealing material (wt%/100) (0.5 in this research);

ρ_d = dry density for each increment (Mg/m^3);

G_n = specific gravity of non-montmorillonite particles in clays (2.65 in this research); and

G_s = specific gravity of aggregate particles (non-clay fraction) (2.65 in this research);

Substituting the above values and dry density for each increment into Eqns. 4.7, 4.8 and 4.9, EMDD can be calculated in Mg/m^3.

4.3 Comparison of Hydro-Mechanical Response of LBF under Different Loading/Wetting Paths [3]

This section compares the 1-D swelling/compression and hydraulic performance of LBF under different loading paths and different reservoir fluids. The relationships between EMDD, hydraulic conductivity and void ratio and applied vertical pressure have been compared in this section.

Dixon et al. (2002a) developed relationships between swelling pressure versus EMDD and hydraulic conductivity versus EMDD for bentonite clays with permeants of varying salinity. These relationships are shown in Figures 4.3 and 4.4. These results are from individual 1-D swelling pressure and hydraulic conductivity tests, respectively. These relationships have been included for comparison with the data generated in this research. It is important to note Dixon used solutions of NaCl as the saline permeant rather than $CaCl_2$. Moreover,

[3] Significant portions of this section have been drawn from:
Baumgartner et al. (2007) – Appendix C, Kjartanson and Batenipour. Light BackFill (LBF), Preliminary Results Of One-Dimensional Consolidation Testing On Bentonite Clay-Based Sealing Components Subjected To Two Pore-Fluid Chemistry Conditions, Ontario Power Generation Report

Chandler (2005) used the trendline relationships from Figure 4.3 in formulating material parameters for the preliminary compliance modelling.

4.3.1 Hydro-Mechanical Response of LBF under Different Loading Paths with Distilled Reservoir Water

The loading/compression and unloading/swelling responses for tests conducted following paths 1, 2a and 2b (see Table 3.4) are shown in Figure 4.5 plotted as the logarithm of the applied vertical pressure versus EMDD. The Dixon et al. (2002a) trendlines for fresh water and 100 g/l NaCl from Figure 4.3 have been superimposed on this figure. The figure shows that loading/compression trendlines for paths 1 and 2b, which allowed about 20% swelling prior to loading/compression, are virtually identical while the loading/compression trendline for path 2a, in which the samples were kept constrained prior to loading/compression, is above the other two paths. The unloading/swelling trendlines for paths 1 and 2b have about the same slope as the loading compression path trendlines, but the applied vertical pressures for the same EMDD value are significantly lower. As the figure shows, and also it was observed in section 4.1, the loading/compression response for each path is distinctly different from the unloading/swelling response. This indicates that there is significant hysteresis in the loading/compression and unloading/swelling paths. Insufficient unloading/swelling data were collected for path 2a to make a

definitive conclusion regarding this response. The figure also shows that the trendlines fit to the loading/compression data for paths 1, 2a and 2b tend to follow the trend of the Dixon et al. (2002a) trendline for fresh water.

The same hysteresis can be seen in Figure 4.6. This figure shows the hydraulic conductivity values for loading/compression and unloading/swelling for paths 1, 2a and 2b plotted as the logarithm of hydraulic conductivity versus EMDD. The Dixon et al. (2002a) trendlines for fresh water and 100 g/l NaCl from Figure 4.4 have been superimposed on this figure. The loading/compression hydraulic conductivity data for paths 1 and 2b have about the same slope as the unloading/swelling hydraulic conductivity data, but the hydraulic conductivity values for the same EMDD value are generally higher. This is because the amount of interconnected pore spaces in the loading/compression phase is likely higher than in the unloading/swelling phase. The hydraulic conductivity results are interpreted from 1-D compression tests in which soil fabric and thus interconnected porosity are significantly affected by the deformations, and not from hydraulic conductivity tests in which samples are rigidly restrained. The figure also shows that the trendlines for the loading/compression hydraulic conductivity data for paths 1 and 2b tend to follow the trend of the Dixon et al. (2002) trendline for fresh water.

Figure 4.7 shows the void ratio values for tests following path 1 (e.g. HB6 and HB8), path 1a (e.g. HB4) and path 2b (e.g. HB9) plotted as void ratio versus the

logarithm of applied vertical pressure. The two sets of tests for path 1 (HB6 and HB8) show a high level of repeatability of test response. The compression curves for all three paths tend to converge towards a narrow range of void ratio at stresses higher than 1100 KPa. These curves have similar shape with the curves developed by Miao 2004 (see Figs. 2.10 and 2.11). The flattening of the shape of void ratio versus logarithm of applied vertical pressure curves in the higher stress ranges is evident in Figure 4.7.

4.3.2 Hydro-Mechanical Response of LBF with Distilled Reservoir Water and 100 g/l $CaCl_2$ Reservoir Solution

Figure 4.8 compares the loading/compression and unloading/swelling responses for paths 1 and 3 plotted as the logarithm of applied vertical pressure versus EMDD. Distilled water was used as the reservoir fluid for path 1 while 100 g/l $CaCl_2$ solution was used as the reservoir fluid for path 3. Both these paths allowed swelling of samples up to 20% strain on water (or solution) uptake. The Dixon et al. (2002a) trendlines for fresh water and 100 g/l NaCl from Figure 4.3 have been superimposed on this figure. This figure shows that the loading/compression and unloading/swelling responses have distinctly different behaviour when 100 g/l $CaCl_2$ solution is used as the reservoir fluid as opposed to distilled water. The path 3 applied vertical pressures for the same EMDD value are substantially lower than the path 1 pressures, showing trends similar to

those described in section 2.4.1. The LBF samples exposed to 100 g/l $CaCl_2$ solution undergo significantly more compression, with significantly higher EMDD values for the same applied vertical pressures than the LBF samples exposed to distilled water.

The same behaviour between samples with distilled water in the reservoir and 100 g/l $CaCl_2$ solution in the reservoir can be seen in Figure 4.9. This figure shows the hydraulic conductivity values for loading/compression and unloading/swelling for paths 1 and 3 plotted as the logarithm of hydraulic conductivity versus EMDD. The Dixon et al. (2002a) trendlines for fresh water and 100 g/l NaCl from Figure 4.4 have been superimposed on this figure. Path 3 loading/compression and unloading/swelling hydraulic conductivity values are substantially higher than the path 1 hydraulic conductivity values for the same EMDD. This indicates that LBF samples exposed to 100 g/l $CaCl_2$ solution are more permeable than the LBF samples exposed to distilled water. Path 3 hydraulic conductivity values are generally higher than the Dixon et al. (2002a) trendline for 100 g/l NaCl.

The void ratio values for tests following path 1 (e.g. HB6) and path 3 (e.g. HB19) are shown in Figure 4.10 plotted as void ratio versus the logarithm of applied vertical pressure. The void ratio curve of path 1 is above the void ratio curve of path 3. The same behaviour was observed by Miao 2004 (see Figs. 2.10 and 2.11) and Castellanos et al. 2006 (see Figs. 2.16 and 2.17). Because test HB6

achieved the targeted 20% vertical strain, the sample had a void ratio of 1.45 at the beginning of the compression phase, higher than the initial, as-placed void ratio of 1.06 (see Table 3.3). On the other hand, test HB19 did not achieve the targeted 20% initial swelling, therefore the void ratio of 1.1 at the beginning of the loading phase for this test is close to the initial, as-placed void ratio of about one (see Table 3.3). The $CaCl_2$ solutions suppresses the thickness of diffuse double layers, therefore swelling strains are significantly lower. Figure 4.10 also shows that the void ratio curve of path 1 is steeper than the void ratio curve of path 3. As the stress decreases, the void ratio values for path 1 (HB6) increases significantly as opposed to path 3 (HB19). It is important to note that these curves have similar shape with the curves developed by Miao 2004 (see Fig. 2.10).

4.3.3 Hydro-Mechanical Response of LBF under Different Loading Paths with 100 g/l $CaCl_2$ Reservoir Solution

The loading/compression and unloading/swelling responses for paths 3, 4 and 5 are shown on Figure 4.11 plotted as the logarithm of applied vertical pressure versus EMDD. The 100 g/l $CaCl_2$ solution was used as the reservoir fluid for all the paths. The samples for path 5 also used 100 g/l $CaCl_2$ solution as the mixing fluid. Paths 3 and 5 allowed for swelling on fluid uptake while for path 4 the sample was kept constrained during fluid uptake. Figure 4.11 shows that the

general trends of behaviour for paths 3, 4 and 5 are similar. Path 5 loading/compression and unloading/swelling trendlines are above the trendlines for paths 3 and 4. This indicates that the use of 100 g/l $CaCl_2$ solution as the mixing fluid (path 5) decreases the amount of compression on loading and increases the sample rebound on unloading. Path 4 has the highest compression on loading and for a given EMDD, the lowest applied vertical pressure on unloading. This may be due to the inability of diffuse double layers to form and expand around the clay mineral path 4 test because of the restricted initial swelling. As described in Section 4.3.1, the hysteresis is evident between loading/compression and unloading/swelling in Figure 4.11.

The same behaviour can be seen in Figure 4.12. The figure shows the hydraulic conductivity values for loading/compression and unloading/swelling for paths 3, 4 and 5 plotted as the logarithm of the hydraulic conductivity versus EMDD. The figure shows that the trends in hydraulic conductivity for paths 3, 4 and 5 are very similar. The path 5 hydraulic conductivity values for both loading/compression and unloading/swelling paths are slightly lower than the other two paths. The use of 100 g/l $CaCl_2$ solution as the mixing fluid (path 5) tended to decrease the hydraulic conductivity for the loading/compression path, particularly at the higher range of EMDD and make LBF less permeable.

Figure 4.13 shows the void ratio values for path 3 (e.g. HB19), path 4 (e.g. HB14) and path 5 (e.g. HB15) plotted as void ratio versus the logarithm of applied

vertical pressure. The curves for paths 3, 4 and 5 are similar. Path 4 test sample (HB14) is seen to be more compressible than the other two path tests at stresses greater than 0.06 MPa. The flattening of the curves at higher stresses is also evident in this figure.

4.3.4 Hydro-Mechanical Response of LBF with 100 g/l $CaCl_2$ Solution Reservoir and 200 g/l $CaCl_2$ Solution Reservoir

The loading/compression and unloading/swelling responses for paths 3 and 6 are shown in Figure 4.14 plotted as the logarithm of applied vertical pressure versus EMDD. The 100 g/l $CaCl_2$ solution was used as the reservoir fluid for path 3 while 200 g/l $CaCl_2$ solution was used as the reservoir fluid for path 6. The figure shows that the loading/compression and unloading/swelling trendlines for paths 3 and 6 are similar. This indicates that increasing the $CaCl_2$ concentration in the reservoir fluid from 100 g/l to 200 g/l does not have a significant impact on the loading/compression and unloading/swelling responses of the LBF.

The same behaviour can be seen in Figure 4.15. The figure shows the hydraulic conductivity values for loading/compression and unloading/swelling for paths 3 and 6 plotted as the logarithm of hydraulic conductivity versus EMDD. The figure shows that the hydraulic conductivity trendlines for path 6 do not differ significantly from the path 3 trendlines. Increasing the $CaCl_2$ concentration in the

reservoir fluid from 100 g/l to 200 g/l does not appear to have a significant impact on the hydraulic performance of the LBF.

Figure 4.16 shows the void ratio values for path 3 (e.g. HB19) and path 6 (e.g. HB20) plotted as void ratio versus the logarithm of applied vertical pressure. The void ratio curve for path 6 does not differ significantly from the path 3 curve. This effect is not as significant as that shown by Miao 2004 (see Figs. 2.10 and 2.11). This may be due to higher initial void ratios at the beginning of compression for the Miao (2004).

The loading/compression and unloading/swelling results for all paths are summarized on Figures 4.17 and 4.18 (applied vertical pressure versus EMDD) and 4.19 and 4.20 (hydraulic conductivity versus EMDD). Figures 4.17 and 4.18 again highlight the distinct differences in response when $CaCl_2$ is used as the reservoir fluid as opposed to distilled water. Also, path 4 is seen to give the lowest applied vertical pressure for a given EMDD for both the loading/compression and unloading/swelling paths. Figure 4.19 shows that the hydraulic conductivity values derived from the loading increments show similar trends to the trendlines shown by Dixon et al. (2002a); i.e. hydraulic conductivity values decrease with increasing EMDD and generally increase with increasing salinity. Figure 4.20 shows that the hydraulic conductivity values determined from the unloading/swelling response of the compression tests gave generally

low values and the trends that were apparent in Figure 4.19 are not apparent in this figure.

4.4 Bulk Modulus and Water Activity

The bulk elastic properties of a material determine how much it will compress under a given amount of external pressure. The bulk modulus (K) of a substance is a measure of the substance's resistance to uniform compression. The bulk modulus value is an input requirement for FLAC for elastic modelling. This section compares the relationships between bulk modulus and vertical strain for distilled water reservoir (paths 1, 2a and 2b) and different $CaCl_2$ solutions reservoirs (paths 3, 4, 5 and 6). Chandler (2005) used existing relationships between swelling pressure and EMDD from Dixon et al. (2002a) (see Fig. 4.3) to define relationships between bulk modulus and vertical strain for sealing materials. The trendline of Chandler's relationship for LBF in the range of fresh water to 60 g/l NaCl conditions has been included for comparison with the data generated in this research. The relationships between water activity and EMDD are also compared for paths 3, 4, 5 and 6 in this section. The values of bulk modulus (K) and water activity (a_w) for each loading and unloading increment of the tests are included in Appendix C. The equations used for calculation of bulk modulus and water activity are given in Appendix D.

Figure 4.21 shows the bulk modulus values versus vertical strain for loading/compression paths for all the reservoir fluids. The Chandler (2005) trendline is superimposed on this figure. The figure shows the significant difference in bulk modulus values for the loading/compression path when different $CaCl_2$ solutions are used as the reservoir fluid as opposed to distilled water. The $CaCl_2$ solution bulk modulus values for the same vertical strain are lower than the distilled water values. As indicated from previous sections, the LBF samples with $CaCl_2$ reservoir solutions have lower resistance to compression than the LBF samples exposed to distilled water. This observation shows that the presence of saline pore fluid ($CaCl_2$ in this research) makes the LBF more compressible than in the presence of distilled water.

The loading/compression and unloading/swelling path bulk modulus values for all tests are summarized in Figure 4.22. The unloading/swelling path bulk modulus values generally tend to trend below the loading/compression path values.

Figure 4.23 shows the water activity values for loading/compression for all the reservoir fluids. The trendlines show that for a given reservoir fluid, as EMDD increases, the water activity value decreases. These trends are similar to those shown in Kjartanson et el. (2003a, c). Moreover, trendlines for tests using $CaCl_2$ reservoir solutions are above the trendline for tests using distilled reservoir water. According to this graph, the LBF samples with EMDD values less than 1.50 Mg/m^3 and saturated with $CaCl_2$ solution, would have a_w values greater than the

0.96 threshold value. Interestingly, the 100 g/l constrained (path 4) test gives the highest water activity values for a given EMDD (even higher than the water activity values for the tests conducted with 200 g/l reservoir fluid).

4.5 Analytical Modelling

In this section, the interaction between HCB (inner material) and LBF (outer material) in a hypothetical emplacement room sealing system is modelled using a two-material axisymmetric linear elastic analytical model. The situation modelled is illustrated in Figure 4.24. The assumption has been made that inner and outer boundaries are rigidly fixed and incompressible (Chandler 2005). In this scenario, the inner rigid boundary could represent a used fuel container and the outer rigid boundary could represent the emplacement room wall. It must be realized that while this geometry could not be installed in an in-room configuration as shown, the arrangement may be a possible configuration for an in-floor borehole container emplacement method (see Fig. 1.3a) (The diameter of the borehole in this case would be in the order of 1.87 m (Kjartanson et al. 2003a)). The results of the modelling give some insight into HCB/LBF interactions.

The model results represent the long term condition once the HCB and LBF have saturated and generated their full swelling pressures. As described earlier, the

expected long term condition in an emplacement room is swelling of the HCB and compression of the LBF. The assumption has been made that the LBF is compressing 10% (vertical strain = 10%). The radial stress, mean stress, displacement and water activity in the HCB and LBF in the emplacement room were computed using the analytical model equations listed in Appendix E. The analytical solution for the modelling has been drawn from Chandler 2005, Appendix B, Numerical Modelling of the Stress and Displacement of Emplacement Room Swelling-Clay Material, Ontario Power Generation report.

The inner material (HCB) properties are drawn from Baumgartner et al. (2007) – HCB6 test results, Appendix A, Preliminary Results of One-Dimensional Consolidation Testing on Bentonite Clay-Based Sealing Components Subjected to Two Pore-Fluid Chemistry Conditions, Ontario Power Generation Report. For test HCB6, the HCB was tested in the presence of 75 g/l $CaCl_2$ solution. The derived data for HCB6 has been drawn from Baumgartner et al. (2007) and is shown in Table 4.5. The swelling pressure of HCB was taken as the applied pressure required to recompress the sample height to the original height (i.e. 7.94 MPa) (ASTM D4546) and the bulk modulus (K) used for the modelling was determined from the constrained modulus value (M) for this increment using the equation (Bardet 1997):

$$K = \frac{M}{3}\frac{(1+v)}{(1-v)} \qquad (4.10)$$

HCB properties (i.e. swelling pressure and bulk modulus) are shown on Figure 4.24. Poisson's ratio (v) was arbitrarily selected to be 0.3.

Four different LBF conditions have been used as an outer material in the analytical modelling. These four conditions are represented by the compression phase in paths 3, 4, 5 and 6. The bulk modulus values of the LBF for these paths have been drawn from Figure 4.21 by assuming that vertical strain is equal to 10%. The swelling pressure of LBF is assumed to be equal to the applied vertical pressure at the vertical strain of 10% and has been drawn from Figure 4.25. Figure 4.25 also shows an example of the swelling pressure for Path 4 (e.g. HB14). LBF properties (i.e. swelling pressure and bulk modulus) are included in Table 4.3. As with the HCB, Poisson's ratio (v) was arbitrarily selected to be 0.3.

Figures 4.26, 4.27, 4.28 and 4.29 show the analytical results (the radial stress, mean stress and displacement) for paths 3, 4, 5 and 6, respectively. As Figures 4.26a to 4.29a show, the mean stress (swelling pressure) in the HCB decreased relative to the initial as-placed value. Because HCB is a high swelling pressure material compared to the LBF (relative to the initial as-placed value), it expanded. Conversely, the LBF is a low swelling pressure material and has relatively low bulk modulus value. Therefore it compressed and its volume decreased, so the mean stress increased. The two materials are in equilibrium when the radial stress and displacement values in HCB and LBF are equal at the location where

they are in contact. Comparison of Figures 4.26b to 4.29b shows that the displacement in paths 3, 4, 5 and 6 are quite similar. In addition, the four plots indicate that the radial stress for the inner portion of the HCB, including that in contact with the container (i.e. inner rigid boundary), is positive (i.e. tensile stress occurs in the radial direction in this region). This is likely a result of the assumption that LBF and HCB are behaving as elastic materials.

Figures 4.30 and 4.31 show a summary of analytical results at the container surface. Figures 4.30 and 4.31 show the radial stress and mean stress values versus LBF swelling pressure and LBF bulk modulus values at the container surface for paths 3, 4, 5, and 6, respectively.

The water activity values in the HCB and the LBF for the same LBF paths are tabulated in Table 4.4. These water activity values correspond to the equilibrium condition after the HCB has expanded and the LBF has compressed, and were calculated using equation E.13 from Appendix E. The a_w for HCB is in the range from 0.990 to 0.992 and for LBF is in the range of 0.996 to 0.998. These water activity values are greater than the 0.96 threshold value.

Property	Test Number *						
	HB2	HB3	HB4	HB6	HB7	HB8	HB9
Final sample height (mm)	7.48	11.12	7.77	10.14	8.11	7.79	11.11
Sample volume (cm^3)	14.7	21.8	15.3	19.9	15.9	15.3	21.8
Mass of water (gr)	5.7	12.4	6.5	11.2	6.4	6.8	13.2
Total Mass of Solid + Mass of Salt (gr)	24.5	25.1	25.2	25.9	25.1	25.1	25.1
Total Dissolved Solid TDS (g/l)	0	0	0	0	0	0	0
Water Density ρ_w (Mg/m^3)	0.998	0.998	0.998	0.998	0.998	0.998	0.998
Density of Solution ρ_l (Mg/m^3) (Fig. B.2)							
Percent mass of the solute to the solution C_m (%) (Eqn. B.5)	0	0	0	0	0	0	0
Specific Gravity Gs	2.7	2.7	2.7	2.7	2.7	2.7	2.7
Specific Gravity of Solids to Solution G's (Eqn. B.6c)							
Bulk Water Content W (Eqn. B.8)	0.23	0.49	0.26	0.43	0.25	0.27	0.53
Gravimetric Water Content W_w (Eqn. B.18)							
Gravimetric Solution Content W_l (Eqn. B.19)							
Mass of Solid M_s (gr) (Eqn. B.16)	**24.5**	**25.1**	**25.2**	**25.9**	**25.1**	**25.1**	**25.1**
Dry Density ρ_d (Mg/m^3) (Eqn. B20)	**1.67**	**1.15**	**1.66**	**1.30**	**1.58**	**1.64**	**1.15**

* see test matrix in Table 3.4

Table 4.1: The volume-mass parameters for final conditions for the distilled water test samples

Property	Test Number *							
	HB11	HB12	HB13	HB14	HB15	HB16	HB19	HB20
Final sample height (mm)	7.52	7.65	7.71	7.31	7.49	7.46	7.68	7.25
Sample volume (cm^3)	14.8	15	15.1	14.3	14.7	14.7	15.1	14.2
Mass of water (gr)	5.7	5.9	6.2	5.7	5.7	5.2	6.0	5.2
Total Mass of Solid + Mass of Salt (gr)	26.6	26.0	25.7	26.1	26.0	26.6	26.2	26.8
Total Dissolved Solid TDS (g/l)	100	100	100	100	100	200	100	200
Water Density ρ_w (Mg/m^3)	0.998	0.998	0.998	0.998	0.998	0.998	0.998	0.998
Density of Solution ρ_l (Mg/m^3) (Fig. B.2)	1.08	1.08	1.08	1.08	1.08	1.15	1.08	1.15
Percent mass of the solute to the solution C_m (%) (Eqn. B.5)	9.28	9.28	9.28	9.28	9.28	17.36	9.28	17.36
Specific Gravity Gs	2.7	2.7	2.7	2.7	2.7	2.7	2.7	2.7
Specific Gravity of Solids to Solution G's (Eqn. B.6c)	2.50	2.50	2.50	2.50	2.50	2.34	2.50	2.34
Bulk Water Content W (Eqn. B.8)	0.21	0.23	0.24	0.22	0.22	0.2	0.23	0.19
Gravimetric Water Content W_w (Eqn. B.18)	0.22	0.23	0.25	0.22	0.22	0.21	0.24	0.2
Gravimetric Solution Content W_l (Eqn. B.19)	0.24	0.26	0.27	0.25	0.25	0.25	0.26	0.24
Mass of Solid M_s (gr) (Eqn. B.16)	**26.0**	**25.4**	**25.1**	**25.6**	**25.4**	**25.5**	**25.5**	**25.7**
Dry Density ρ_d (Mg/m^3) (Eqn. B20)	**1.77**	**1.69**	**1.66**	**1.78**	**1.73**	**1.74**	**1.69**	**1.80**

* see test matrix in Table 3.4

Table 4.2: The volume-mass parameters for final conditions for the $CaCl_2$ solution test samples

LBF Condition	Swelling Pressure (Mpa)	Bulk Modulus (Mpa)	Poisson's Ratio
Path 3	0.25	1.192	0.3
Path 4	0.15	0.628	0.3
Path 5	0.21	1.794	0.3
Path 6	0.20	1.586	0.3

Table 4.3: The LBF properties for analytical modelling

LBF Condition	Water Activity	
	HCB	LBF
Path 3	0.991	0.996
Path 4	0.992	0.998
Path 5	0.990	0.996
Path 6	0.990	0.996

Table 4.4: Water Activity Values for HCB and LBF from analytical modelling

	Vertical Stress (Mpa)	Vertical Strain (%)	Void Ratio	Dry Density (Mg/m^3)	EMDD (Mg/m^3)	1-D Constrained Modulus (Mpa)
start	1.01	0%	0.859	1.474	1.285	
1	0.97	-13%	1.098	1.306	1.118	
2	1.99	-11%	1.060	1.330	1.141	56
3	4.10	-6%	0.970	1.391	1.201	48
4	**7.94**	**0%**	0.865	1.469	1.280	**72**
5	15.82	5%	0.772	1.546	1.359	157
6	7.94	4%	0.791	1.530	1.342	729
7	3.99	2%	0.831	1.497	1.308	179
8	1.95	-2%	0.891	1.449	1.259	62
9	1.02	-5%	0.956	1.401	1.211	27
10	1.98	-5%	0.951	1.405	1.215	352
11	4.04	-3%	0.908	1.436	1.247	93
12	7.94	1%	0.840	1.489	1.300	110
13	15.94	5%	0.774	1.544	1.357	219

Table 4.5: HCB6 Derived Data (Baumgartner et al. 2007)

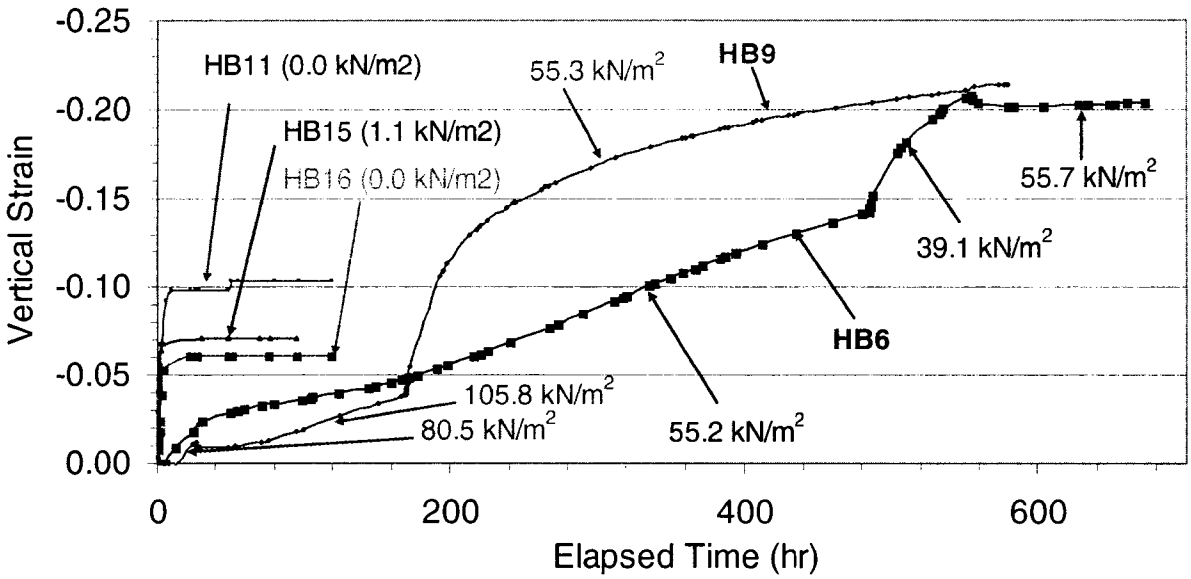

Figure 4.1: Strain versus Time for Tests with Distilled Reservoir Water (HB6 and HB9) and Tests with 100g/l $CaCl_2$ Reservoir Solution (HB11 and HB15) and Test with 200g/l $CaCl_2$ Reservoir Solution (HB16)

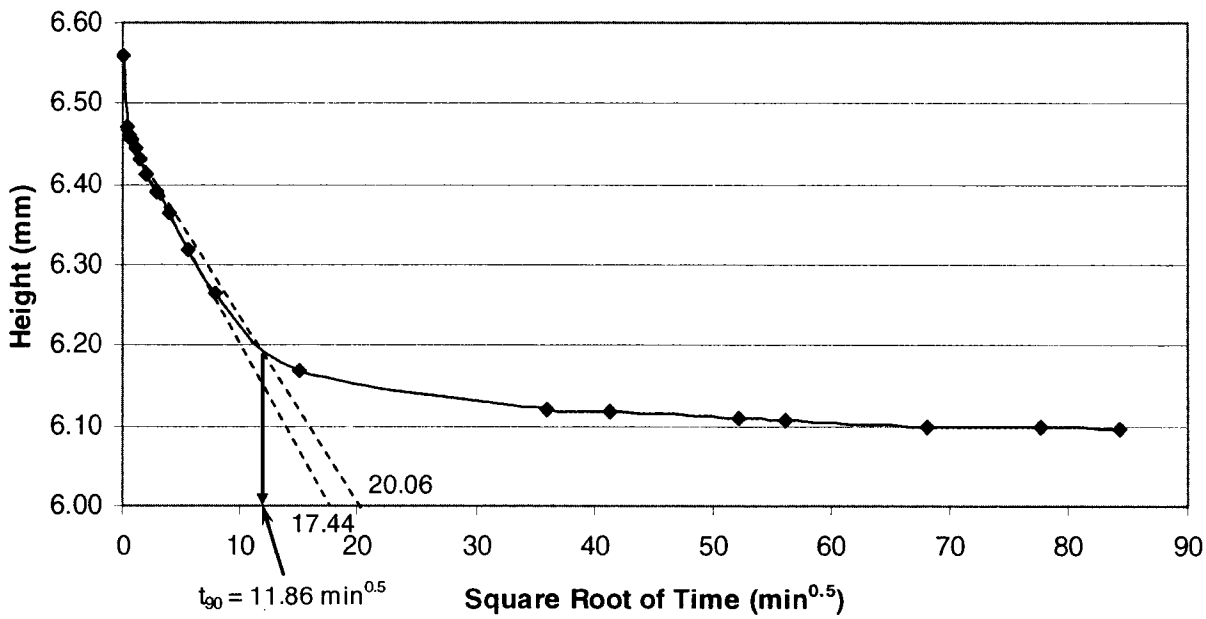

Figure 4.2: Example Sample Height versus Square Root of Time Graph: This Increment is from Test HB 14 with an Applied Stress of 2673 KN/m^2 on the Loading Path

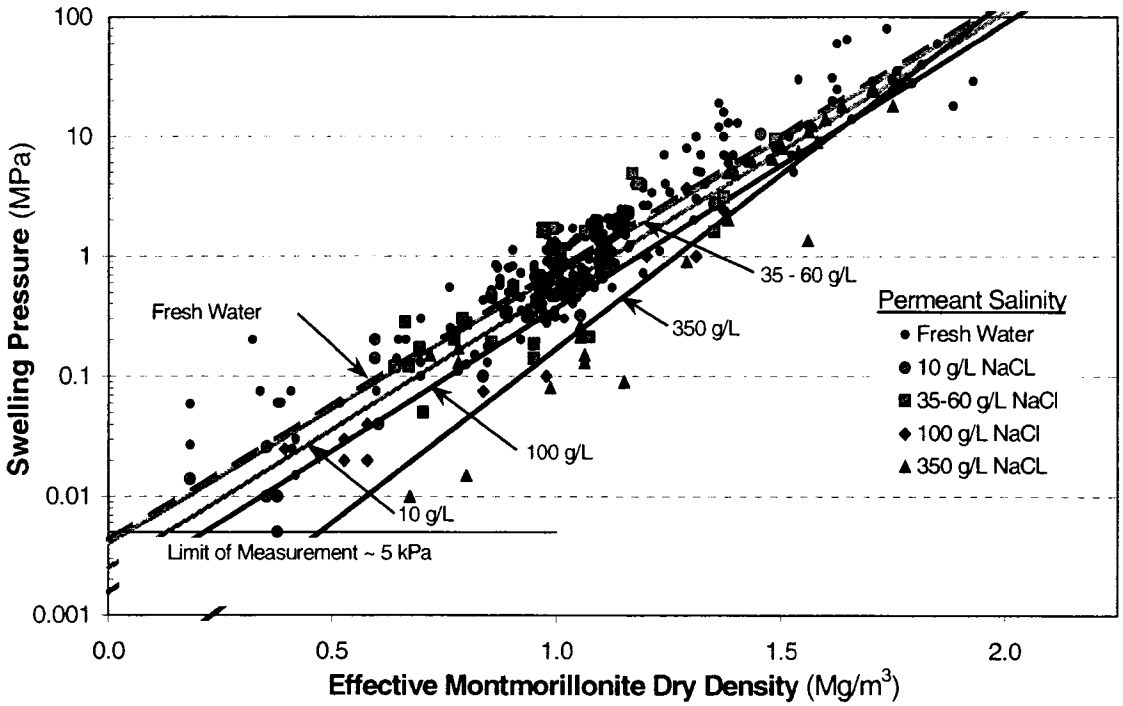

Figure 4.3: Relationship between Swelling Pressure and EMDD for Bentonite Clays with Varying Salinities (after Dixon et al. 2002a)

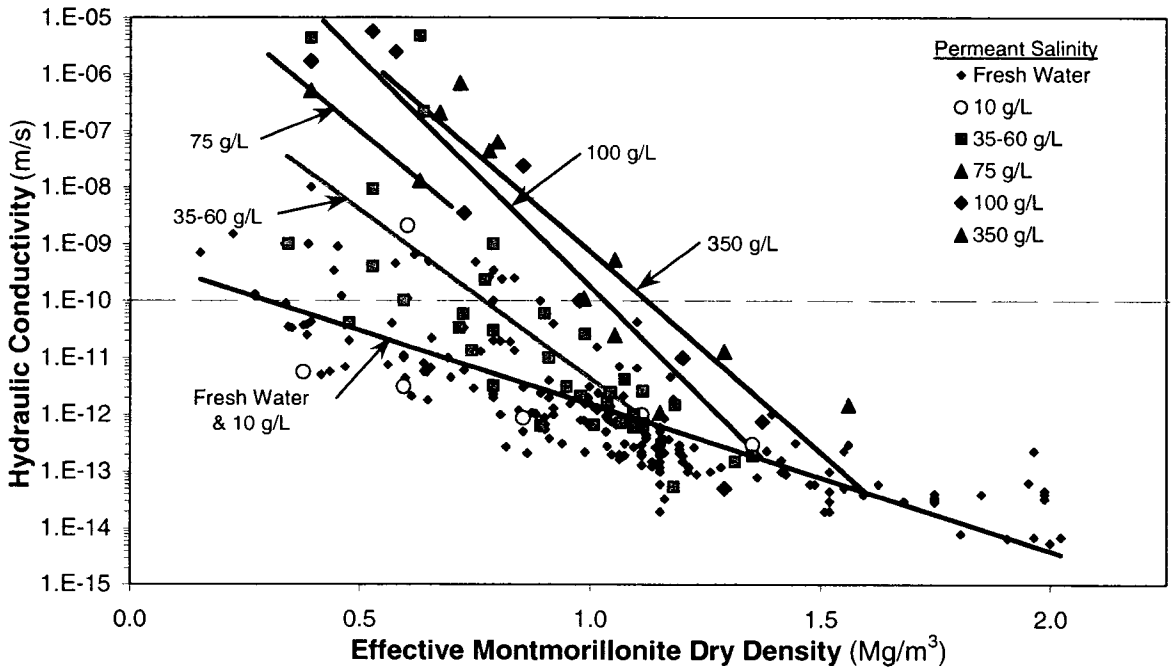

Figure 4.4: Relationship between Hydraulic Conductivity and EMDD in Bentonite clays with Varying Salinities (after Dixon et al. 2002a)

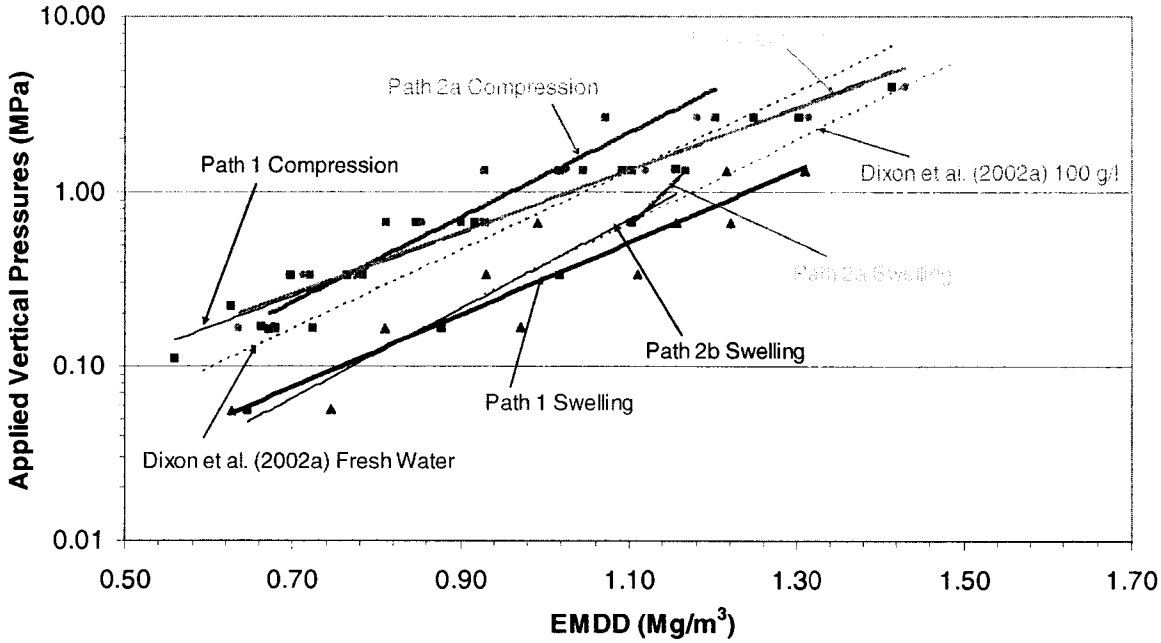

Figure 4.5: Applied Vertical Pressure versus EMDD for Paths 1, 2a and 2b

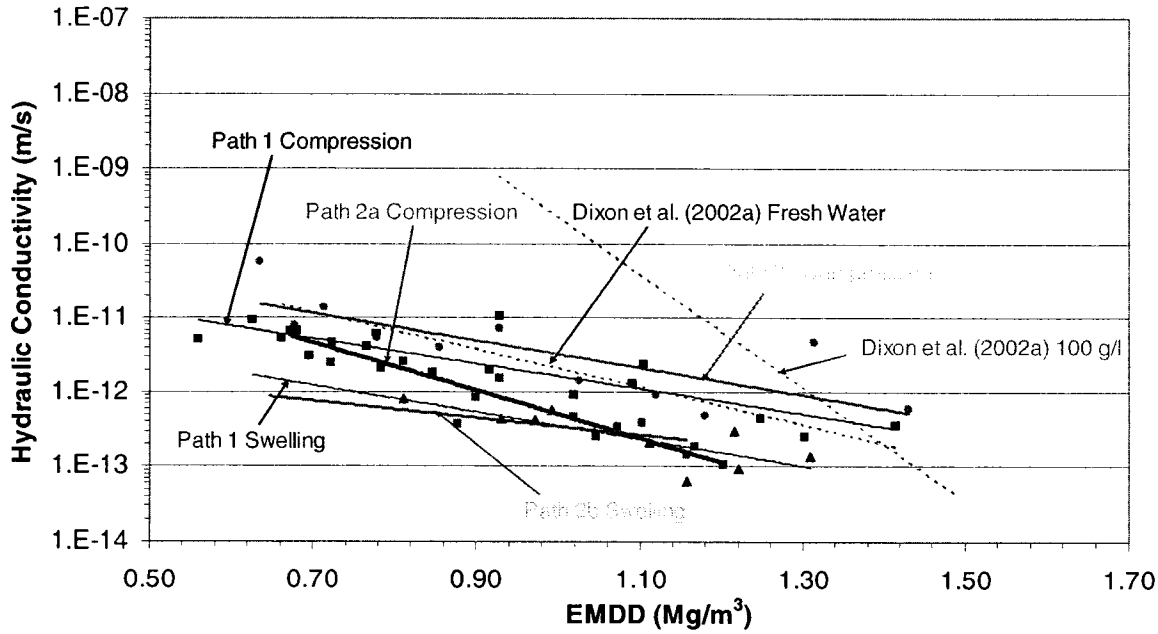

Figure 4.6: Hydraulic Conductivity versus EMDD for Paths 1, 2a and 2b

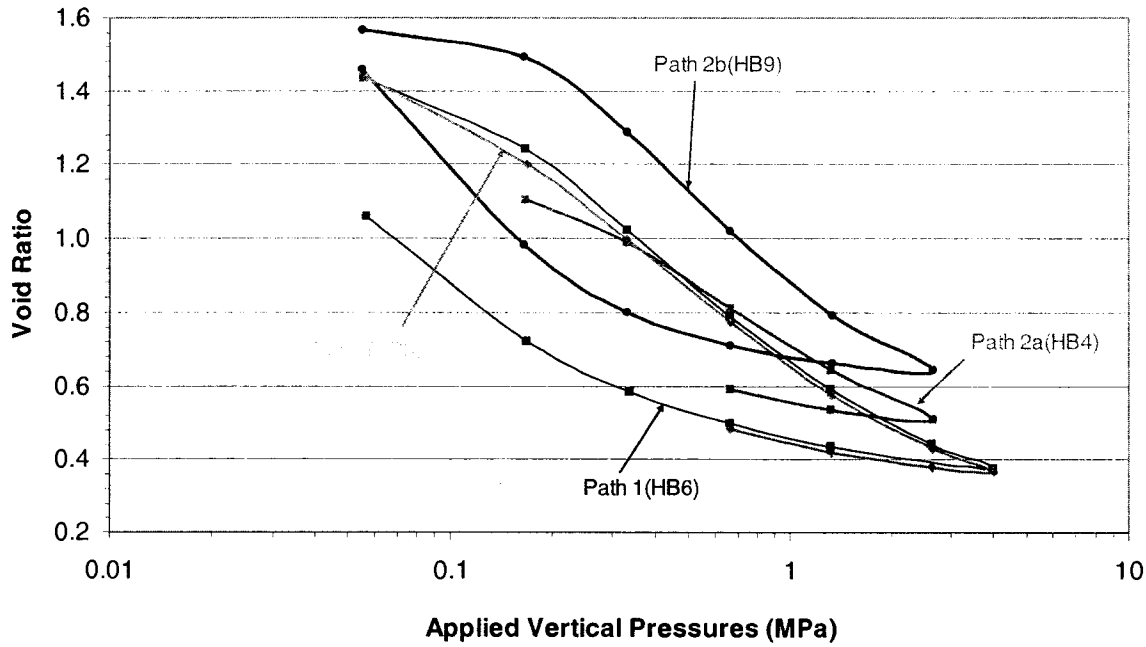

Figure 4.7: Void Ratio versus Applied Vertical Pressure for Paths 1, 2a and 2b

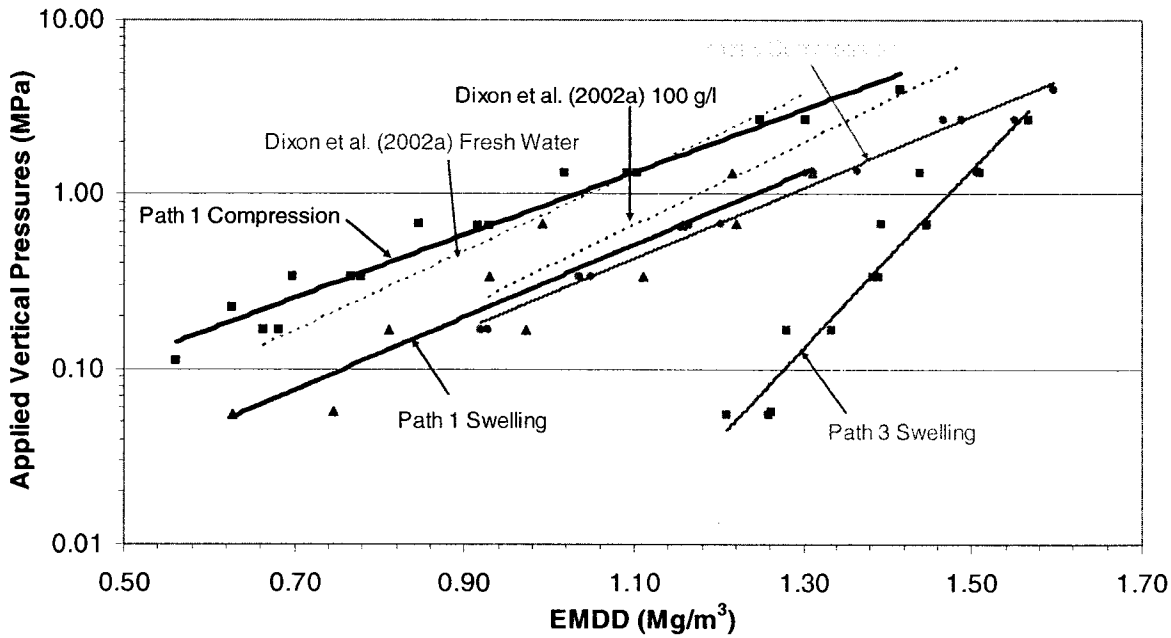

Figure 4.8: Applied Vertical Pressure versus EMDD for Paths 1 and 3

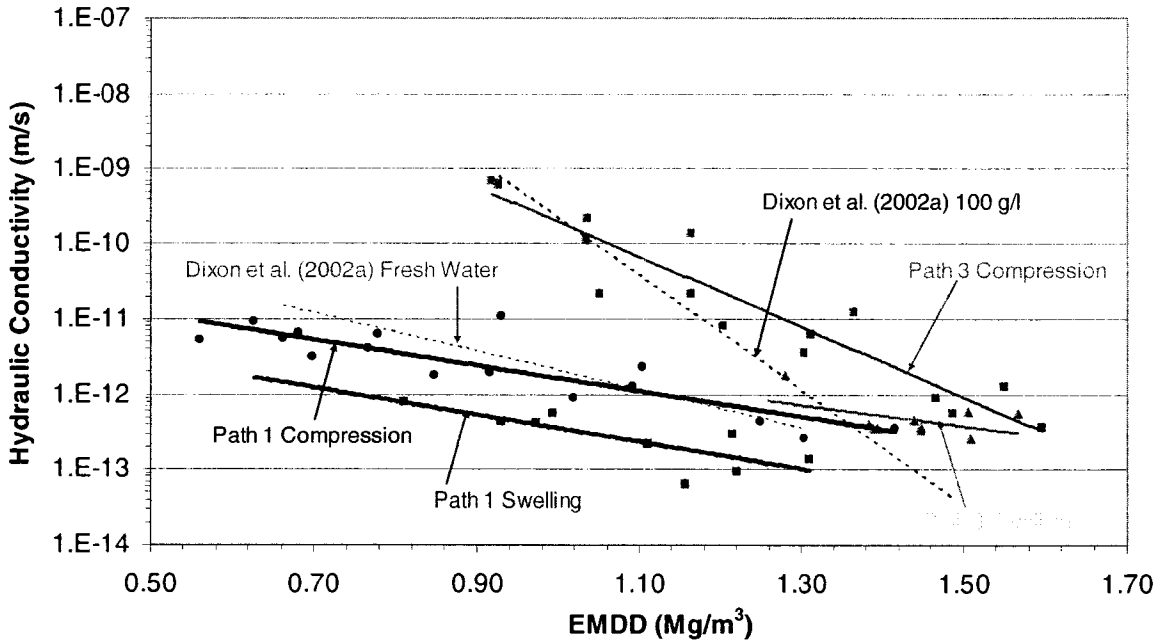

Figure 4.9: Hydraulic Conductivity versus EMDD for Paths 1 and 3

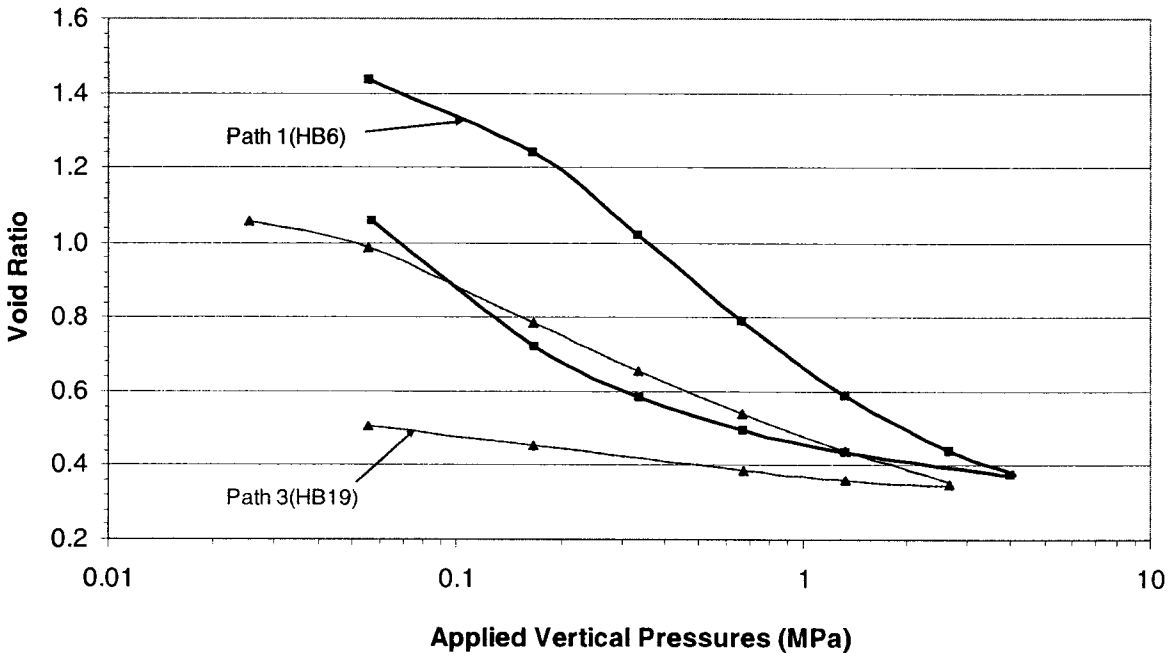

Figure 4.10: Void Ratio versus Applied Vertical Pressure for Paths 1 and 3

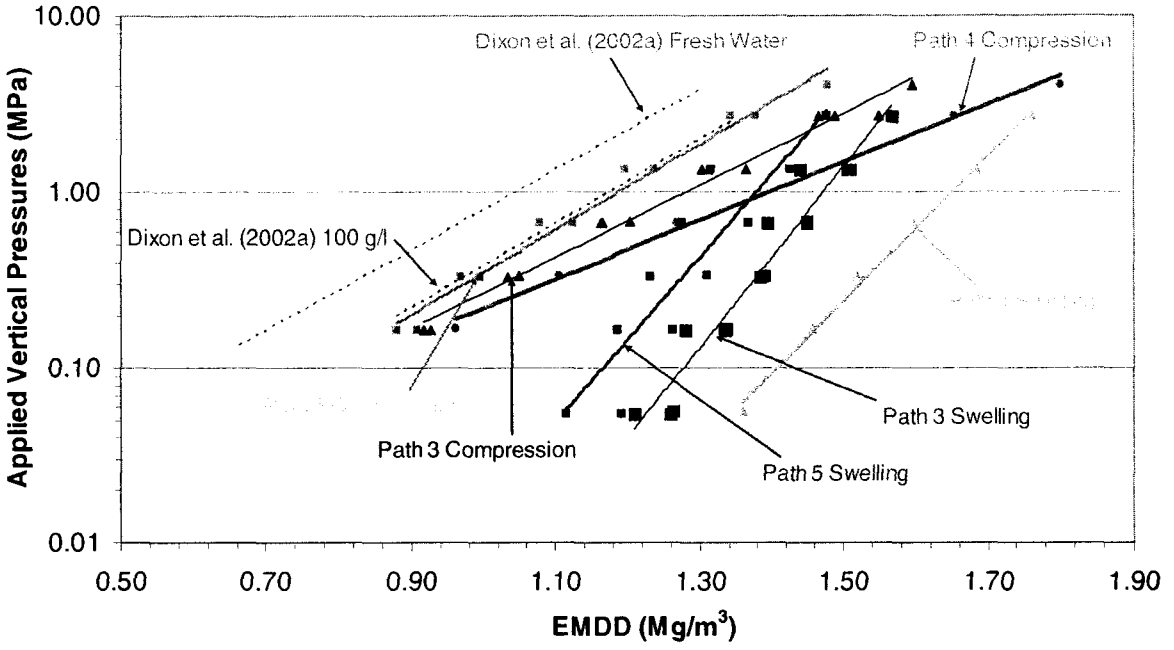

Figure 4.11: Applied Vertical Pressure versus EMDD for Paths 3, 4 and 5

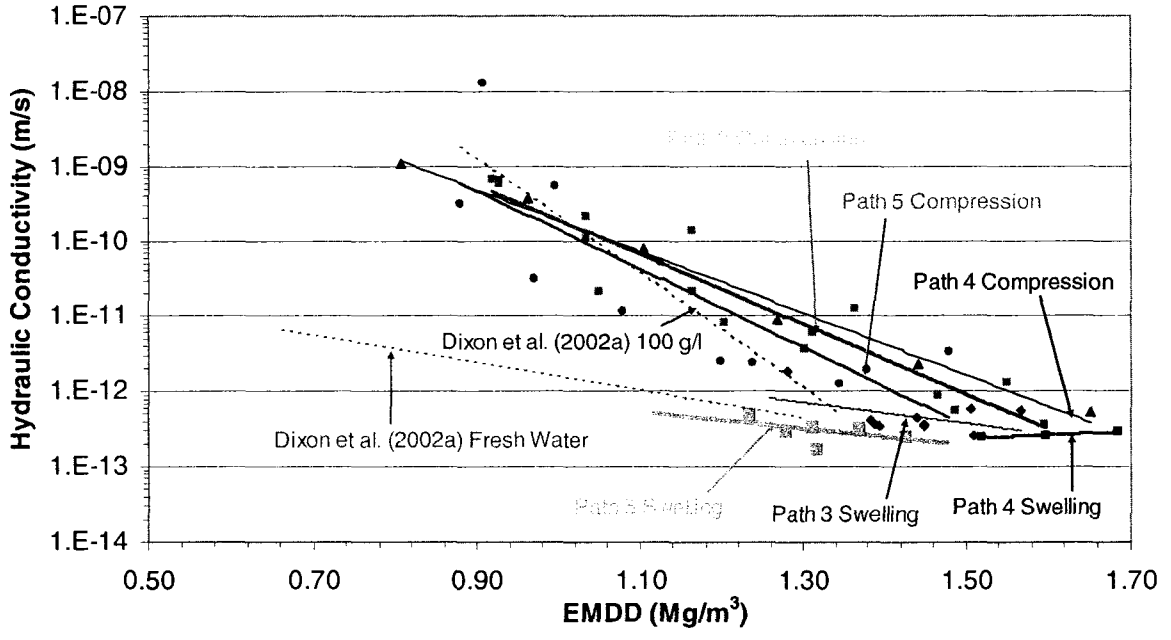

Figure 4.12: Hydraulic Conductivity versus EMDD for Paths 3, 4 and 5

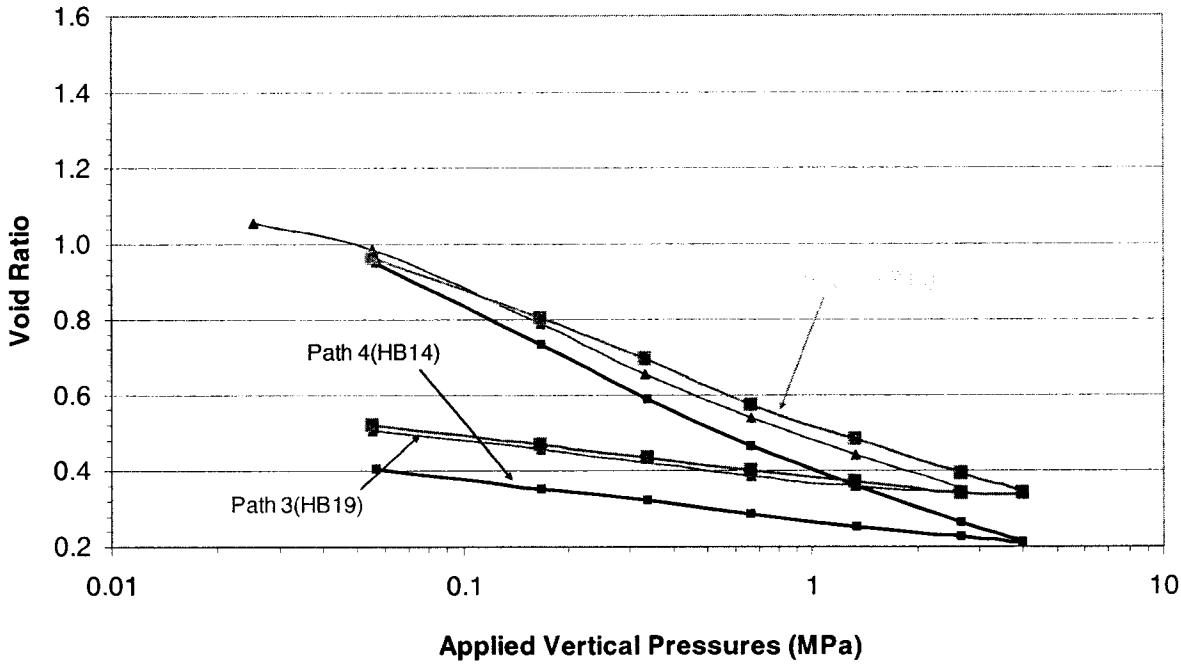

Figure 4.13: Void Ratio versus Applied Vertical Pressure for Paths 3, 4 and 5

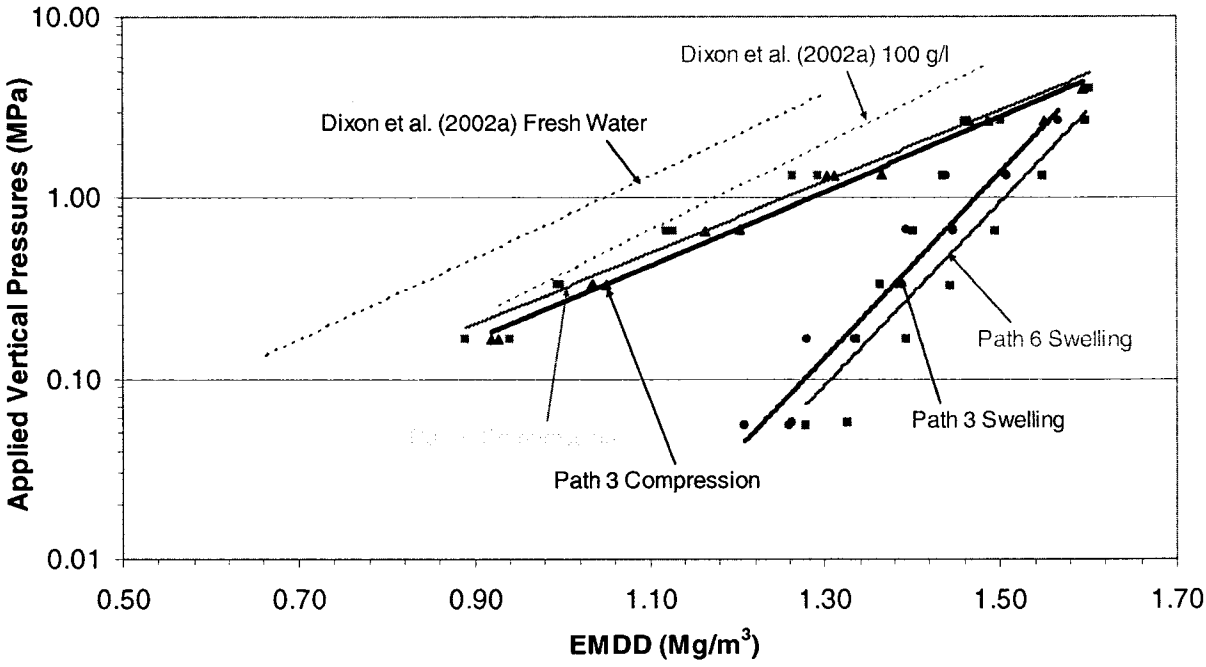

Figure 4.14: Applied Vertical Pressure versus EMDD for Paths 3 and 6

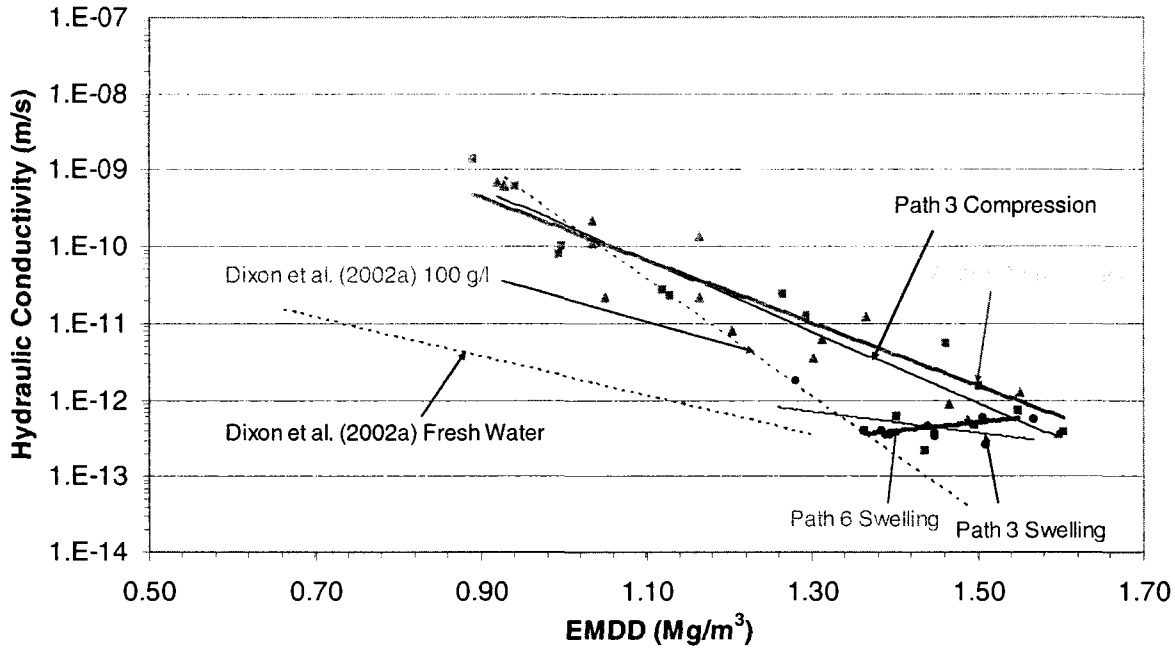

Figure 4.15: Hydraulic Conductivity versus EMDD for Paths 3 and 6

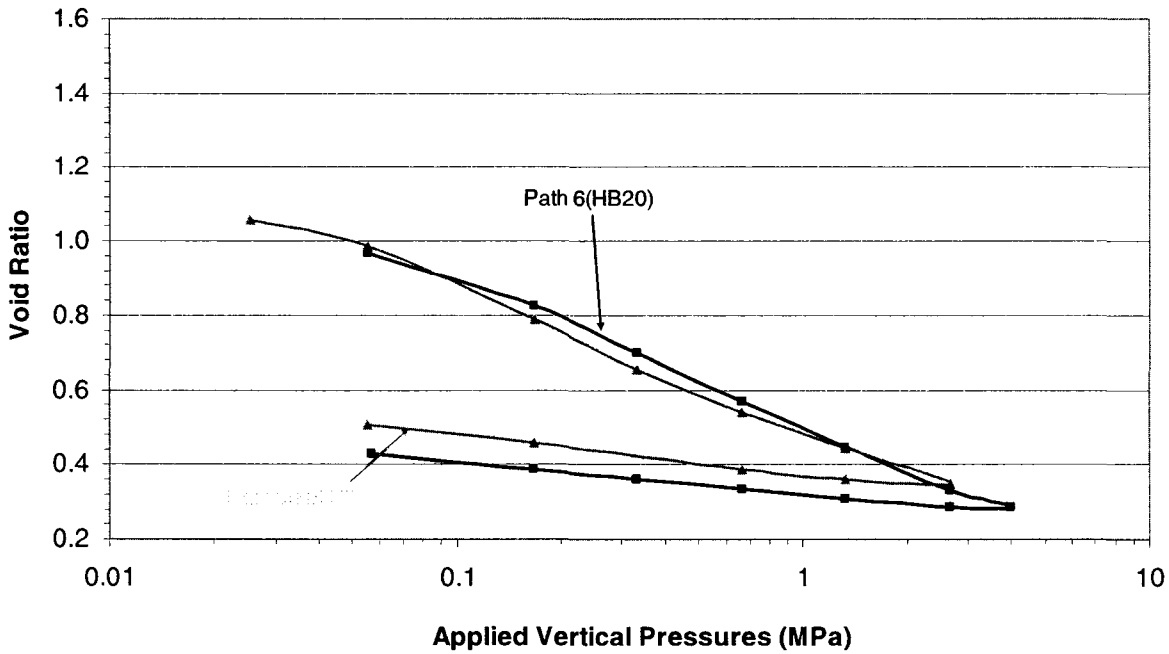

Figure 4.16: Void Ratio versus Applied Vertical Pressure for Paths 3 and 6

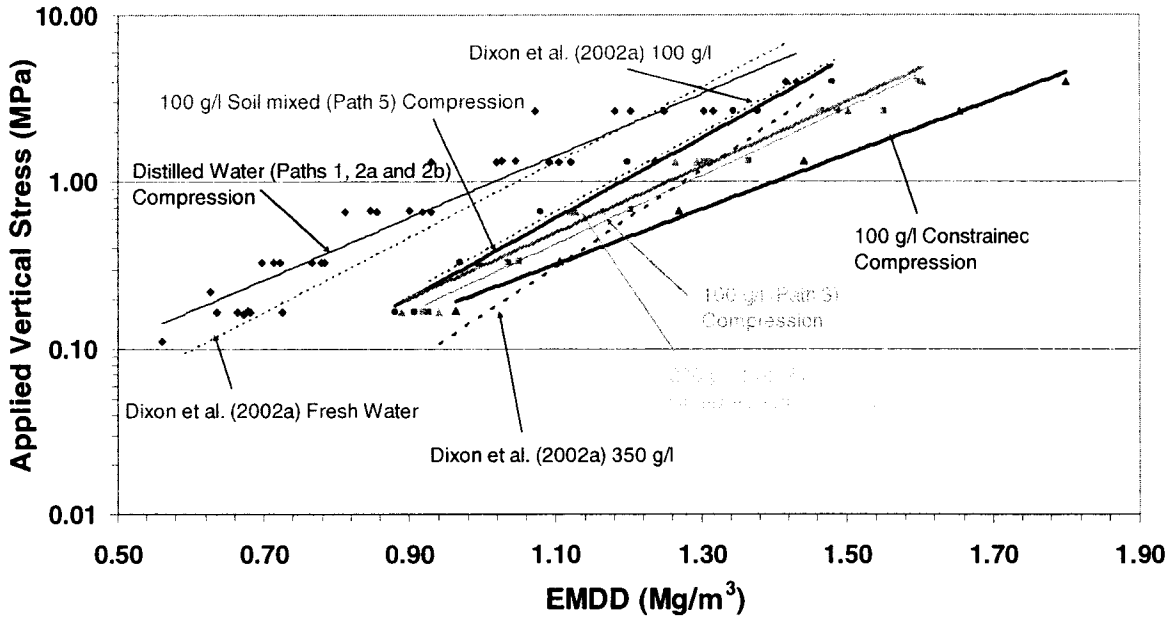

Figure 4.17: Applied Vertical Pressure versus EMDD for all Loading/Compression Path Data

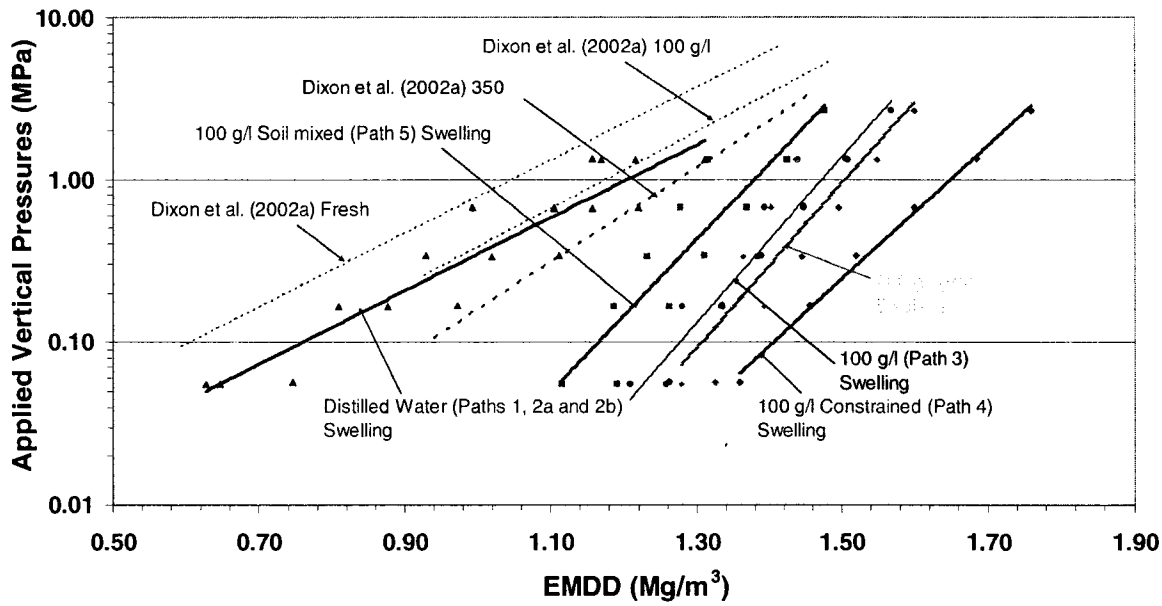

Figure 4.18: Applied Vertical Pressure versus EMDD for all Unloading/Swelling Path Data

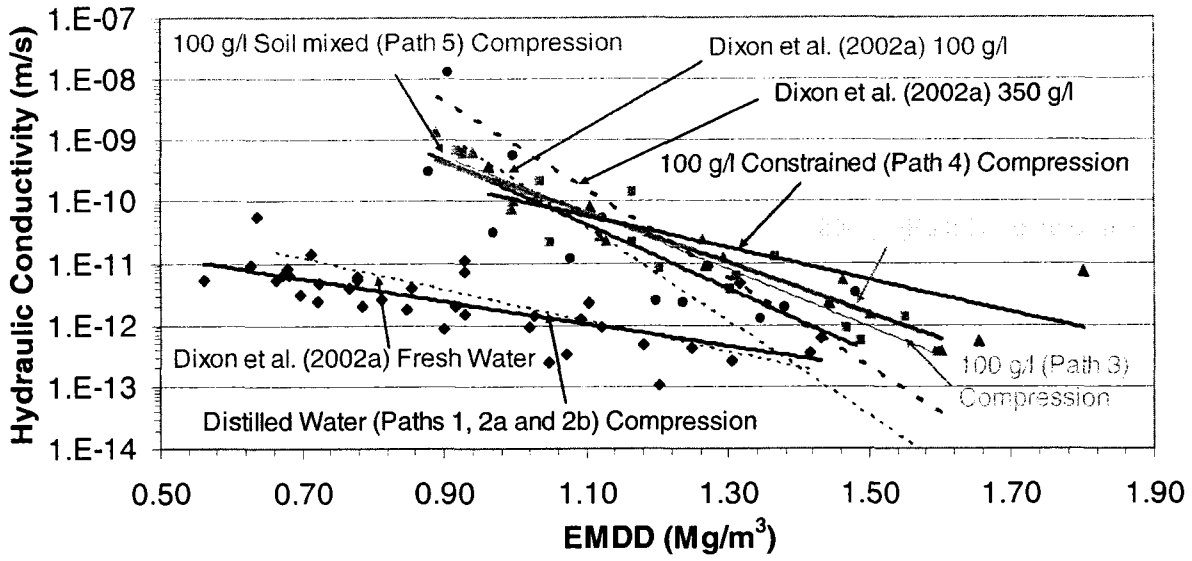

Figure 4.19: Hydraulic Conductivity versus EMDD for all Loading/Compression Path Data

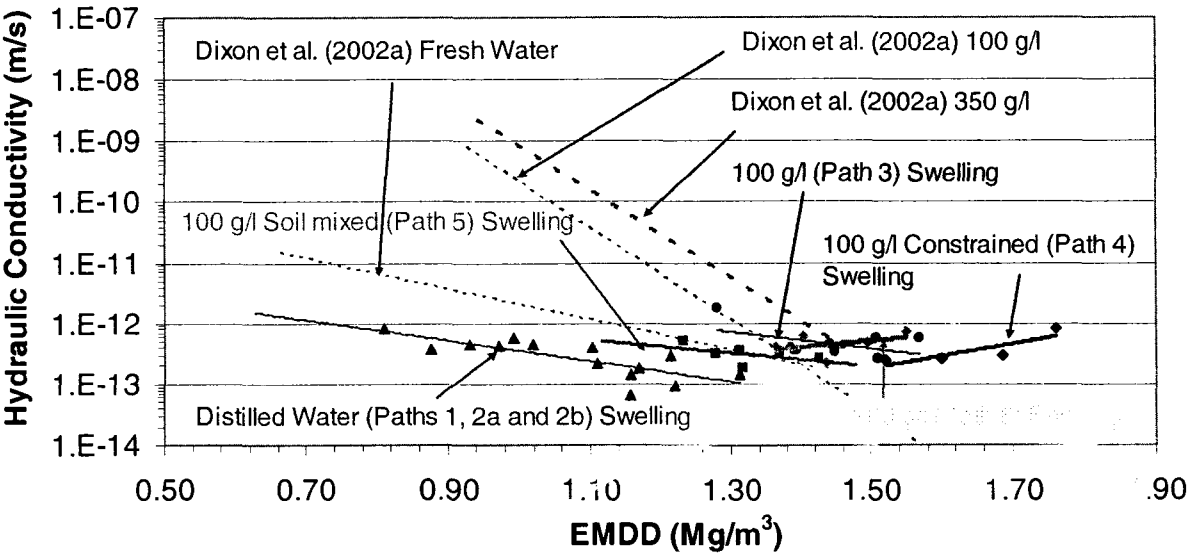

Figure 4.20: Hydraulic Conductivity versus EMDD for all Unloading/Swelling Path Data

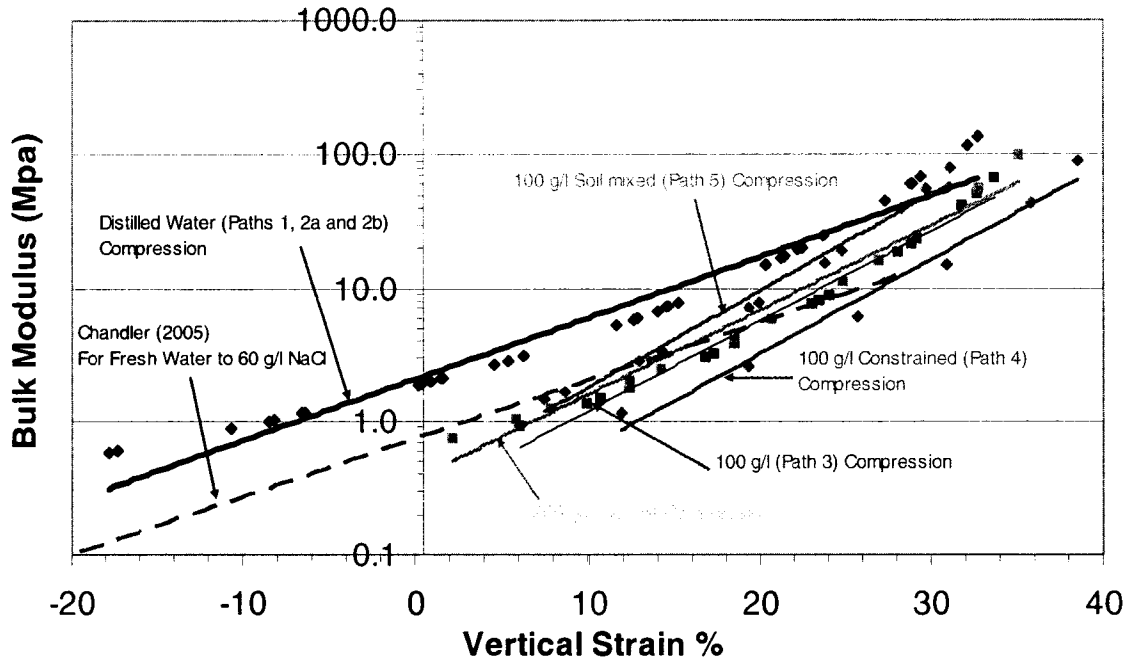

Figure 4.21: Bulk Modulus versus Vertical Strain for Loading/Compression for all Reservoir Fluids

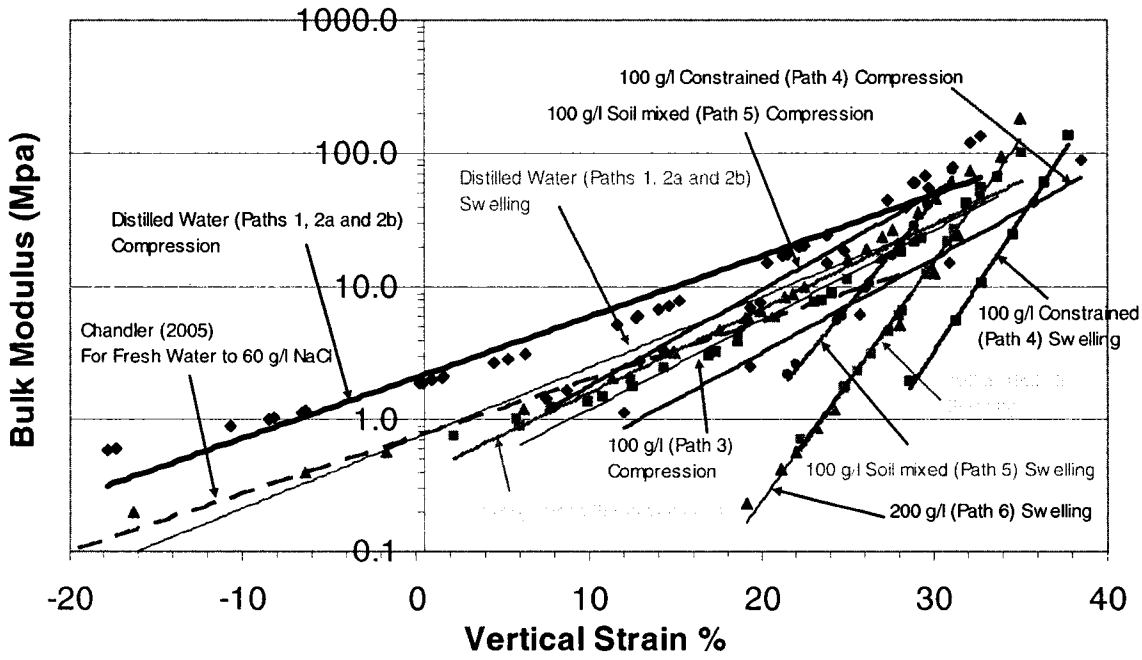

Figure 4.22: Bulk Modulus versus Vertical Strain for Loading/Compression and Unloading/Swelling for all Reservoir Fluids

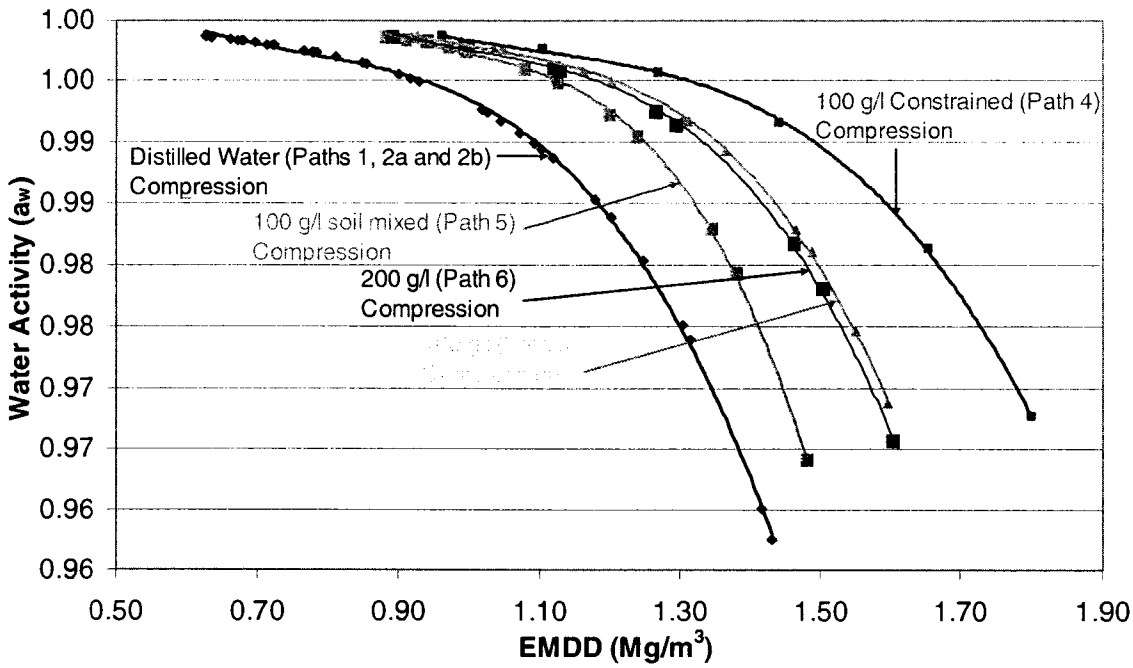

Figure 4.23: Water Activity versus EMDD for Loading/Compression for all Reservoir Fluids

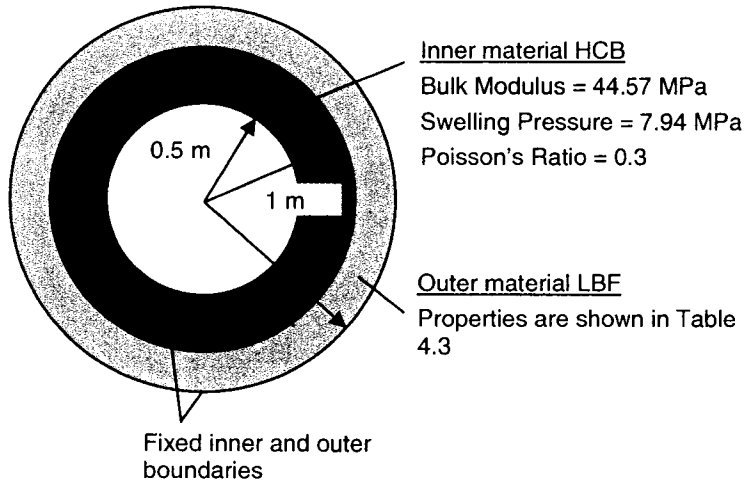

Figure 4.24: Illustration of the Axisymmetric Two-Material Linear-Elastic Model (Revised from Chandler 2005)

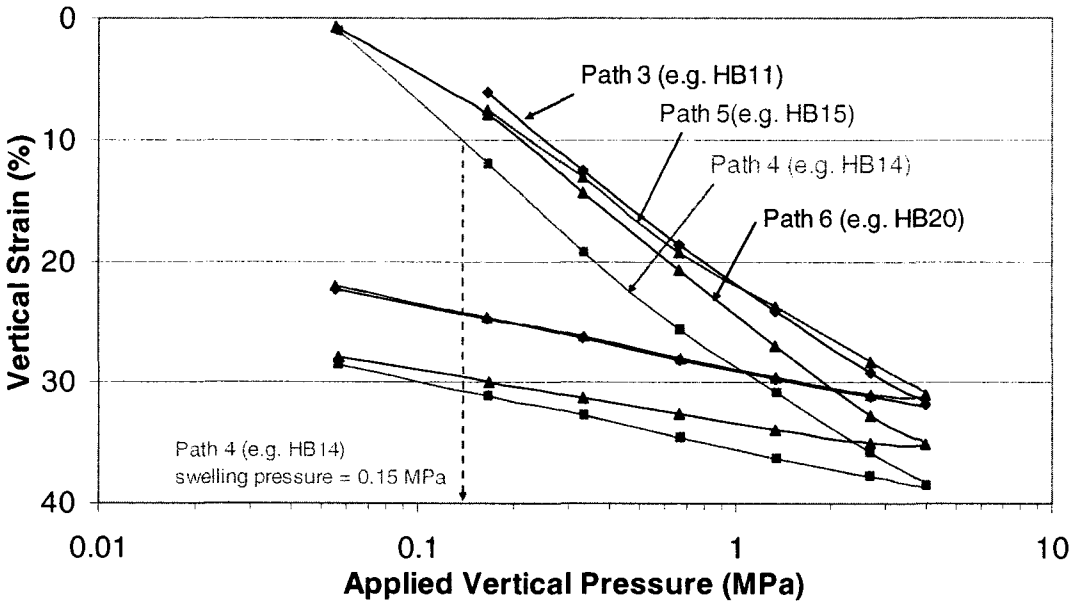

Figure 4.25: Vertical Strain versus Applied Vertical Pressure for Paths 3, 4, 5 and 6

a)

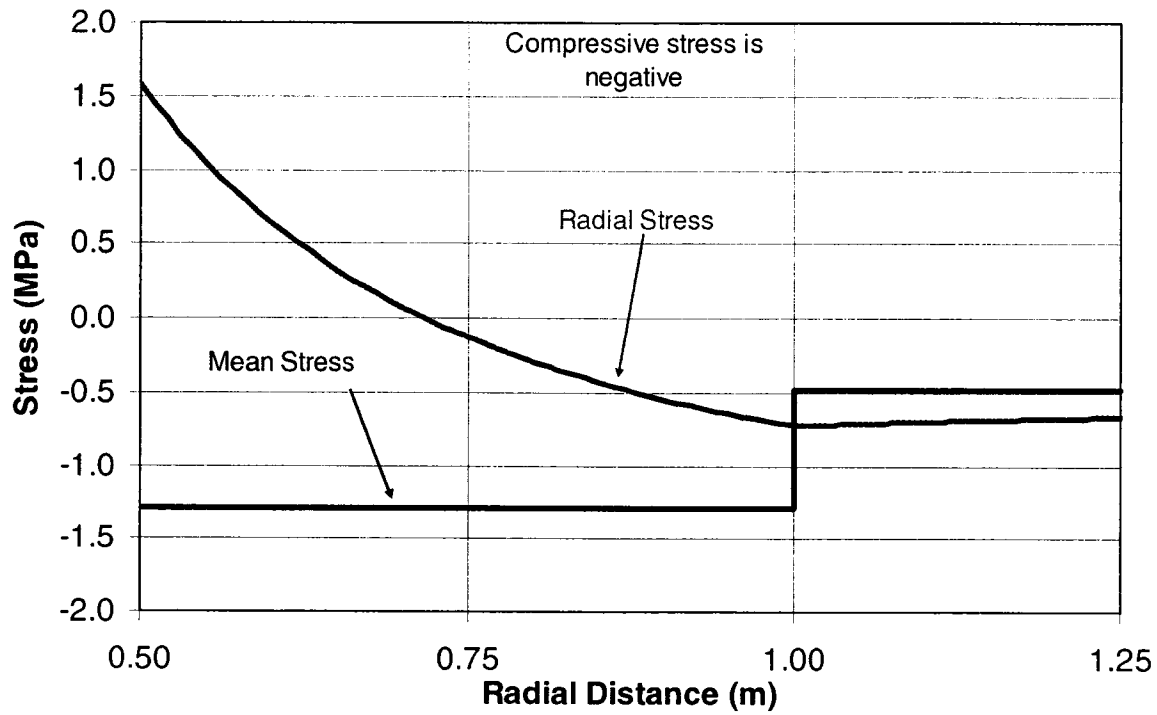

b)

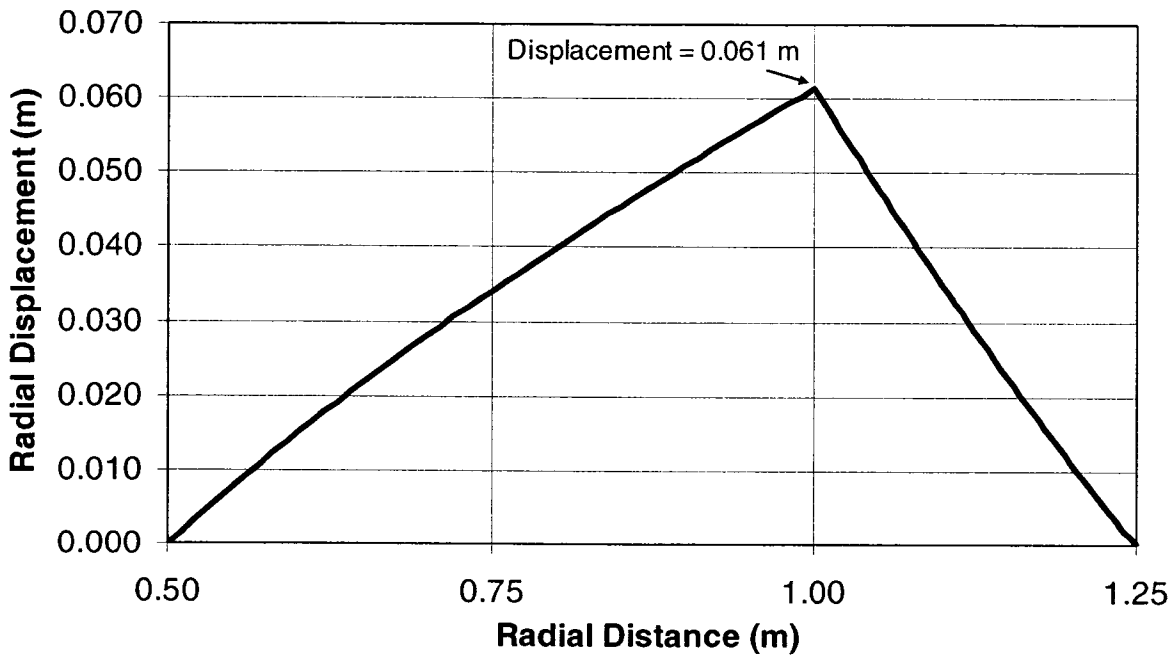

Figure 4.26: Axisymmetric Linear-Elastic Analytical Model for Path 3 a)Radial and Mean Stress, b)Radial Displacement

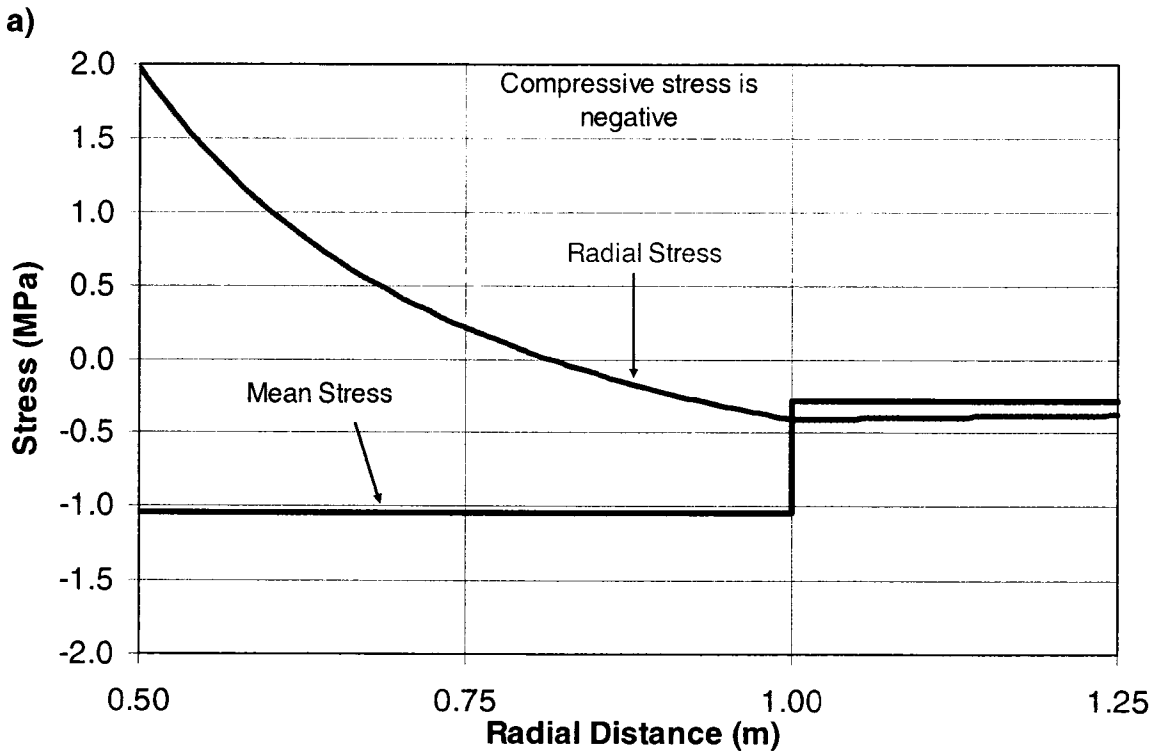

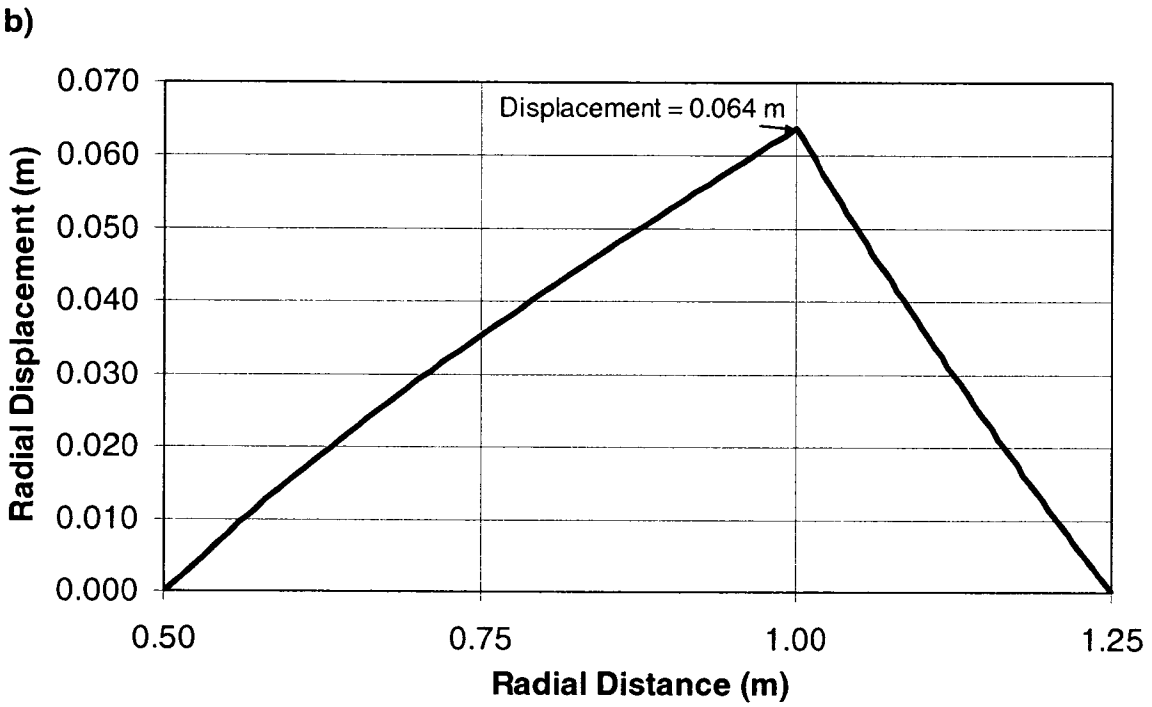

Figure 4.27: Axisymmetric Linear-Elastic Analytical Model for Path 4 a)Radial and Mean Stress, b)Radial Displacement

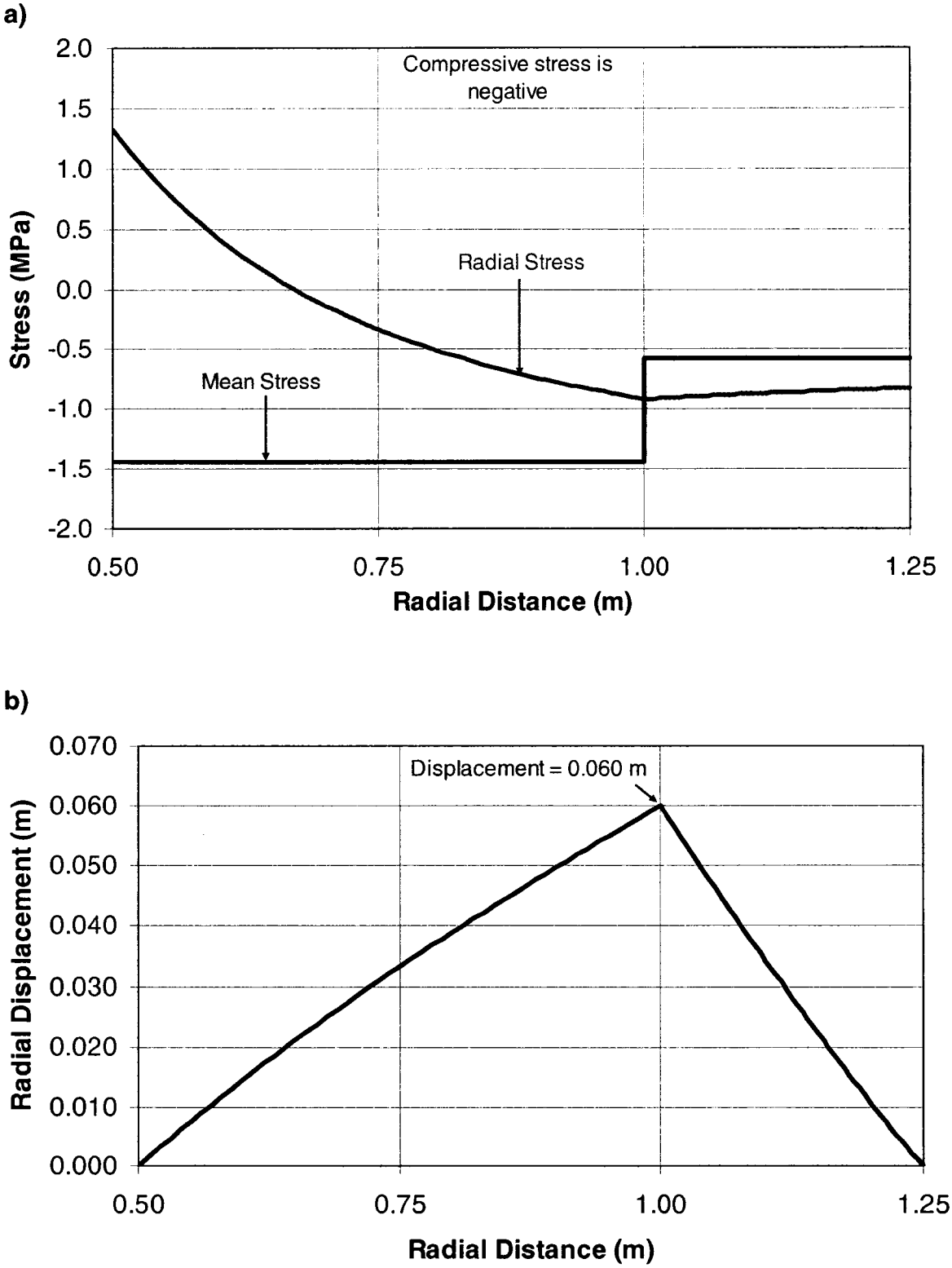

Figure 4.28: Axisymmetric Linear-Elastic Analytical Model for Path 5 a)Radial and Mean Stress, b)Radial Displacement

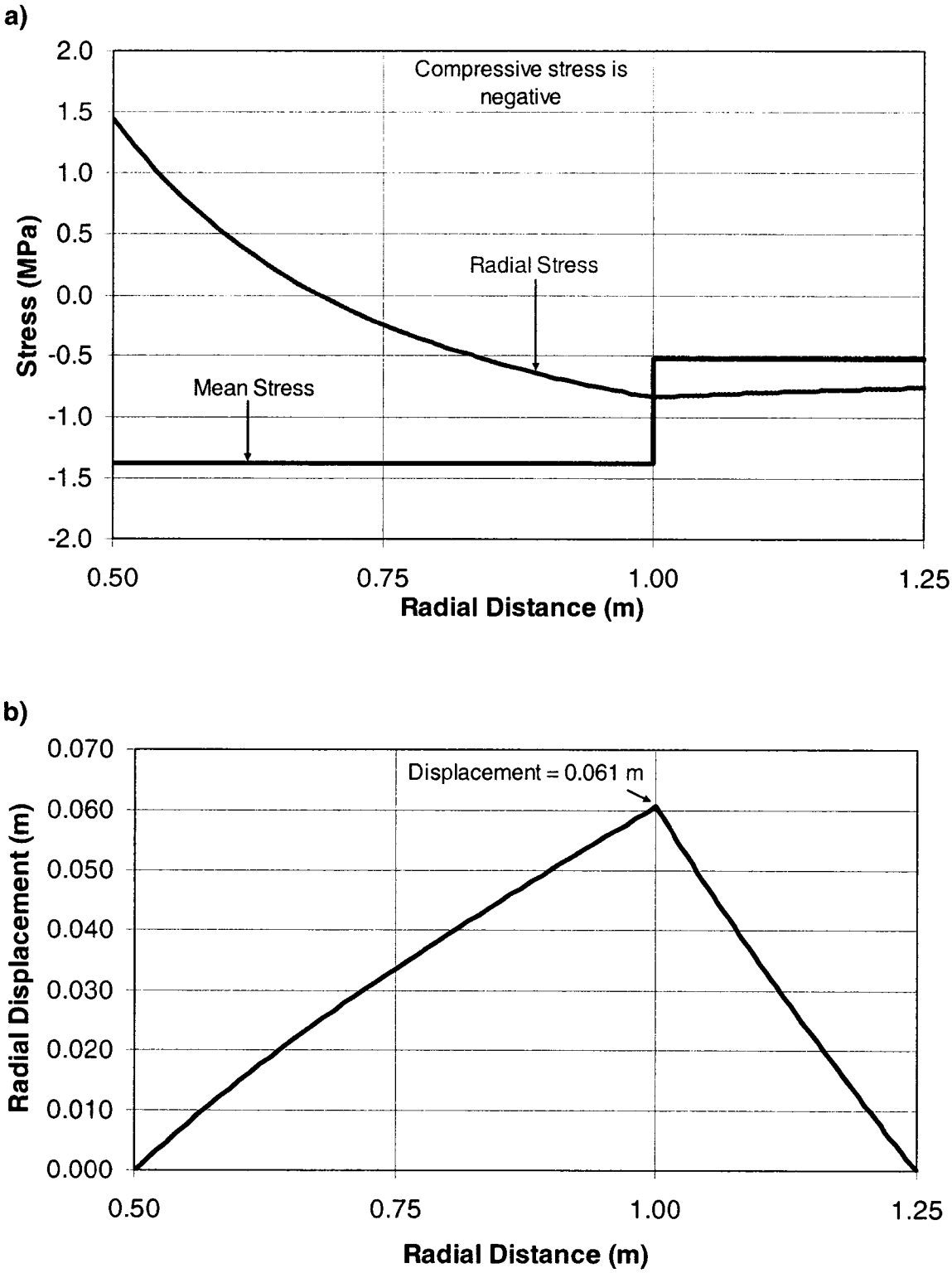

Figure 4.29: Axisymmetric Linear-Elastic Analytical Model for Path 6 a)Radial and Mean Stress, b)Radial Displacement

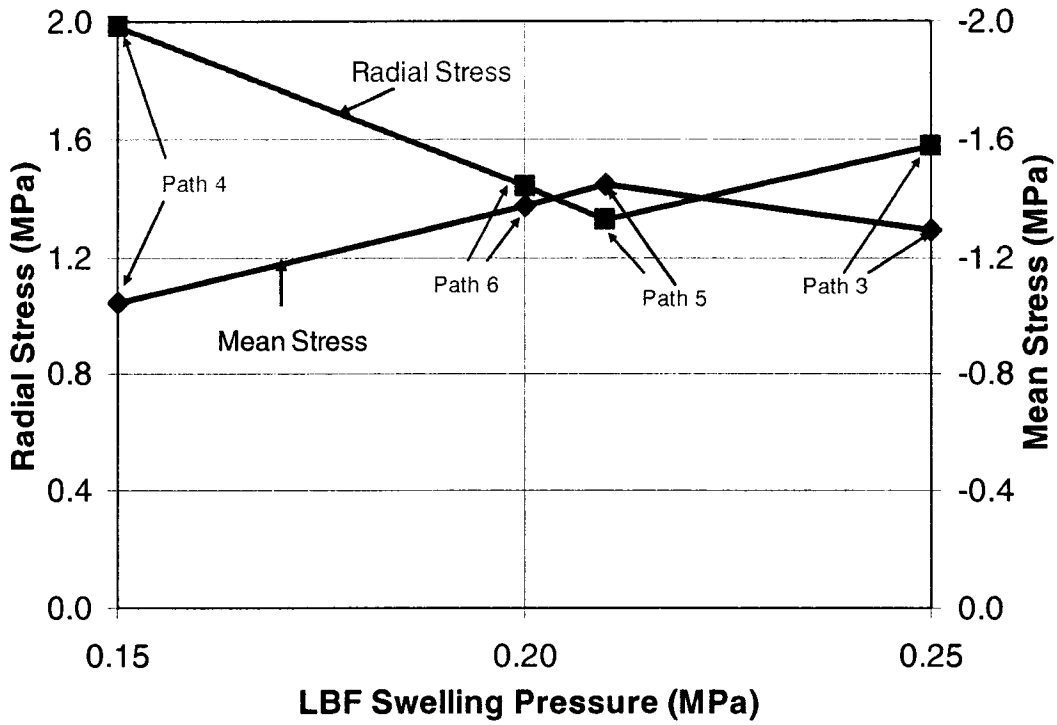

Figure 4.30: Radial Stress and Mean Stress versus LBF Swelling Pressure at the Container Surface for Paths 3, 4, 5, and 6

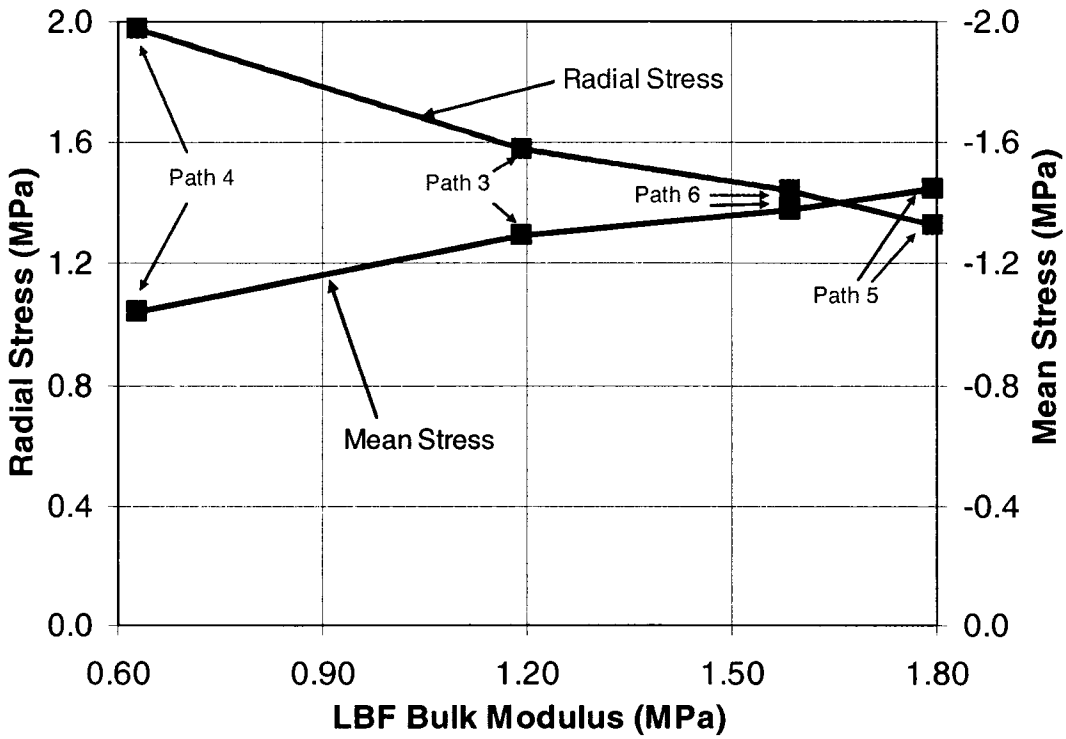

Figure 4.31: Radial Stress and Mean Stress versus LBF Bulk Modulus at the Container Surface for Paths 3, 4, 5, and 6

Chapter 5 : CONCLUSIONS AND RECOMMENDATIONS FOR FURTHER WORK

5.1 Summary of the Work

The objectives of this research are to describe and compare the one-dimensional compression, swelling and hydraulic behaviour of LBF material composed of 50% bentonite and 50% sand in the presence of distilled water and 100 g/l $CaCl_2$ and 200 g/l $CaCl_2$ solutions and to determine the hydro-mechanical parameters of LBF required for compliance modelling of the DGR emplacement room sealing system. The tests were conducted on 50-mm-diameter by 10-mm-thick LBF samples, placed to an initial average water content of 20.5% and an initial average EMDD of 0.79, using standard lever arm consolidation equipment. The initial average void ratio of the samples was 0.99. Several different loading and wetting paths were examined, including allowing the LBF to swell up to 20%

vertical strain on distilled water or solution uptake and constraining the LBF from swelling on distilled water or solution uptake. The samples were loaded in increments to a maximum vertical applied stress of about 4000 kN/m^2 following initial distilled water or solution uptake, and then unloaded in increments. Except for some of the initial increments during distilled water or solution uptake, each test increment was allowed to come to equilibrium.

The results of individual test loading and unloading increments were used to compute void ratio (e), hydraulic conductivity (k), EMDD, bulk modulus (K) and water activity (a_w). The hydraulic conductivity versus EMDD and vertical applied pressure versus EMDD results were compared to results compiled by Dixon et al. (2002a). The interaction between HCB (inner material) and LBF (outer material) in a hypothetical emplacement room sealing system was simulated using a two-material axisymmetric linear elastic analytical model.

5.2 Conclusions

Following are key results and observations of this research.

1. The test results show linear relationships between the logarithm of vertical applied pressure and EMDD and the logarithm of hydraulic conductivity and EMDD, both for loading/compression and unloading/swelling paths.

These exponential relationships follow the form of the exponential relationships between swelling pressure and EMDD and hydraulic conductivity and EMDD presented by Dixon et al. (2002a). The loading/compression relationships tend to follow the trend of the Dixon et al. (2002a) relationships. Conversely, the unloading/swelling relationships do not follow the trend of the Dixon et al. (2002a) relationships.

2. The tests results show that the relationship between vertical applied pressure and EMDD and the hydraulic conductivity and EMDD depend on loading path and stress and strain history. All of the tests showed significant hysteresis between the loading/compression and unloading/swelling paths. The hysteresis was more pronounced in the tests that used $CaCl_2$ in the consolidation cell reservoir. This means that future hydro-mechanical compliance modelling must use different constitutive parameters for the loading/compression and unloading/swelling paths.
3. The compression, swelling and hydraulic behaviour of LBF with 100 g/l or 200 g/l $CaCl_2$ cell reservoir solution is distinctly different than the behaviour of LBF with distilled water in the cell reservoir. The LBF is much more compressible with 100 g/l or 200 g/l $CaCl_2$ cell reservoir solution and its swelling capability and hydraulic performance are adversely affected. In the initial swelling portion of the compression tests, the samples with distilled water achieved swelling strains of about 20% under applied vertical stresses of 55 kN/m^2 while the samples with 100 g/l

or 200 g/l $CaCl_2$ solution achieved only about 6% to 10% swelling strain under essentially unloaded conditions. The samples with 100 g/l or 200 g/l $CaCl_2$ solution have higher hydraulic conductivity values than the samples with distilled water. For the tests with samples tested in the presence of $CaCl_2$ solutions, k values tend to be greater than 10^{-10} m/s with EMDD values less than about 1.0 Mg/m^3.

4. Increasing the cell reservoir $CaCl_2$ solution concentration from 100 g/l to 200 g/l does not create a significant difference in the compression, swelling and hydraulic response of LBF. The change in compression, swelling and hydraulic response is much more pronounced in the change from distilled water to 100 g/l cell reservoir fluid.
5. The effects of the 100 g/l $CaCl_2$ reservoir solution on the compression, swelling and hydraulic behaviour of LBF were somewhat suppressed by preconditioning (i.e. mixing) the LBF mixture with the same $CaCl_2$ solution as contained in the cell reservoir, in this case with a $CaCl_2$ concentration of 100 g/l. The use of 100 g/l $CaCl_2$ solution as the mixing fluid tended to decrease the hydraulic conductivity and the amount of compression on loading and increase the sample rebound on unloading relative to the other tests conducted in the presence of $CaCl_2$ solutions.
6. The resistance to uniform compression for LBF, in terms of bulk modulus (K) for the loading/compression path, increases exponentially with vertical strain. The tests conducted in the presence of distilled water generally have higher K values than the tests conduced in the presence of $CaCl_2$

solutions. This was unexpected, as other researches (e.g. Castellanos et al. 2006), have observed the opposite (i.e. increasing stiffness with increasing salinity). The LBF results may be due to the initially low density of the bentonite/sand material. Of the tests conducted in the presence of $CaCl_2$ solutions, the samples that used 100 g/l $CaCl_2$ as the mixing fluid have the highest K values while the test that was initially constrained from swelling during 100 g/l $CaCl_2$ solution uptake has the lowest K values.

7. The compression test results show that the water activity (a_w) values decrease as EMDD increases. The tests conducted in the presence of distilled water generally have lower a_w values than the tests conduced in the presence of $CaCl_2$ solutions. Of the tests conducted in the presence of $CaCl_2$ solutions, the samples that used 100 g/l $CaCl_2$ as the mixing fluid have the lowest a_w values while the samples that were initially constrained from swelling during 100 g/l $CaCl_2$ solution uptake have the highest a_w values.
8. The results of two-material axisymmetric linear elastic analytical simulations of the interaction between HCB and LBF in a hypothetical emplacement room sealing system show that the mean stress (assumed to be equal to swelling pressure) in the HCB decreases relative to the initial as-placed value. This is because it expanded while the mean stress in LBF increased as it was compressed. The results of the simulations show that the water activity values in HCB and LBF are greater than the 0.96 threshold value.

5.3 Recommendations for Future Work

The following work is recommended for future research based on the results of this research:

1. Carry out one-dimensional compression tests on LBF material composed of 100% granular bentonite or bentonite pellets in the presence of distilled water and $CaCl_2$ solutions of varying salinities. Emplacement trials indicate that higher initial as-placed EMDD values may be achievable for this type of material. Compare these results with the results from this research and results from Dixon et al. (2002a).
2. Carry out one-dimensional compression tests on LBF in the presence of a 250 g/l $CaCl_2$ solution (250 g/l $CaCl_2$ is closer to the concentration of Ca-rich groundwaters in the sedimentary rocks of Southern Ontario).
3. Carry out further compliance modelling of the emplacement room sealing system. Further work could include examining the assumption that swelling pressure is equal to mean stress and using FLAC so that the non-linearity of the elastic parameters could be included in the analysis.
4. Further work should aim towards having a sealing system design that will maintain the a_w of the HCB adjacent to the containers < 0.96.

REFERENCES

ASTM. 1998. Standard Test Method for One-Dimensional Consolidation Properties of Soils – D 2435-90. Annual Book of ASTM Standards, Vol. 04.08, American Society for Testing and Materials, Philadelphia.

ASTM. 2003. Standard test methods for one-dimensional swell or settlement potential of cohesive soils. Standard D4546-03, ASTM International, West Conshohocken, Pennsylvania, USA.

Bardet, J.-P. 1997. Experimental Soil Mechanics. Prentice Hall Inc., Upper Saddle River, N.J.

Batenipour, H. and Kjartanson, H., 2007. Effect of Water Salinity on the Hydro-Mechnical Behaviour of a Low Density Bentonite-Based Backfill Material. In proceedings of the 60th Canadian Geotechnical Conference & 8th Joint CGS/IAH-CNC Groundwater Conference. Ottawa.

Baumgartner, P. and Snider, G.R., 2002. Seal Evaluation and Assessment Study (SEAS): Loght Backfill Placement Trials. Atomic Energy of Canada Limited Technical Memorandum 90.70.20.

Baumgartner, P., Priyanto, D.G., Baldwin, J.R., Blatz, J.A., Kjartanson, B.H. and Batenipour, H., 2007. Preliminary Results of One-Dimensional Consolidation Testing on Bentonite Clay-Based Sealing Components Subjected to Two Pore-Fluid Chemistry Conditions, Ontario Power Generation Report.

Bolt, G.H., 1956. Physico-chemical analysis of the compressibility of pure clays. Géotechnique, 6(2): 86–93.

Castellanos, E., Gens, A., Lloret A. and Romero, E., 2006. Influence of water chemistry on the swelling capacity of a high density bentonite. Unsaturated soils. ASCE Geo-Institute, 2006, p. 962-972.

Chandler, N.A., 2005. Numerical Modelling of The Stress And Displacement of Emplacement Room Swelling-Clay Materials. Ontario Power Generation, Technical Memorandum, 06819(UF)-03782.02-T10, Toronto, Ontario.

Craig, R.F., 2004. Craig's Soil Mechanics 7th Edition. E and FN Spon. London and New York.

Dixon, D.A., 1994. Sodium bentonites of Canada, the United States and Mexico: sources, reserves and properties. Engineering Materials for Waste Isolation, CSCE-Engineering Division-Special Publication, 37-65.

Dixon, D.A., Campbell, S.L. and Hnatiw, D.S., 1994. Pre-placement quality control and as-placed properties of the buffer materials used in the URL Isothermal Buffer Experiment. Atomic Energy of Canada Limited Technical Record, TR-612, COG-94-35.

Dixon, D.A., Chandler, N.A, Stroes-Gascoyne, S.and Kozak, E. 2001. The Isothermal Buffer-Rock-Concrete Plug Interaction Test: Results, Issues, Synthesis, Ontario Power Generation, Supporting Technical Report, 06819-REP-01200-10056-R00, Toronto, Ontario.

Dixon, D.A., Chandler, N.A. and Baumgartner, P., 2002a. The influence of groundwater salinity and interfaces on the performance of potential backfilling materials. In Trans. 6th International Workshop on Design and Construction of Final Repositories: Backfilling in Radioactive Waste Disposal. ONDRAF/NIRAS, Brussels, Belgium, 2002 March 11-13.

Dixon, D., Chandler, N.A., Graham, J. and Gray, M.N., 2002b. Two large-scale sealing tests conducted at Atomic Energy of Canada's underground research laboratory: the buffer-container experiment and the isothermal test. Canadian Geotechnical Journal, 39: 503-518.

Gascoyne, M., Davison, C.C, Ross, J.D. and Pearson, R., 1987. Saline groundwaters and brines in pultons in the Canadian Shield. In Saline Water and Gases in Crystalline Rocks. Editors: Fritz, P. and Frape, S.K., Geological Association of Canada Special Paper 33.

Gierszewski, P., Jensen, M., Maak, P. and Vorauer, A., 2004. Third Case Study – Site and design description. Ontario Power Generation Nuclear Waste Management Division Report 06819-REP-01200-10124-R00.

Graham, J., Chandler, N.A., Dixon, D.A., Roach, P.J., To, T., and Wan, A.W.L., 1997. The Buffer Container Experiment: Results, Synthesis, Issues. Atomic Energy of Canada Limited Report, AECL-11746, COG-97-46-I.

Grim, R. E.1962. Applied clay mineralogy. New York: McGraw-Hill.

Hillel, D., 1980. Fundamentals of Soil Physics. Academic Press.

Kjartanson, B. H., Dixon, D.A. and Stroes-Gascoyne, S., 2003a. Effects of container/buffer gap fill on buffer performance. Ontario Power Generation, Nuclear Waste Management Division Report 06819-REP-01200-10102-R00.

Kjartanson, B.H., Dixon, D.A. and Baumgartner, P. 2003b. Concepts and Technologies for Backfilling a Nuclear Fuel Waste Repository. Ontario Power Generation, Nuclear Waste Management Division, Report No. 06819-REP-01200-10103-R00.

Kjartanson, B. H., Dixon, D.A. and Stroes-Gascoyne, S., 2003c. Microbe Viability and Activity in Bentonite-based Barriers. 56th Canadian Geotechnical Conference.

Kjartanson, B.H., Dixon, D. A. and Kohle, C.L., 2005. Placement of bentonite pellets to fill repository sealing systems voids and gaps. Ontario Power Generation, Nuclear Waste Management Division Report 06819-REP-01200-10136-R00.

Komine, H., 2004. Simplified evaluation for swelling characteristics of bentonites. Engineering Geology, Vol. 71, 3-4, pp. 265-279.

Lide, D.R., ed. 2007. CRC Handbook of Chemistry and Physics, Internet Version 2007, (87th Edition), http://www.hbcpnetbase.com.

Maak, P. and Simmons, G.R., 2005. Deep Geologic Repository Concepts for Isolation of Used Fuel in Canada. Canadian Nuclear Society Waste Management, Decommissioning and Environmental Restoration for Canada's Nuclear Activities: Current Practices and Future Needs Ottawa, Ontario, Canada May 8-11 2005.

Maio, C. Di, Santoli, L. and Schiavone, R., 2004. Volume change behaviour of clays: the influence of mineral composition, pore fluid composition and stress state. Mechanics of materials. Vol. 36, Issues 5-6, pp. 435-451.

Mazurek, M. 2004. Long-term used nuclear fuel waste management – Geoscientific review of the sedimentary sequence in southern Ontario. Institute of Geological Sciences, Univ. of Bern, Technical Report TR 04-01, Bern, Switzerland.

Mitchell J. K. and Soga K., 2005. Fundamentals of Soil Behavior, John Wiley & Sons.

NWM0 (Nuclear Waste Management Organization), 2005. Choosing A Way Forward, The Future Management of Canada's Used Nuclear Fuel.

OMNI Laboratories, Inc. http://webmineral.com/specimens/picshow.php?id=1285 May 2007.

Priyanto, D.G. and Baumgartner, P., 2007. Appendix D Volume-Mass Relationships of Soil with Fresh Water and Saline Solutions. Waste Technologies Division Atomic Energy of Canada Limited.

Pusch, R., 2001. The Buffer and Backfill Handbook, Part 2: Materials and techniques. Swedish Nuclear Fuel and Wastes Management Co. (SKB), TR-02-12.

Rowe, R.K., Quigley, R.M. and Booker, J.R., 1995. Clayey Barrier Systems for Waste Disposal Facilities, E & FN Spon (Chapman & Hall).

Stewart D.I., Studds, P.G. and Cousens, T.W., 2003. The factors controlling the engineering properties of bentonite-enhanced sand. Applied clay science, 23(1-4), 2003, pp. 97 – 110.

Stroes-Gascoyne, S. and King, F., 2002. Microbially influenced corrosion issues in high-level nuclear waste repositories. In proceedings of the Corrosion/2002 Research Topical Symposium: Microbiologically Influenced Corrosion. B. Little (Editor). NACE International, The Corrosion Society, Houston TX.

Studds, P.G., Stewart D.I., and Cousens, T.W., 1996. The effect of ion valance on the swelling behaviour of sodium bentonite. Polluted and Marginal Land-96, Proc. 4th Int. Conf. on Re-use of Contaminated Land and Landfills, Engineering Technics Press, Edinburgh, 139-142.

Studds, P.G., Stewart D.I., and Cousens, T.W., 1998. The effects of salt solutions on the properties of bentonite-sand mixtures. Clay Minerals; December 1998; v. 33; no. 4; p. 651-660.

Tripathy, S., Sridharan, A. and Schanz, T., 2004. Swelling pressures of compacted bentonites from diffuse double layer theory. Canadian Geotechnical Journal, Vol. 41, pp. 437-450.

Van Olphen, H., 1963. An introduction to clay colloid chemistry: for clay technologists, geologists and soil scientists. Interscience, New York.

Yong, R.N. and Mohamed, A.M.O., 1992. A study of particle interaction energies in wetting of unsaturated expansive clays. Canadian Geotechnical Journal, 29: 1060–1070.

Appendix A: Sample Height versus Time Graphs

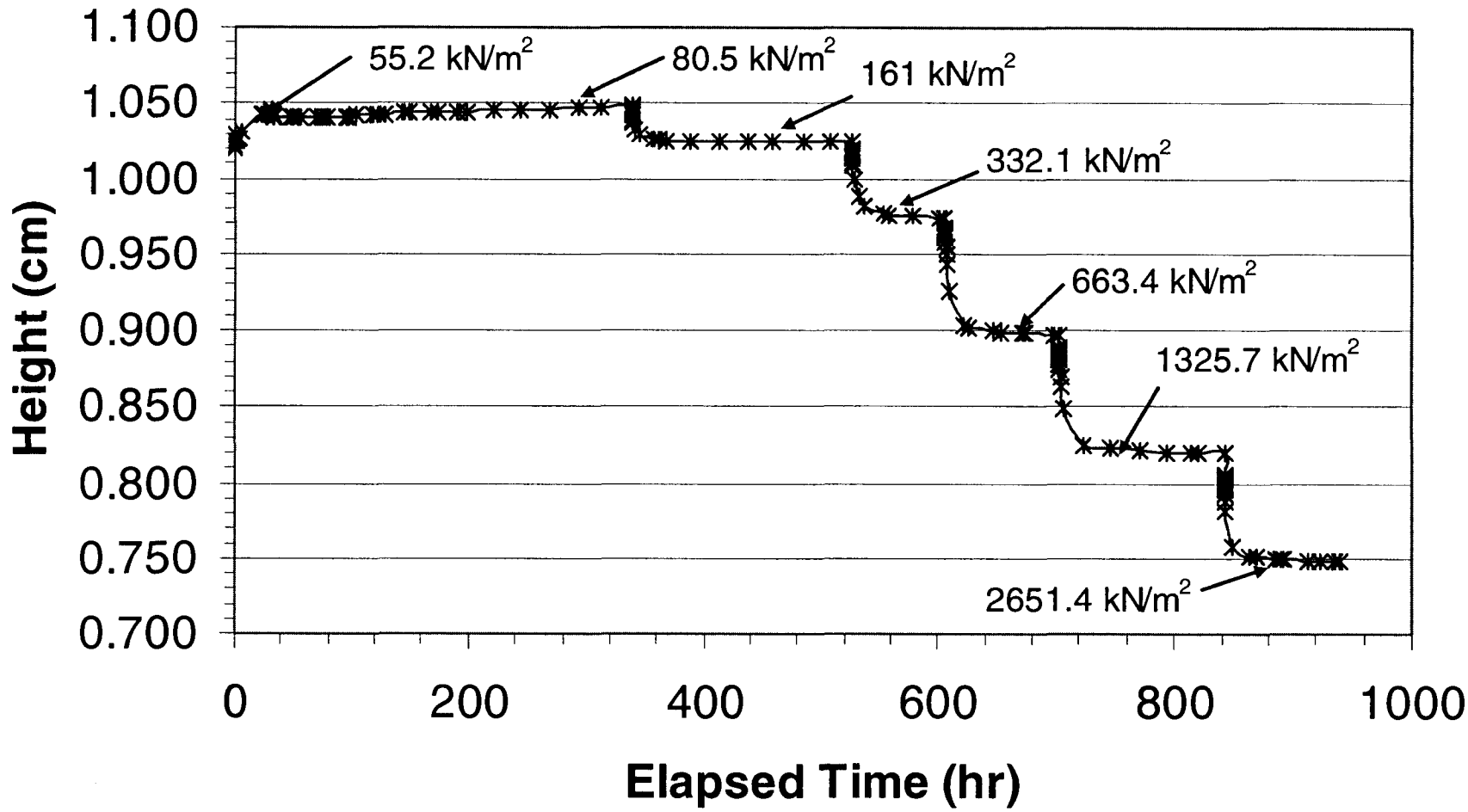

Figure A.1 Test HB2 sample height versus time – stresses for loading increments are shown.

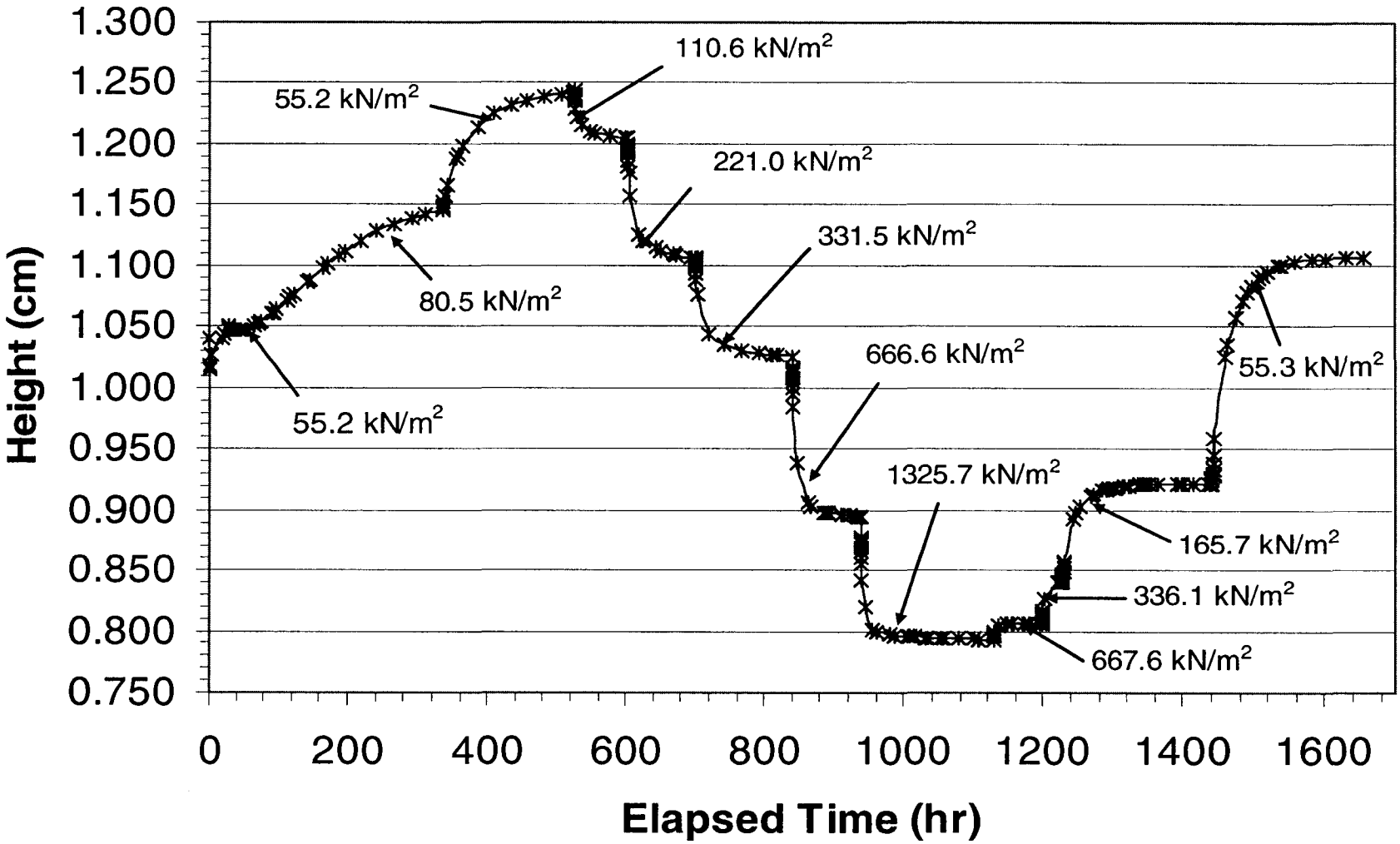

Figure A.2 Test HB3 sample height versus time – stresses for loading and unloading increments are shown.

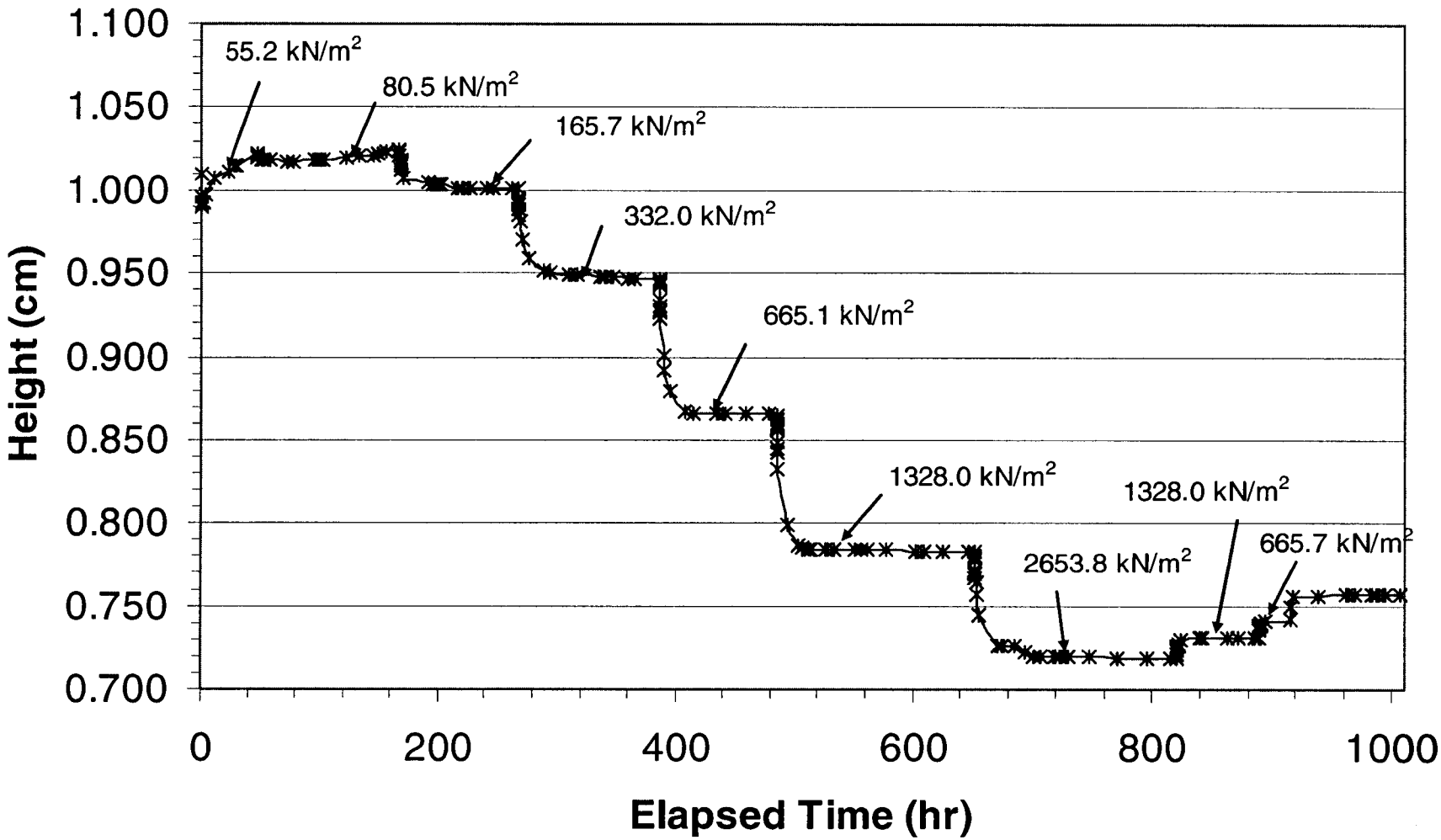

Figure A.3 Test HB4 sample height versus time – stresses for loading and unloading increments are shown.

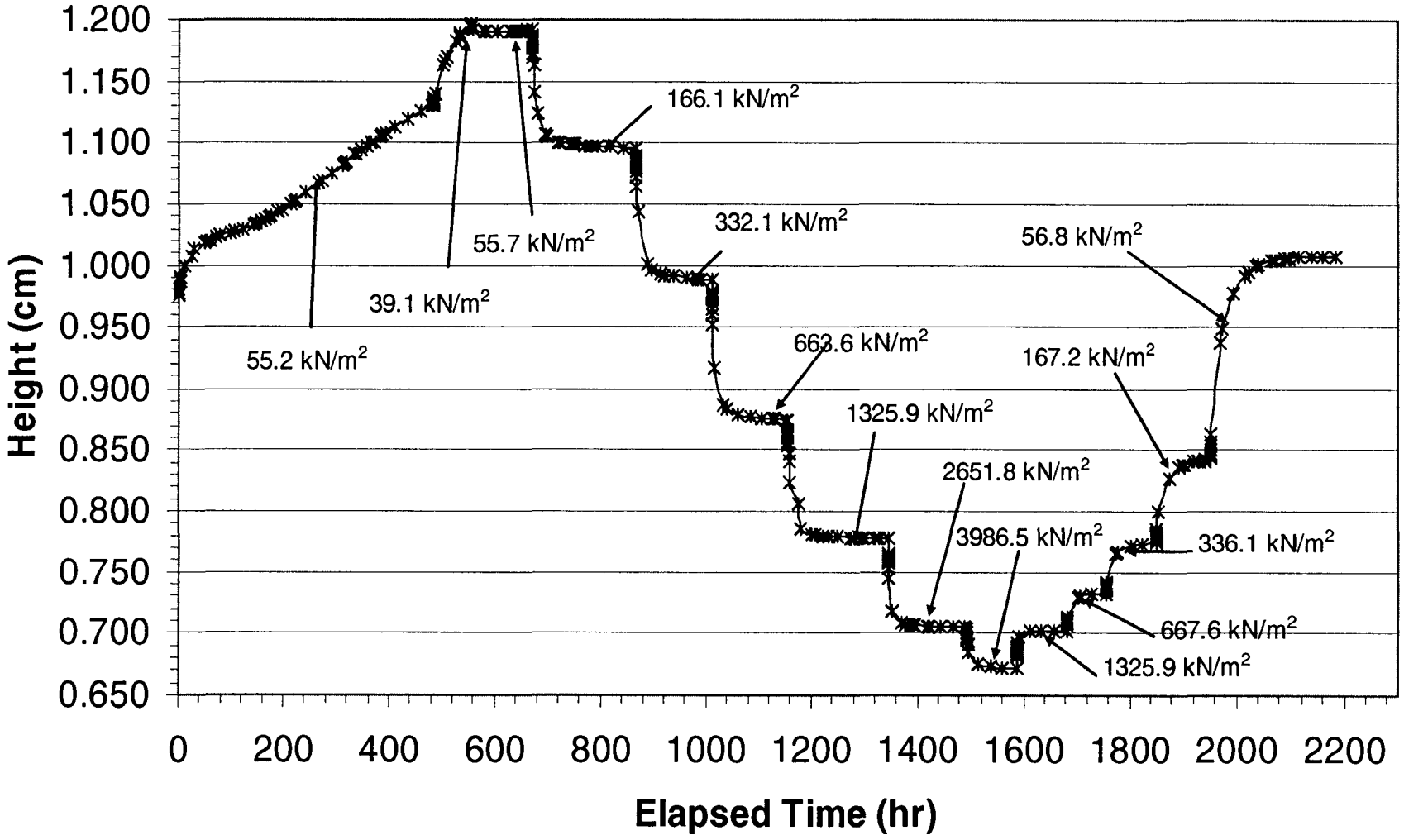

Figure A.4 Test HB6 sample height versus time – stresses for loading and unloading increments are shown.

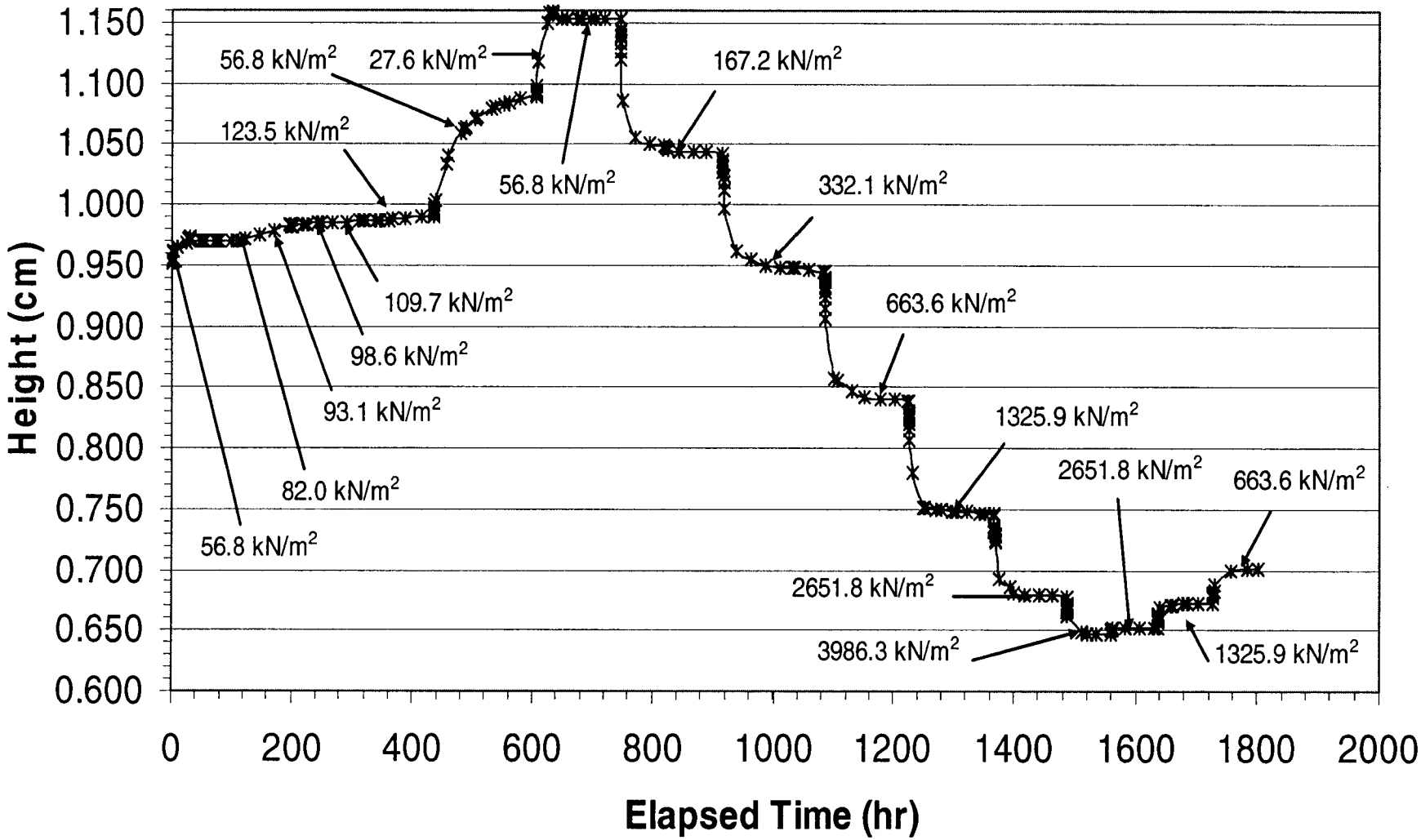

Figure A.5 Test HB7 sample height versus time – stresses for loading and unloading increments are shown.

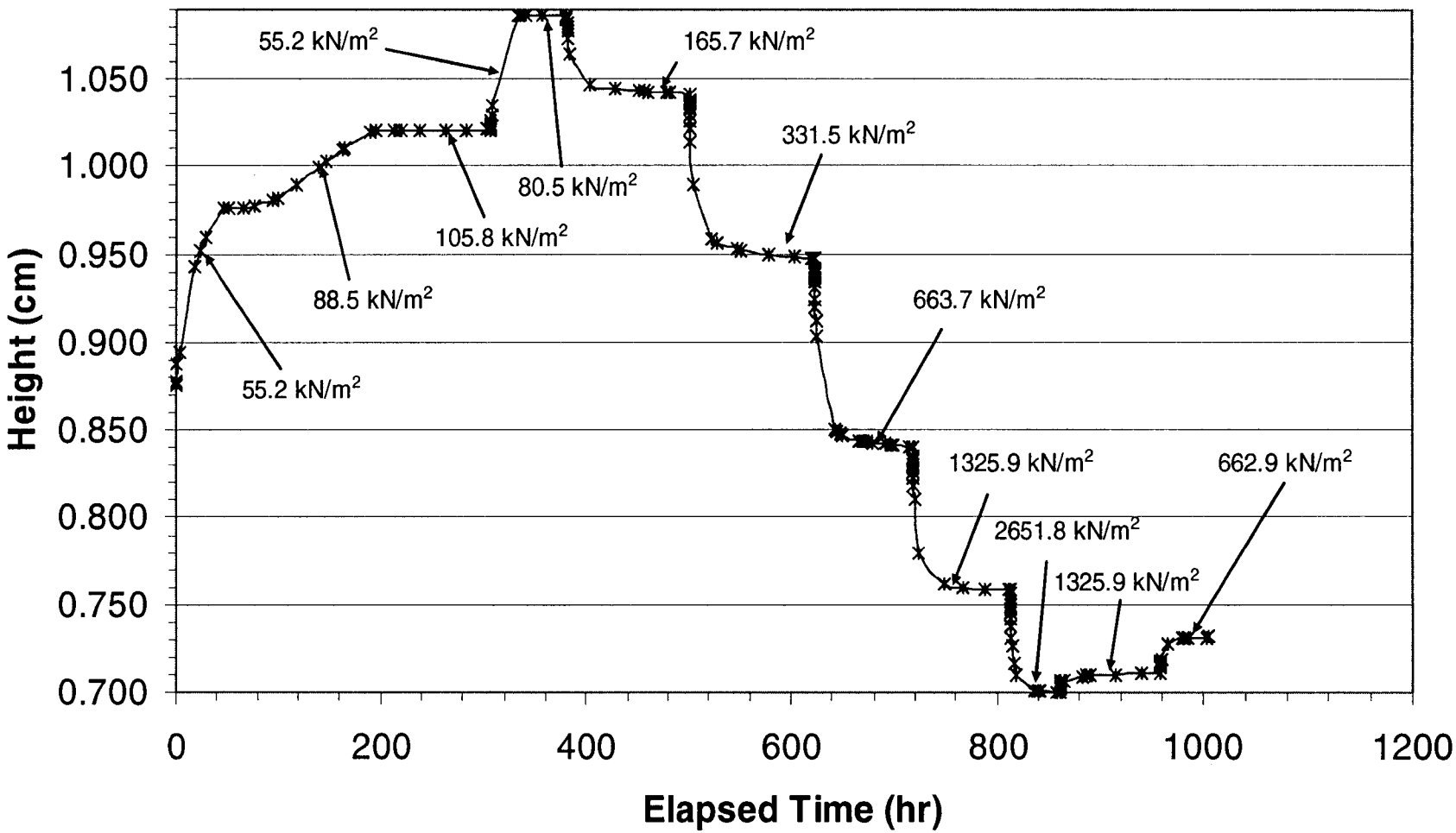

Figure A.6 Test HB8 sample height versus time – stresses for loading and unloading increments are shown.

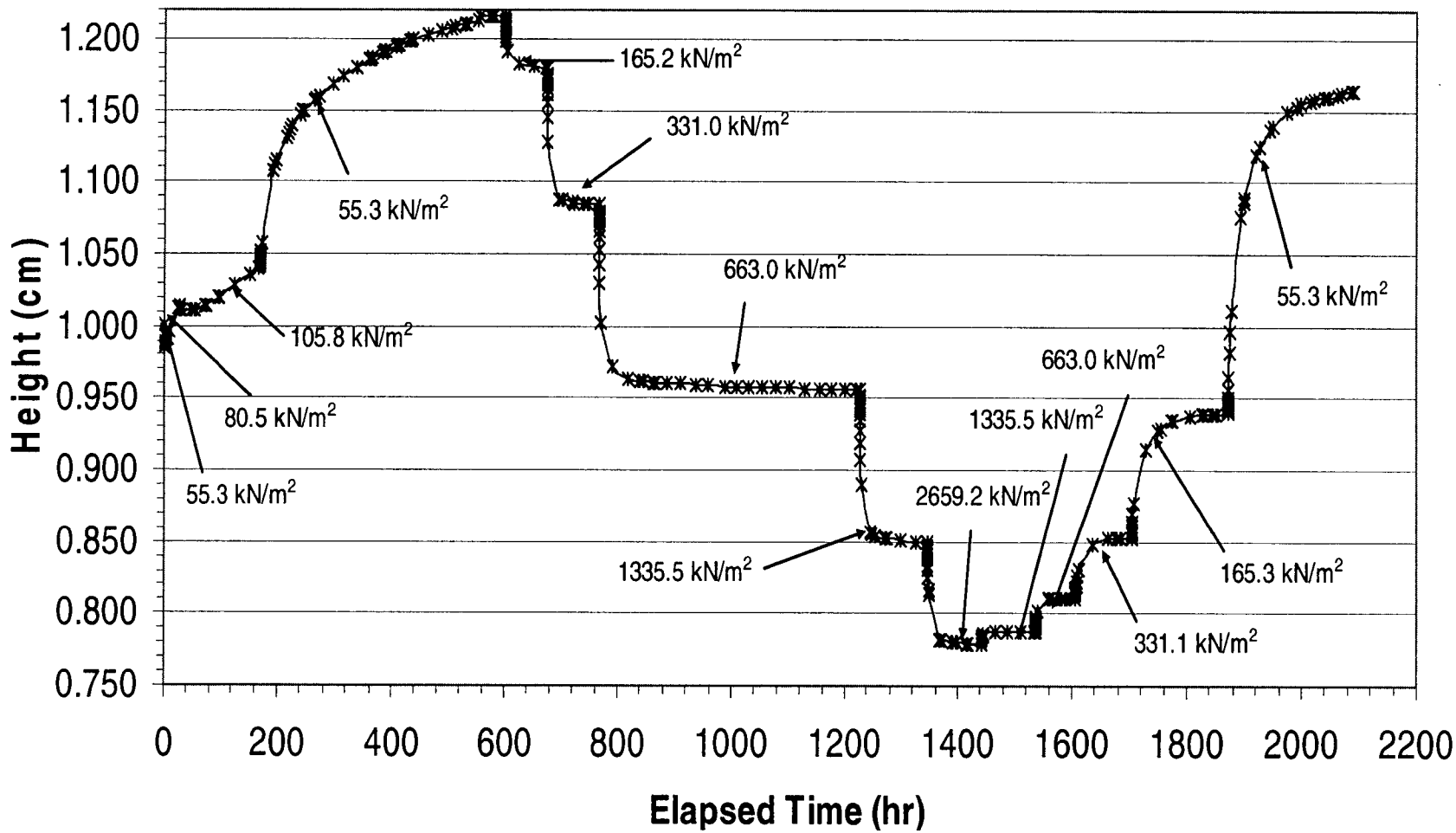

Figure A.7 Test HB9 sample height versus time – stresses for loading and unloading increments are shown.

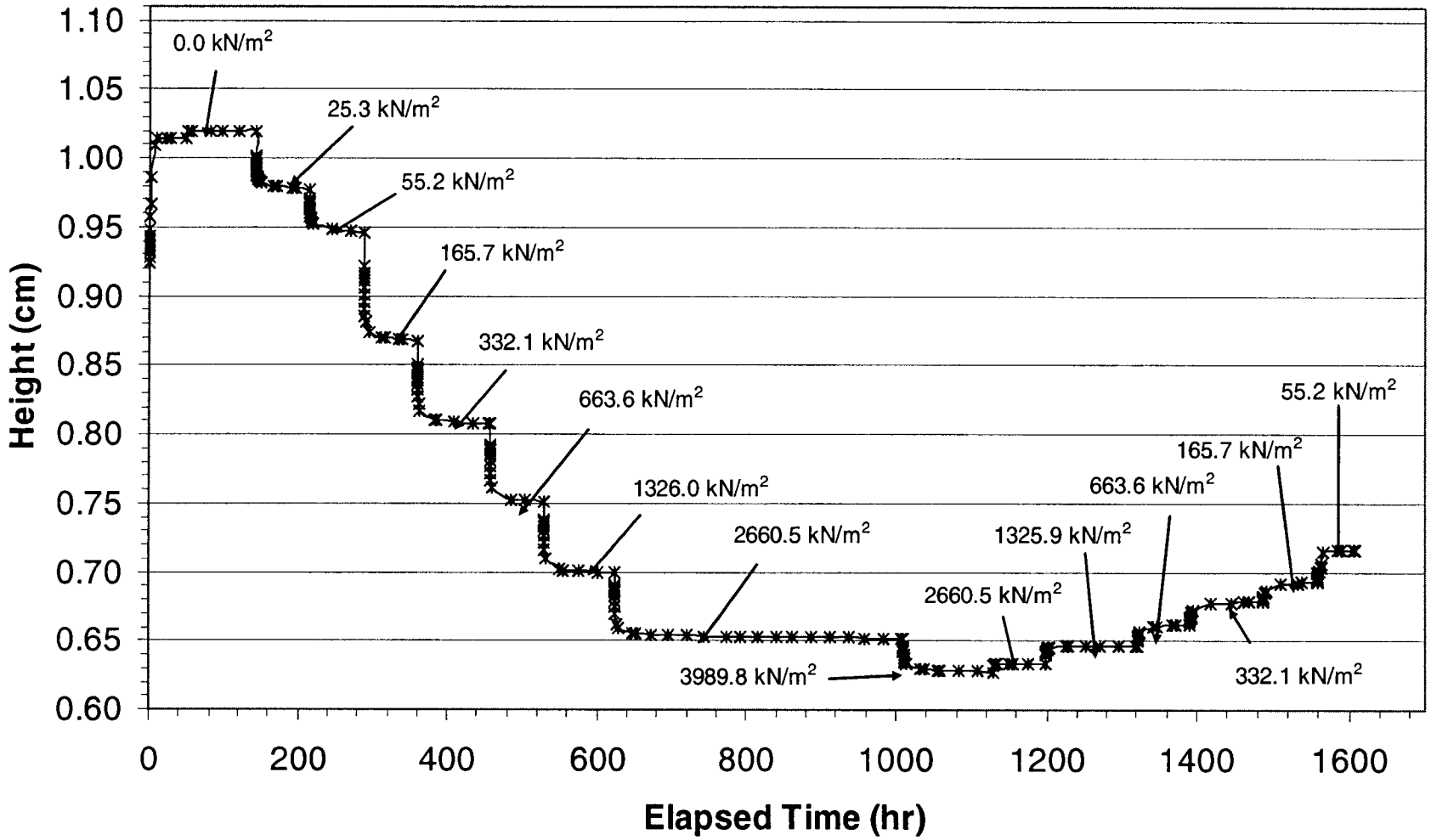

Figure A.8 Test HB11 sample height versus time – stresses for loading and unloading increments are shown.

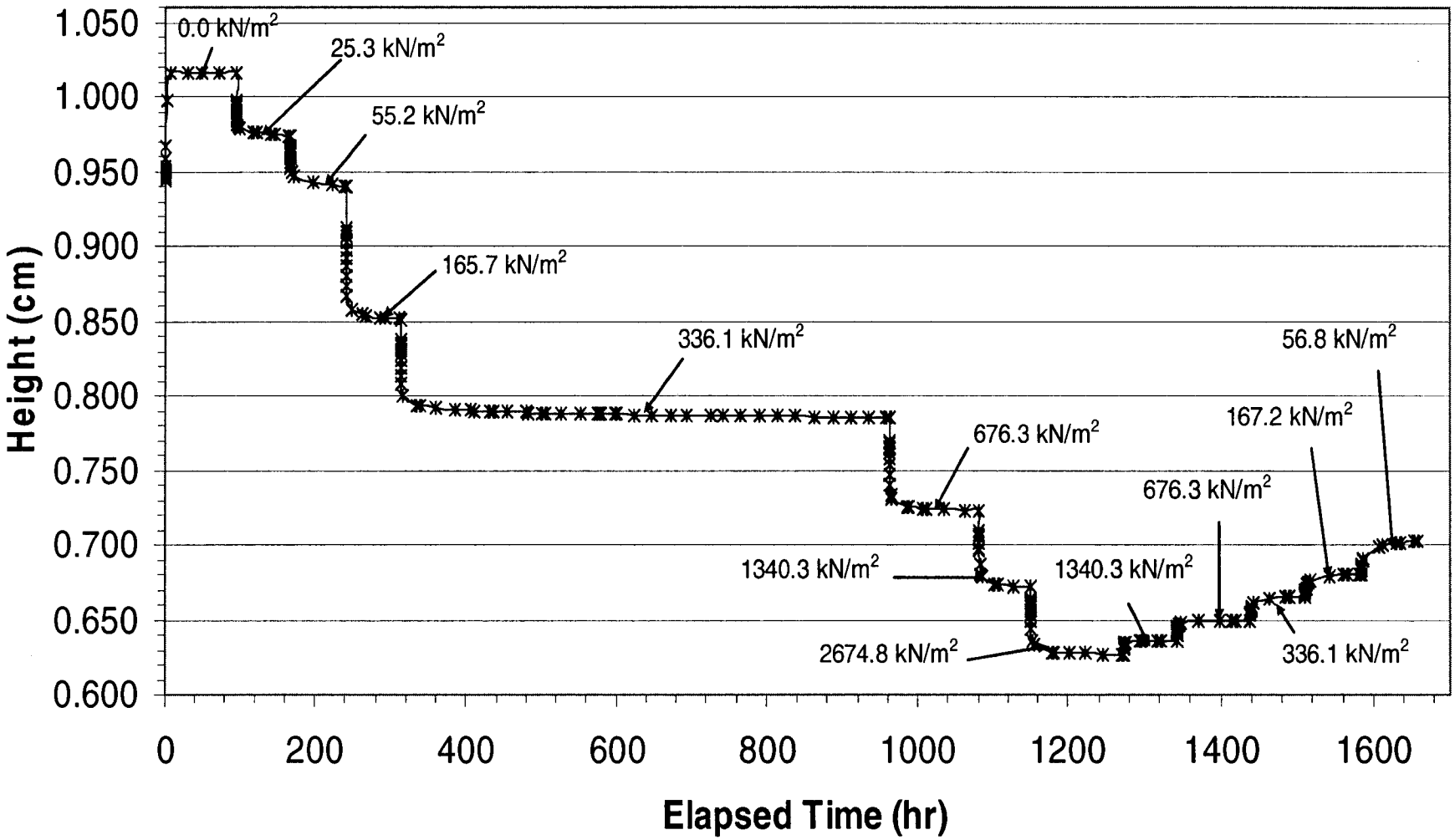

Figure A.9 Test HB12 sample height versus time – stresses for loading and unloading increments are shown.

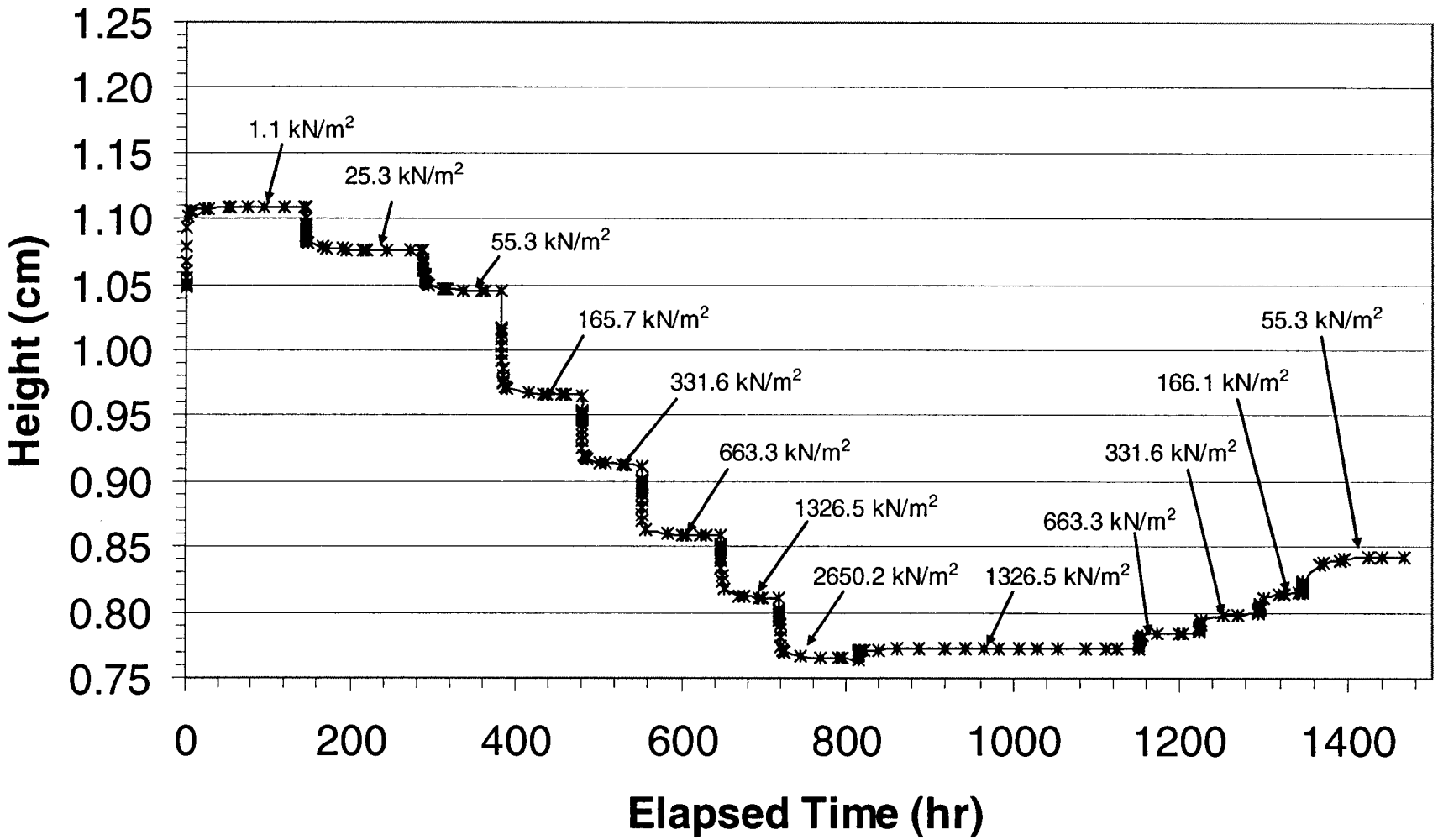

Figure A.10 Test HB13 sample height versus time – stresses for loading and unloading increments are shown.

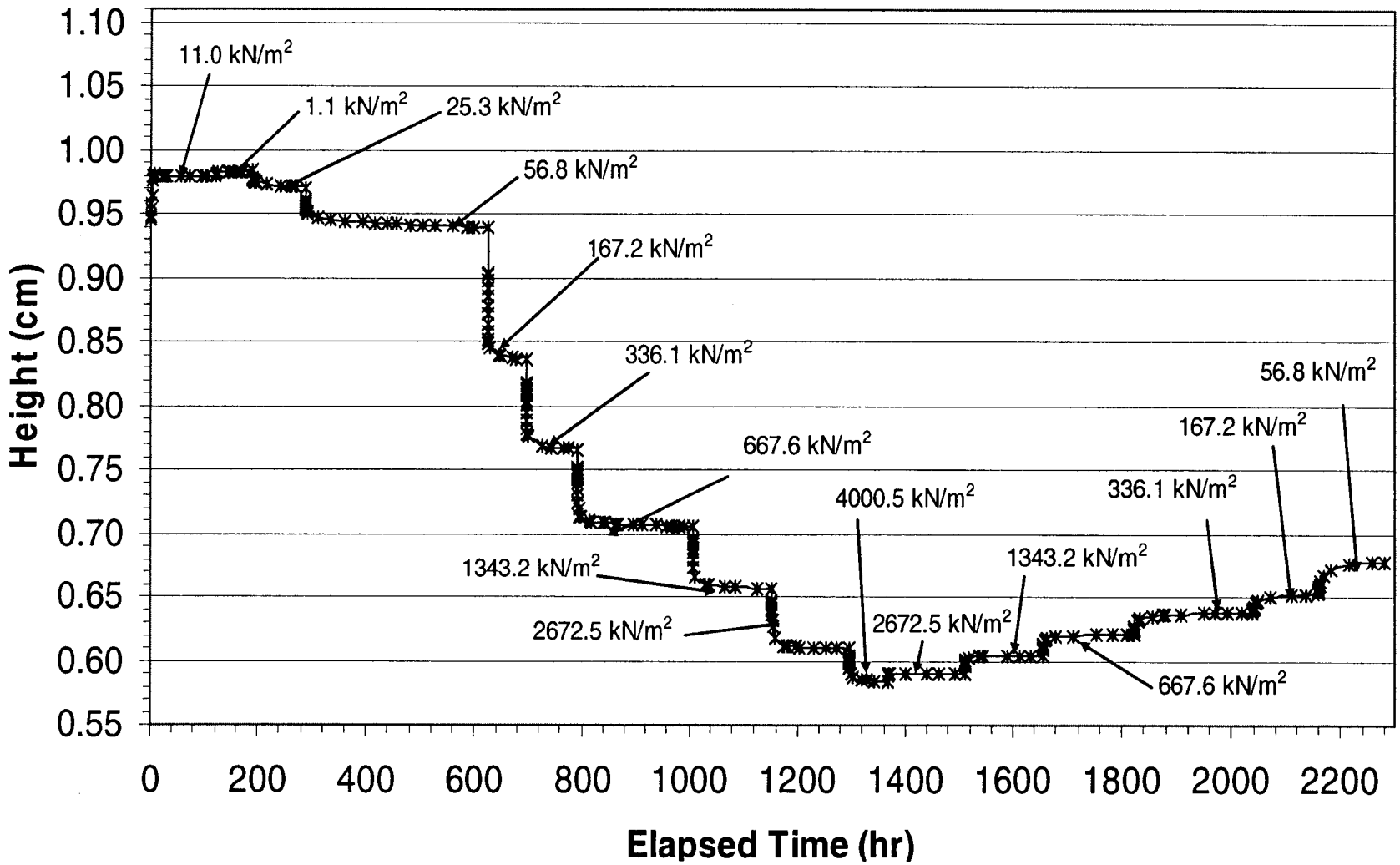

Figure A.11 Test HB14 sample height versus time – stresses for loading and unloading increments are shown.

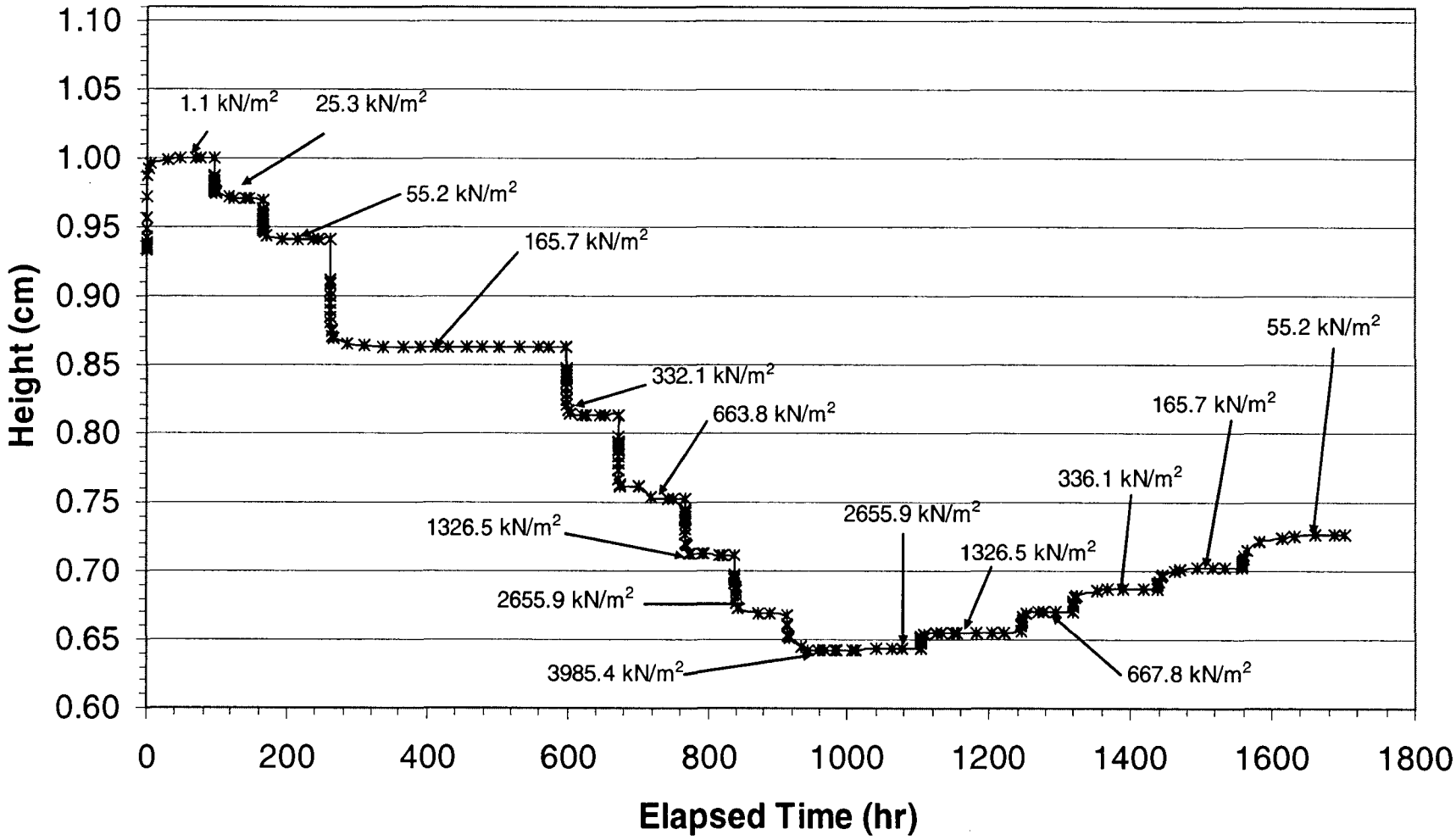

Figure A.12 Test HB15 sample height versus time – stresses for loading and unloading increments are shown.

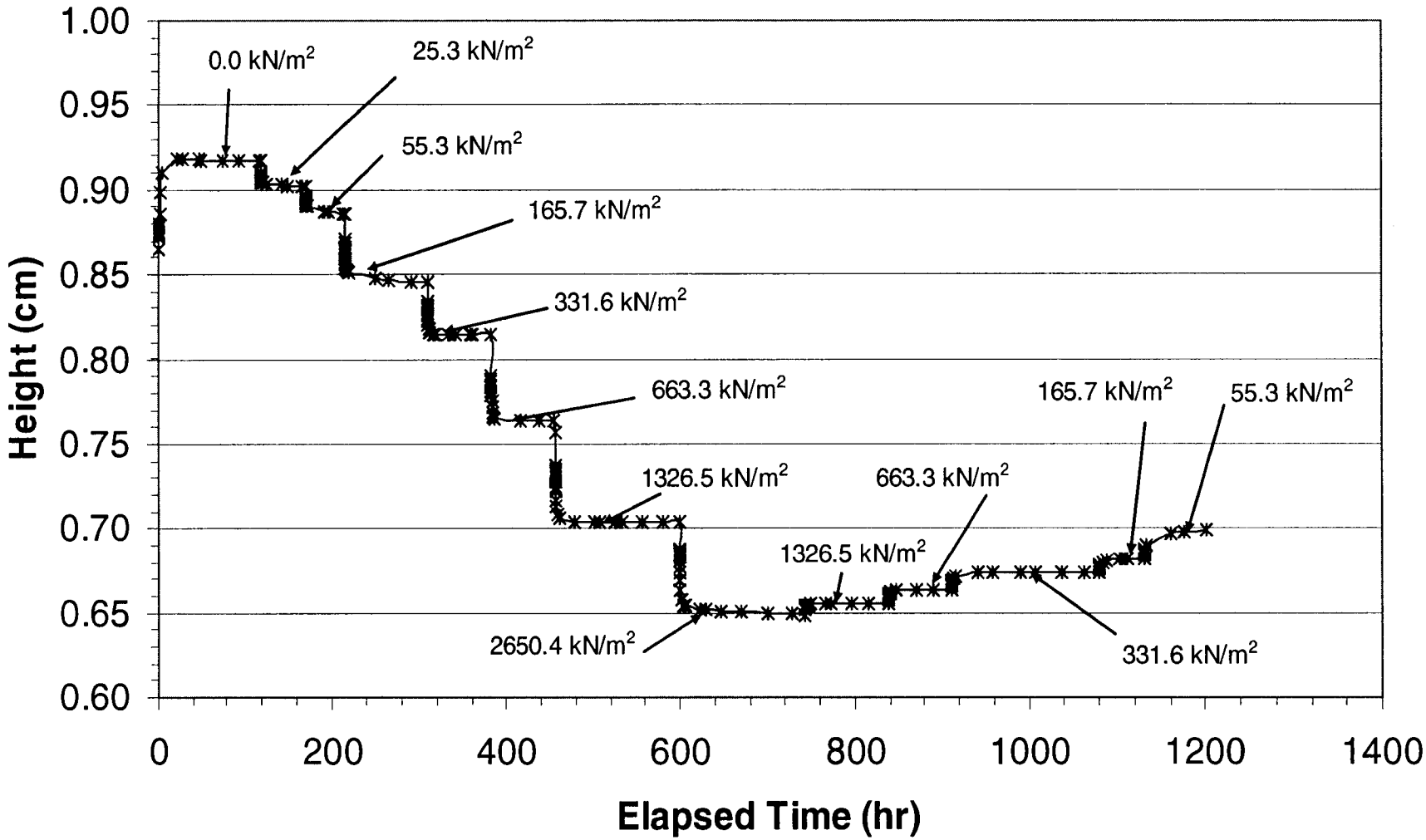

Figure A.13 Test HB16 sample height versus time – stresses for loading and unloading increments are shown.

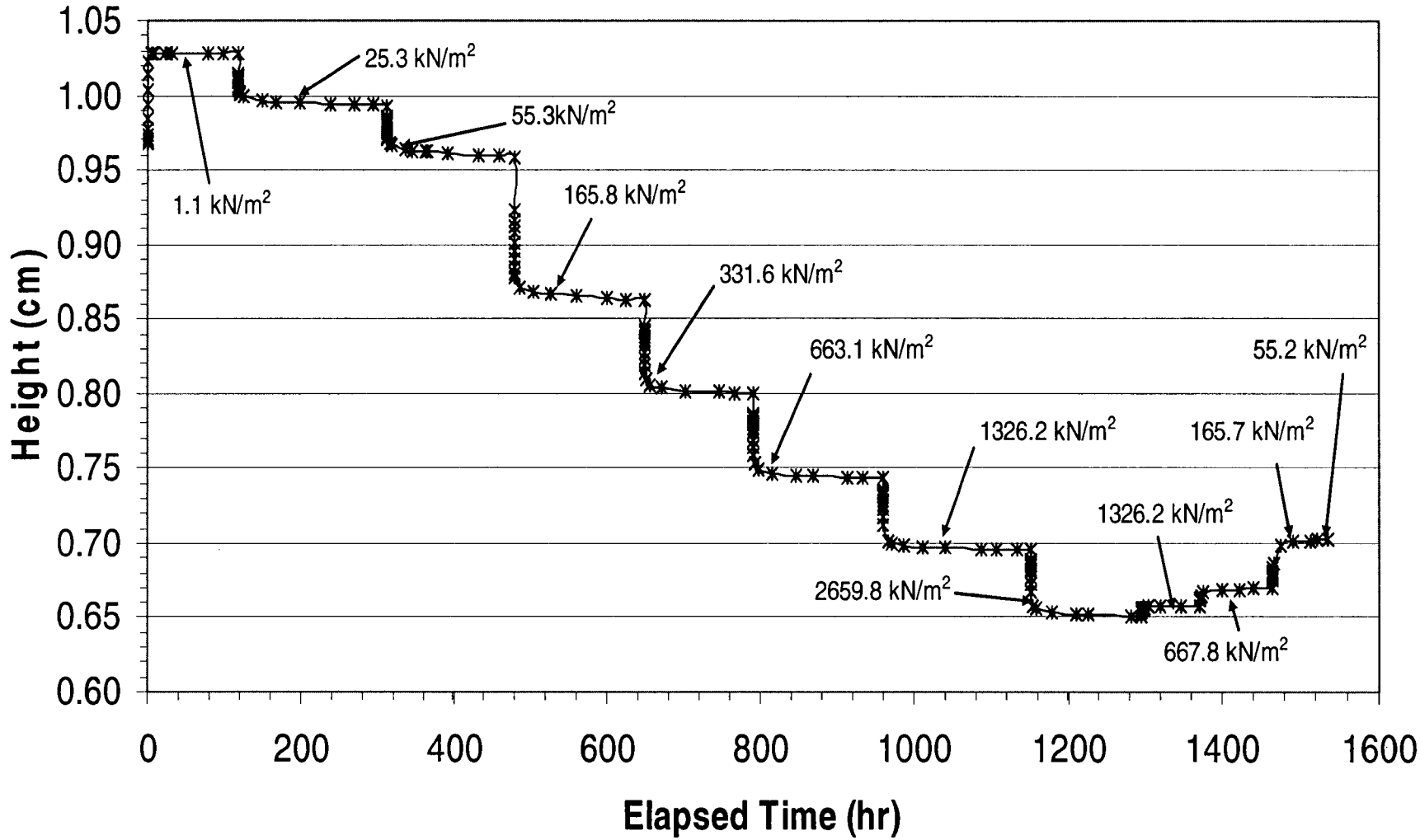

Figure A.14 Test HB19 sample height versus time – stresses for loading and unloading increments are shown.

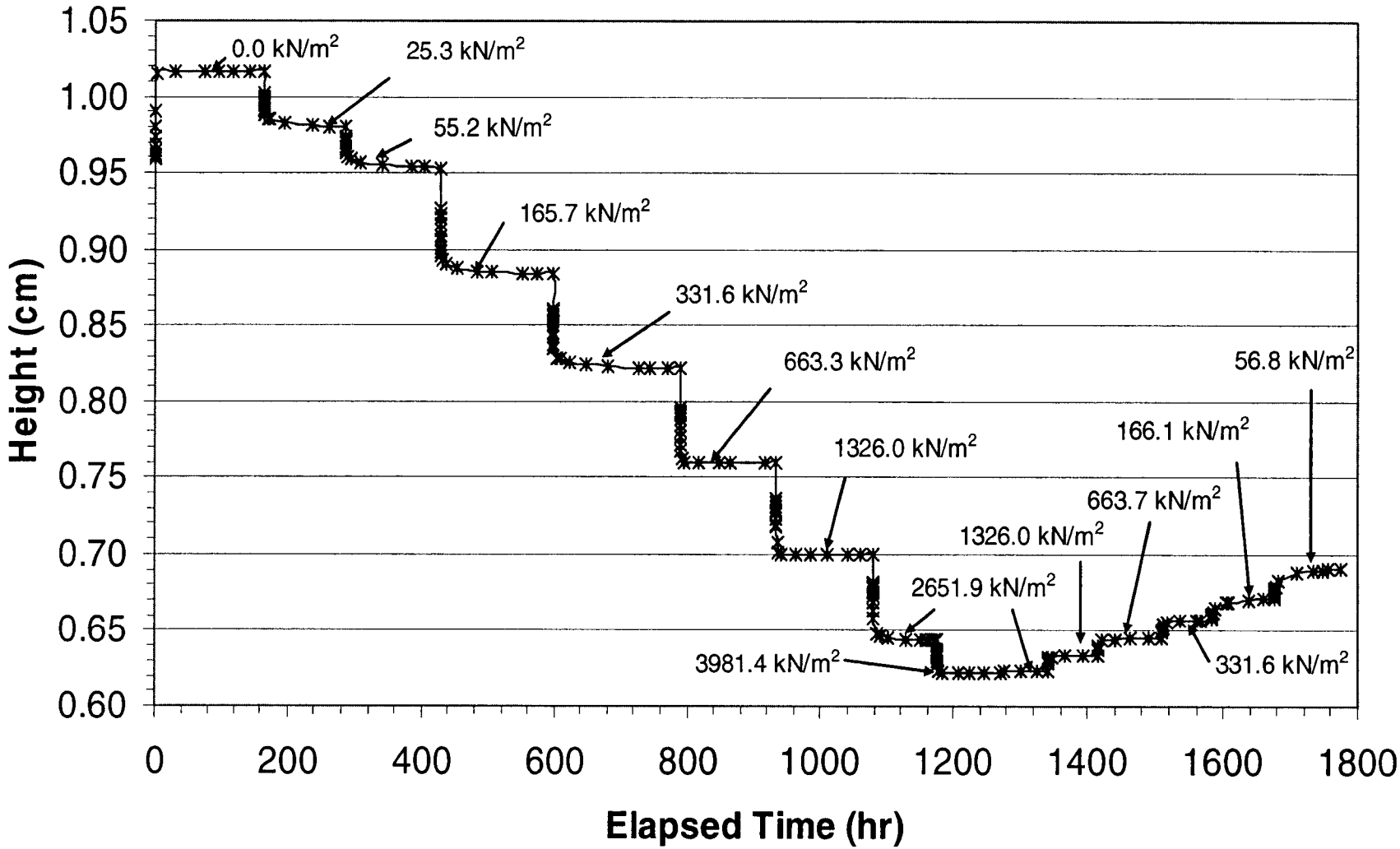

Figure A.15 Test HB20 sample height versus time – stresses for loading and unloading increments are shown.

Appendix B: Equations for Calculation of Volume-Mass Parameters

This appendix includes the equations for calculation of volume-mass parameters using both saline solutions ($CaCl_2$ in this research) and distilled water as consolidation cell reservoir fluids. These equations have been drawn from D.G. Priyanto and P. Baumgartner (2007) – Appendix D, Volume-Mass Relationships of Soil with distilled Water and Saline Solutions, Waste Technologies Division, Atomic Energy of Canada Limited. The full derivation is provided in that appendix and is not repeated here.

$$V = V_S + V_g + V_l \qquad \text{(B.1)}$$

where V = total volume of the soil sample (see Fig. B.1);

V_s = volume of solid;

V_g = volume of gas; and

V_l = volume of liquid.

and

$$V_l = V_W + V_{salt} \qquad \text{(B.2)}$$

where V_w = volume of water (solvent); and

V_{salt} = volume of salt (solute).

$$M = M_S + M_l \qquad \text{(B.3)}$$

where M = total mass of the sample;

M_s = mass of solid; and

M_l = mass of liquid.

and

$$M_l = M_W + M_{salt} \qquad \text{(B.4)}$$

where M_w = mass of water (solvent); and

M_{salt} = mass of salt (solute).

The density of the $CaCl_2$ solution (ρ_l) is dependent on the total dissolved solids (TDS, in units of g/l of solution: 100 g/l and 200 g/l in this research). The density of the $CaCl_2$ solution has been drawn from the empirical equation in Figure B.2 (after Lide 2007).

$$C_m = \frac{TDS}{(\rho_l \times 1000)} \times 100 \qquad \text{(B.5)}$$

where ρ_l = solution density (Mg/m^3); and

C_m = percent mass of the solute to the solution (%).

:

$$G_S = \frac{\rho_S}{\rho_W} \qquad \text{(B.6a)}$$

where ρ_s = density of solid phase;

ρ_w = density of water; and

G_s = specific gravity of soil solids (a value of 2.7 is used in this research).

$$G'_S = \frac{\rho_S}{\rho_l} \qquad \text{(B.6b)}$$

where ρ_l = density of liquid phase (i.e. the saline solution); and

G'_s = specific gravity of soil solids relative to solution density.

$$G_S' = \frac{\rho_S}{\rho_l} = \frac{\rho_S}{\rho_W} \cdot \frac{\rho_W}{\rho_l} = G_S \times \frac{\rho_W}{\rho_l} \qquad \text{(B.6c)}$$

$$w_W = \frac{M_W}{M_S} \qquad \text{(B.7)}$$

where w_w = gravimetric water content.

$$w = \frac{M_W}{M_S + M_{salt}} \qquad \text{(B.8)}$$

where w = bulk water content.

$$w_W = \frac{M_W}{M_S} = \frac{M_l - M_{salt}}{M_S} \qquad \text{(B.9)}$$

$$w_l = \frac{M_l}{M_S} = \frac{M_W + M_{salt}}{M_S} \qquad \text{(B.10)}$$

where w_l = gravimetric solution content.

$$M_S = G'_S \cdot \rho_l \cdot V_S = G_S \cdot \rho_W \cdot V_S \qquad \text{(B.11)}$$

$$M_l = M_W + M_{salt} = w_l \cdot G'_S \cdot \rho_l \cdot V_S = w_l \cdot G_S \cdot \rho_W \cdot V_S \qquad \text{(B.12)}$$

$$M_{salt} = C_m \cdot M_l = C_m \cdot w_l \cdot G'_S \cdot \rho_l \cdot V_S = C_m \cdot w_l \cdot G_S \cdot \rho_W \cdot V_S \qquad \text{(B.13)}$$

$$w_W = w_l(1 - C_m) \qquad \text{(B.14)}$$

$$M_{salt} = M_l - M_W = M_S(w_l - w_W) \qquad \text{(B.15)}$$

$$M_S = \frac{M_S + M_{salt}}{1 + w_l - w_w} \qquad \text{(B.16)}$$

where $M_s + M_{salt} = M$ = Total dry mass of soilds (total mass of sample after drying in oven)

$$w = \frac{w_w}{1 + w_l - w_w} \qquad \text{(B.17)}$$

$$w_w = \frac{w(1 - C_m)}{1 - C_m(1 + w)} \qquad \text{(B.18)}$$

$$w_l = \frac{w}{1 - C_m(1 + w)} \qquad \text{(B.19)}$$

$$\rho_d = \frac{M_S}{V} \qquad \text{(B.20)}$$

where ρ_d = dry density.

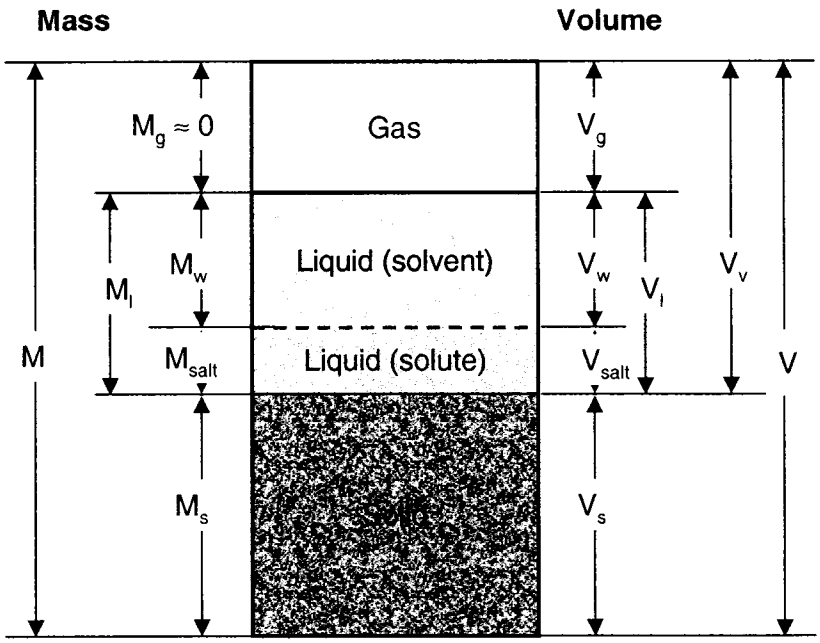

Figure B.1: Three-Phase, Four-Component Soil system (after Priyanto and Baumgartner 2007)

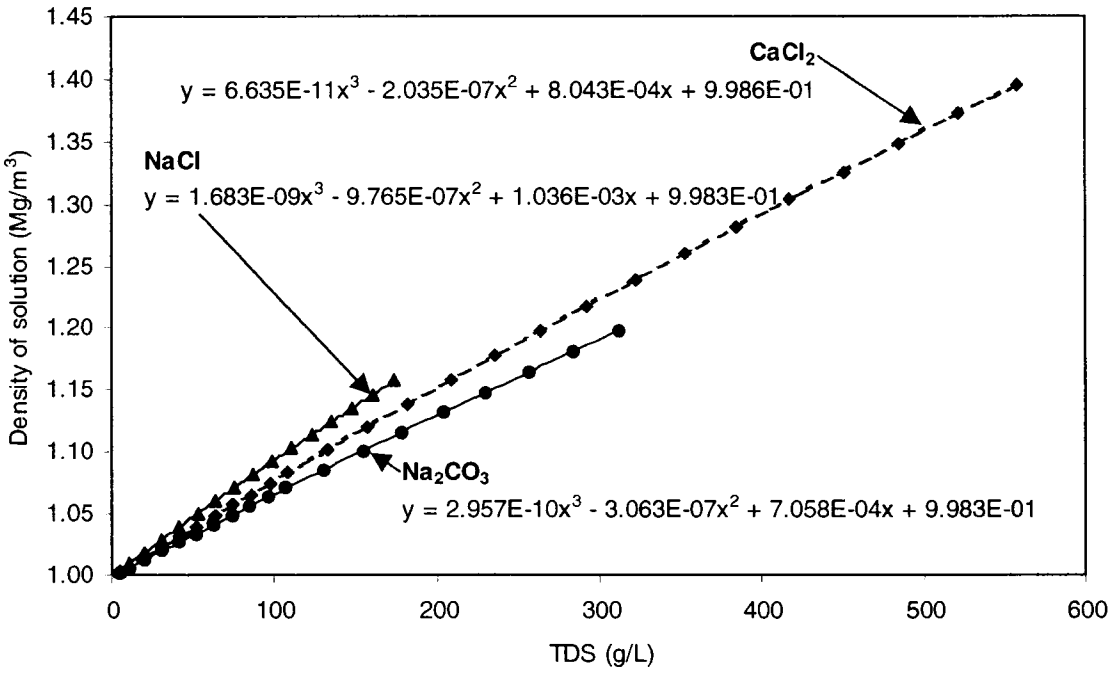

Figure B.2: Common Solution Densities as a Function of Concentration at Room Temperature (after Lide 2007)

Appendix C: Hydro-Mechanical Parameters for Loading and Unloading Increments

Test*	Applied Pressure (kN/m^2)	Log Applied Stress	Equilibrium Vertical Strain	Void Ratio	Dry Density (g/cm^3)	m_v (m^2/MN)	Hydraulic Conductivity (m/s)	EMDD (Mg/m^3)	Bulk Modulus (MPa)	Water Activity
	55.2	1.7	-0.016	1.264	1.193	0.294		0.65		
	80.5	1.9	-0.019	1.270	1.189	0.117		0.65		
	161.0	2.2	0.004	1.218	1.217	0.284	6.46E-12	0.67	1.89	0.9983
HB2	332.1	2.5	0.053	1.109	1.280	0.289	2.44E-12	0.72	2.85	0.9979
	663.4	2.8	0.128	0.942	1.390	0.239	2.53E-12	0.81	5.94	0.9970
	1325.7	3.1	0.203	0.774	1.522	0.131	1.54E-12	0.93	14.99	0.9950
	2651.4	3.4	0.273	0.619	1.667	0.066	3.41E-13	1.07	45.08	0.9907
	55.2	1.7	-0.010	1.216	1.218	0.188		0.67		
	80.5	1.9	-0.102	1.417	1.117	3.596		0.60		
	55.2	1.7	-0.195	1.622	1.030	3.352		0.54		
	110.6	2.0	-0.158	1.539	1.063	0.567	5.17E-12	0.56		
	221.0	2.3	-0.064	1.334	1.157	0.733	9.27E-12	0.63	1.15	0.9986
HB3	331.5	2.5	0.015	1.161	1.250	0.672	3.09E-12	0.70	2.06	0.9981
	666.6	2.8	0.140	0.886	1.432	0.379	1.80E-12	0.85	6.78	0.9965
	1325.7	3.1	0.238	0.672	1.615	0.172	8.99E-13	1.02	24.84	0.9926
	667.6	2.8	0.225	0.700	1.588	0.026	5.69E-13	0.99	10.10	0.9975
	336.1	2.5	0.192	0.773	1.523	0.129	4.42E-13	0.93	5.92	0.9982
	165.7	2.2	0.113	0.945	1.388	0.568	7.96E-13	0.81	2.08	0.9990
	55.3	1.7	-0.064	1.334	1.157	1.812		0.63	0.39	0.9996
	55.2	1.7	-0.012	1.148	1.257	0.226		0.70		
	80.5	1.9	-0.015	1.152	1.254	0.085		0.70		
	165.7	2.2	0.009	1.103	1.284	0.270	4.71E-12	0.72	1.96	0.9979
	332.0	2.5	0.063	0.989	1.358	0.327	2.04E-12	0.78	3.10	0.9973
HB4	665.1	2.8	0.146	0.811	1.491	0.268	8.45E-13	0.90	7.28	0.9955
	1328.0	3.1	0.225	0.644	1.642	0.139	2.49E-13	1.05	20.43	0.9917
	2653.8	3.4	0.288	0.510	1.788	0.062	1.06E-13	1.20	59.91	0.9838
	1328.0	3.1	0.276	0.536	1.758	0.013	1.84E-13	1.17	26.61	0.9860
	665.7	2.8	0.250	0.590	1.698	0.053		1.10	16.02	0.9894
	55.2	1.7	-0.142	1.313	1.167	2.579		0.63		
	39.1	1.6	-0.208	1.447	1.104	3.575		0.59		
	55.7	1.7	-0.204	1.437	1.108	0.232		0.59		
	166.1	2.2	-0.107	1.242	1.204	0.727	5.40E-12	0.66	0.87	0.9984
	332.1	2.5	0.002	1.022	1.336	0.591	4.03E-12	0.77	1.86	0.9975
	663.6	2.8	0.116	0.790	1.509	0.346	1.97E-12	0.92	5.23	0.9952
HB6	1325.9	3.1	0.215	0.590	1.698	0.168	2.31E-12	1.10	17.58	0.9894
	2651.8	3.4	0.289	0.440	1.875	0.071	2.55E-13	1.30	60.34	0.9752
	3986.5	3.6	0.321	0.374	1.964	0.034	3.47E-13	1.42	118.60	0.9601
	1325.9	3.1	0.291	0.436	1.880	0.017	1.39E-13	1.31	36.71	0.9873
	667.6	2.8	0.261	0.497	1.804	0.064	9.48E-14	1.22	19.53	0.9920
	336.1	2.5	0.218	0.584	1.705	0.176	2.16E-13	1.11	8.97	0.9955
	167.2	2.2	0.149	0.723	1.567	0.520	4.13E-13	0.97	3.25	0.9978
	56.8	1.8	-0.017	1.060	1.311	1.769		0.75	0.57	0.9993

* see test matrix in Table 3.4

Test*	Applied Pressure (kN/m^2)	Log Applied Stress	Equilibrium Vertical Strain	Void Ratio	Dry Density (g/cm^3)	m_v (m^2/MN)	Hydraulic Conductivity (m/s)	EMDD (Mg/m^3)	Bulk Modulus (MPa)	Water Activity
HB7	56.8	1.8	-0.012	1.056	1.313	0.216		0.75		
	82.0	1.9	-0.023	1.077	1.300	0.415		0.74		
	93.1	2.0	-0.024	1.080	1.298	0.092		0.74		
	98.6	2.0	-0.025	1.082	1.297	0.258		0.73		
	109.7	2.0	-0.028	1.088	1.293	0.220		0.73		
	123.5	2.1	-0.031	1.093	1.290	0.191		0.73		
	56.8	1.8	-0.134	1.303	1.173	1.502		0.64		
	27.6	1.4	-0.212	1.461	1.097	2.356		0.58		
	56.8	1.8	-0.200	1.436	1.108	0.342	2.83E-11	0.59		
	167.2	2.2	-0.085	1.203	1.225	0.866	7.98E-12	0.68	1.01	0.9983
	332.1	2.5	0.016	0.998	1.351	0.565	5.27E-12	0.78	2.08	0.9974
	663.6	2.8	0.127	0.774	1.522	0.339	7.26E-12	0.93	5.84	0.9950
	1325.9	3.1	0.224	0.576	1.714	0.169	9.18E-13	1.12	20.20	0.9886
	2651.8	3.4	0.295	0.433	1.885	0.068	4.60E-12	1.31	67.67	0.9739
	3986.3	3.6	0.327	0.366	1.976	0.035	6.06E-13	1.43	135.97	0.9575
	2651.8	3.4	0.321	0.379	1.957	0.007		1.41	75.05	0.9792
	1325.9	3.1	0.301	0.420	1.901	0.022		1.34	46.01	0.9855
	663.6	2.8	0.270	0.482	1.822	0.066		1.24	23.68	0.9911
HB8	55.2	1.7	-0.100	1.061	1.310	1.806		0.74		
	80.5	1.9	-0.148	1.152	1.255	1.750		0.70		
	105.8	2.0	-0.149	1.153	1.254	0.008		0.70		
	55.2	1.7	-0.224	1.294	1.177	1.303		0.64		
	80.5	1.9	-0.224	1.294	1.177	0.000		0.64		
	165.7	2.2	-0.173	1.199	1.228	0.490	6.52E-12	0.68	0.60	0.9983
	331.5	2.5	-0.066	0.999	1.351	0.549	6.14E-12	0.78	1.14	0.9974
	663.7	2.8	0.053	0.774	1.522	0.338	1.08E-11	0.93	2.85	0.9950
	1325.9	3.1	0.146	0.601	1.686	0.147	1.26E-12	1.09	7.23	0.9899
	2651.8	3.4	0.212	0.477	1.828	0.058	4.34E-13	1.25	16.88	0.9804
	1325.9	3.1	0.199	0.501	1.799	0.012	2.95E-13	1.21	6.67	0.9922
	662.9	2.8	0.175	0.545	1.747	0.045	6.38E-14	1.16	4.67	0.9942
HB9	55.3	1.7	0.005	1.103	1.284	0.094		0.805		
	80.5	1.9	-0.012	1.138	1.263	0.675		0.785		
	105.8	2.0	-0.039	1.196	1.229	1.070		0.756		
	55.3	1.7	-0.214	1.566	1.052	3.334		0.609		
	165.2	2.2	-0.178	1.490	1.084	0.269	5.74E-11	0.634	0.58	0.9986
	331.0	2.5	-0.082	1.288	1.180	0.491	1.38E-11	0.713	1.02	0.9980
	663.0	2.8	0.045	1.018	1.338	0.355	3.95E-12	0.855	2.65	0.9963
	1335.5	3.1	0.152	0.792	1.507	0.167	1.43E-12	1.025	7.80	0.9924
	2659.2	3.4	0.222	0.643	1.643	0.063	4.70E-13	1.180	19.69	0.9853
	1335.5	3.1	0.213	0.663	1.623	0.009	1.42E-13	1.157	8.31	0.9942
	663.0	2.8	0.190	0.712	1.577	0.043	3.87E-13	1.103	5.79	0.9956
	331.1	2.5	0.148	0.800	1.500	0.155	4.56E-13	1.018	3.22	0.9972
	165.3	2.2	0.062	0.983	1.361	0.615	3.75E-13	0.877	1.18	0.9986
	55.3	1.7	-0.163	1.457	1.099	2.173		0.646	0.20	0.9996

* see test matrix in Table 3.4

Test*	Applied Pressure (kN/m^2)	Log Applied Stress	Equilibrium Vertical Strain	Void Ratio	Dry Density (g/cm^3)	m_v (m^2/MN)	Hydraulic Conductivity (m/s)	EMDD (Mg/m^3)	Bulk Modulus (MPa)	Water Activity
	0.0		-0.104	1.086	1.294			0.73		
	25.3	1.4	-0.058	1.000	1.350	1.629	8.16E-10	0.78		
	55.2	1.7	-0.025	0.938	1.393	1.046	2.65E-10	0.81		
	165.7	2.2	0.060	0.777	1.520	0.751	6.33E-10	0.93	0.90	0.9986
	332.1	2.5	0.125	0.655	1.632	0.413	2.16E-10	1.04	1.76	0.9977
	663.6	2.8	0.186	0.539	1.754	0.210	1.38E-10	1.16	3.79	0.9958
	1326.0	3.1	0.241	0.435	1.882	0.103	6.16E-12	1.31	8.85	0.9916
HB11	2660.5	3.4	0.293	0.337	2.019	0.051	5.51E-13	1.49	23.36	0.9810
	3989.8	3.6	0.319	0.288	2.096	0.028	3.62E-13	1.60	41.71	0.9687
	2660.5	3.4	0.312	0.300	2.076		5.58E-13	1.57	26.47	0.9790
	1325.9	3.1	0.298	0.327	2.034	0.015	2.62E-13	1.51	13.41	0.9894
	663.6	2.8	0.282	0.357	1.989	0.034	3.41E-13	1.45	6.60	0.9948
	332.1	2.5	0.264	0.392	1.940	0.077	4.05E-13	1.38	3.11	0.9975
	165.7	2.2	0.248	0.421	1.900	0.127		1.33	1.72	0.9986
	55.2	1.7	0.223	0.470	1.837	0.309		1.26	0.70	0.9994
	0.0		-0.075	1.121	1.273			0.72		
	25.3	1.4	-0.031	1.034	1.328	1.628	8.32E-10	0.76		
	55.2	1.7	0.005	0.963	1.375	1.151	1.07E-09	0.80		
	165.7	2.2	0.099	0.777	1.520	0.861	5.98E-10	0.93	1.33	0.9986
	336.1	2.5	0.169	0.640	1.646	0.451	2.14E-11	1.05	3.01	0.9975
	676.3	2.8	0.235	0.509	1.789	0.234	8.08E-12	1.20	7.98	0.9950
HB12	1340.3	3.1	0.289	0.403	1.925	0.106	1.25E-11	1.36	21.63	0.9893
	2674.8	3.4	0.337	0.308	2.064	0.051	1.29E-12	1.55	65.53	0.9747
	1340.3	3.1	0.327	0.329	2.032	0.012	5.81E-13	1.51	55.43	0.9897
	676.3	2.8	0.312	0.357	1.989	0.033	3.68E-13	1.45	26.18	0.9948
	336.1	2.5	0.296	0.389	1.944	0.069	3.58E-13	1.39	12.18	0.9974
	167.2	2.2	0.280	0.421	1.900	0.135		1.33	6.00	0.9986
	56.8	1.8	0.256	0.467	1.840	0.295		1.26	2.33	0.9994
	1.1	0.0	-0.064	1.142	1.260			0.706		
	25.3	1.4	-0.030	1.073	1.303	1.339	2.95E-09	0.739		
	55.3	1.7	0.003	1.007	1.345	1.061	7.08E-10	0.774		
	165.7	2.2	0.087	0.839	1.468	0.759	3.10E-10	0.880	1.66	0.9987
	331.6	2.5	0.143	0.726	1.564	0.370	3.12E-11	0.969	3.34	0.9978
	663.3	2.8	0.199	0.613	1.674	0.198	1.17E-11	1.079	7.75	0.9960
HB13	1326.5	3.1	0.248	0.513	1.785	0.093	2.45E-12	1.198	18.95	0.9923
	2650.2	3.4	0.297	0.415	1.908	0.049	1.27E-12	1.343	54.93	0.9829
	1326.5	3.1	0.289	0.432	1.885	0.009	1.78E-13	1.316	28.54	0.9959
	663.3	2.8	0.276	0.457	1.853	0.027	3.05E-13	1.276	17.30	0.9973
	331.6	2.5	0.261	0.488	1.815	0.063	5.01E-13	1.232	9.84	0.9983
	166.1	2.2	0.244	0.522	1.774	0.137		1.186	5.48	0.9990
	55.3	1.7	0.215	0.580	1.709	0.343		1.115	2.20	0.9995

* see test matrix in Table 3.4

Test*	Applied Pressure (kN/m^2)	Log Applied Stress	Equilibrium Vertical Strain	Void Ratio	Dry Density (g/cm^3)	m_v (m^2/MN)	Hydraulic Conductivity (m/s)	EMDD (Mg/m^3)	Bulk Modulus (MPa)	Water Activity
HB14	11.0	1.0	-0.031	1.030	1.330	2.803		0.761		
	1.1	0.0	-0.036	1.040	1.323	0.493		0.756		
	25.3	1.4	-0.023	1.014	1.341	0.539	7.23E-10	0.770		
	56.8	1.8	0.010	0.949	1.385	1.014	1.07E-09	0.807		
	167.2	2.2	0.120	0.734	1.557	1.002	3.73E-10	0.962	1.14	0.9986
	336.1	2.5	0.193	0.589	1.699	0.495	7.90E-11	1.105	2.56	0.9976
	667.6	2.8	0.257	0.463	1.845	0.239	9.03E-12	1.268	6.16	0.9956
	1343.2	3.1	0.309	0.361	1.984	0.103	2.33E-12	1.441	15.06	0.9916
	2672.5	3.4	0.358	0.265	2.135	0.053	5.25E-13	1.653	43.42	0.9813
	4000.3	3.6	0.385	0.211	2.229	0.032	7.31E-12	1.801	88.72	0.9676
	2672.5	3.4	0.378	0.225	2.204		8.30E-13	1.760	133.85	0.9760
	1343.2	3.1	0.364	0.253	2.155	0.017	2.91E-13	1.684	60.61	0.9883
	667.6	2.8	0.346	0.287	2.098	0.041	2.57E-13	1.598	24.73	0.9948
	336.1	2.5	0.328	0.322	2.042	0.083	2.45E-13	1.519	10.74	0.9975
	167.2	2.2	0.313	0.353	1.995	0.139		1.455	5.47	0.9986
	56.8	1.8	0.286	0.406	1.920	0.352		1.359	1.96	0.9995
HB15	1.1	0.0	-0.071	1.087	1.294			0.732		
	25.3	1.4	-0.039	1.024	1.334	1.242	4.72E-09	0.764		
	55.2	1.7	-0.008	0.963	1.375	1.005	1.24E-09	0.799		
	165.7	2.2	0.075	0.802	1.498	0.743	1.31E-08	0.907	1.45	0.9985
	332.1	2.5	0.129	0.696	1.592	0.354	5.51E-10	0.996	2.80	0.9975
	663.8	2.8	0.193	0.572	1.718	0.220	5.27E-11	1.124	7.05	0.9949
	1326.5	3.1	0.238	0.485	1.819	0.084	2.35E-12	1.237	15.42	0.9905
	2655.9	3.4	0.284	0.395	1.935	0.045	1.96E-12	1.378	40.17	0.9794
	3985.4	3.6	0.311	0.341	2.013	0.029	3.35E-12	1.479	78.95	0.9642
	2655.9	3.4	0.311	0.343	2.011			1.477	74.25	0.9773
	1326.5	3.1	0.297	0.369	1.972	0.015	2.53E-13	1.425	40.60	0.9870
	667.8	2.8	0.281	0.401	1.928	0.035	3.32E-13	1.368	21.00	0.9929
	336.1	2.5	0.263	0.436	1.880	0.075	3.49E-13	1.310	10.61	0.9962
	165.7	2.2	0.247	0.467	1.840	0.128		1.262	6.02	0.9977
	55.2	1.7	0.220	0.519	1.778	0.317		1.190	2.57	0.9989
HB16	0.0		-0.061	0.910	1.414			0.83		
	25.3	1.4	-0.043	0.877	1.439	0.681	5.03E-10	0.85		
	55.3	1.7	-0.025	0.845	1.464	0.570	1.09E-10	0.88		
	165.7	2.2	0.022	0.760	1.534	0.415	6.19E-10	0.94	0.74	0.9983
	331.6	2.5	0.058	0.695	1.593	0.224	1.02E-10	1.00	1.01	0.9978
	663.3	2.8	0.124	0.576	1.713	0.211	2.70E-11	1.12	1.98	0.9961
	1326.5	3.1	0.186	0.466	1.842	0.106	2.39E-11	1.26	4.21	0.9925
	2650.4	3.4	0.250	0.351	1.999	0.059	5.47E-12	1.46	11.17	0.9818
	1326.5	3.1	0.242	0.363	1.980	0.007	2.17E-13	1.44	1.21	0.9961
	663.3	2.8	0.232	0.382	1.954	0.020	6.09E-13	1.40	0.85	0.9974
	331.6	2.5	0.220	0.403	1.924	0.047	4.06E-13	1.36	0.57	0.9983
	165.7	2.2	0.211	0.420	1.901	0.072		1.34	0.42	0.9988
	55.3	1.7	0.191	0.456	1.855	0.228		1.28	0.23	0.9994

* see test matrix in Table 3.4

Test*	Applied Pressure (kN/m^2)	Log Applied Stress	Equilibrium Vertical Strain	Void Ratio	Dry Density (g/cm^3)	m_v (m^2/MN)	Hydraulic Conductivity (m/s)	EMDD (Mg/m^3)	Bulk Modulus (MPa)	Water Activity
HB19	1.1	0.0	-0.062	1.129	1.268			0.71		
	25.3	1.4	-0.027	1.057	1.313	1.393	9.16E-10	0.75		
	55.3	1.7	0.009	0.986	1.359	1.148	7.90E-10	0.79		
	165.8	2.2	0.108	0.787	1.511	0.906	6.85E-10	0.92	1.46	0.9987
	331.6	2.5	0.173	0.656	1.631	0.443	1.08E-10	1.03	3.21	0.9977
	663.1	2.8	0.231	0.540	1.753	0.211	2.15E-11	1.16	7.54	0.9958
	1326.2	3.1	0.281	0.440	1.874	0.097	3.61E-12	1.30	18.45	0.9920
	2659.8	3.4	0.327	0.348	2.003	0.048	8.87E-13	1.47	51.21	0.9828
	1326.2	3.1	0.320	0.362	1.983	0.008	4.51E-13	1.44	39.98	0.9953
	667.8	2.8	0.308	0.387	1.947	0.028	3.51E-13	1.39	21.50	0.9973
	165.7	2.2	0.274	0.455	1.855	0.099	1.81E-12	1.28	4.63	0.9993
	55.2	1.7	0.249	0.506	1.793	0.312		1.21	1.74	0.9997
HB20	0.0		-0.060	1.100	1.286			0.726		
	25.3	1.4	-0.021	1.023	1.335	1.448	1.36E-09	0.765		
	55.2	1.7	0.006	0.968	1.372	0.906	2.92E-10	0.796		
	165.7	2.2	0.078	0.826	1.479	0.654	1.35E-09	0.889	1.23	0.9986
	331.6	2.5	0.143	0.698	1.590	0.422	7.68E-11	0.994	2.45	0.9978
	663.2	2.8	0.208	0.569	1.720	0.229	2.24E-11	1.127	5.76	0.9960
	1326.0	3.1	0.270	0.446	1.867	0.118	1.21E-11	1.293	16.02	0.9914
	2651.9	3.4	0.328	0.331	2.029	0.060	1.52E-12	1.501	55.04	0.9782
	3981.4	3.6	0.351	0.285	2.101	0.026	3.83E-13	1.603	98.89	0.9657
	2651.9	3.4	0.350	0.287	2.098			1.599	179.41	0.9744
	1326.0	3.1	0.339	0.309	2.063	0.013	7.25E-13	1.549	94.22	0.9857
	663.7	2.8	0.327	0.334	2.025	0.029	4.83E-13	1.495	47.52	0.9922
	330.9	2.5	0.314	0.359	1.987	0.058		1.444	24.51	0.9957
	166.1	2.2	0.300	0.387	1.947	0.124		1.393	12.56	0.9976
	56.8	1.8	0.280	0.426	1.893	0.262		1.325	5.19	0.9989

* see test matrix in Table 3.4

Appendix D: Equations for the Calculations of Bulk Modulus and Water Activity

This appendix provides equations for the calculation of bulk modulus (K) and the water activity (a_w). These equations have been drawn from Chandler (2005), Appendices A1. and A2., Numerical Modelling of The Stress And Displacement of Emplacement Room Swelling-Clay Material, Ontario Power Generation report.

The following trendline relationships are derived from Figures 4.17 and 4.18:

$$Ps = 0.013\exp\{4.29EMDD\}$$ Distilled Water, compression (D.1a)

$$Ps = 0.002\exp\{5.13EMDD\}$$ Distilled Water, swelling (D.1b)

$$Ps = 0.003\exp\{4.68EMDD\}$$ 100 g/l $CaCl_2$, compression (D.1c)

$$Ps = 3\times10^{-8}\exp\{11.74EMDD\}$$ 100 g/l $CaCl_2$, swelling (D1d)

$$Ps = 0.001\exp\{5.53EMDD\}$$ 100 g/l $CaCl_2$ – soil mixed, compression (D.1e)

$$Ps = 4\times10^{-7}\exp\{10.76EMDD\}$$ 100 g/l $CaCl_2$ – soil mixed, swelling (D.1f)

$$Ps = 0.003\exp\{4.53EMDD\}$$ 200 g/l $CaCl_2$, compression (D.1g)

$$Ps = 3\times10^{-8}\exp\{11.63EMDD\}$$ 200 g/l $CaCl_2$, swelling (D.1h)

$$Ps = 0.005\exp\{3.78EMDD\}$$ 100 g/l $CaCl_2$ Constrained, compression (D.1i)

$$Ps = 2\times10^{-7}\exp\{9.45EMDD\}$$ 100 g/l $CaCl_2$ Constrained, swelling (D.1j)

where P_S = swelling pressure

$$\varepsilon_V = 1 - \frac{\rho_{d0}}{\rho_d} \tag{D.2}$$

where ρ_{d0} = initial as-placed dry density; and

ε_v = vertical strain.

$$\rho_d = \frac{\rho_{d0}}{1-\varepsilon_V} \tag{D.3}$$

where ρ_d = dry density.

$$EMDD = \frac{\rho_{d0}}{1-\varepsilon_V} \frac{f_m f_c}{\left\{1 - \frac{\rho_{d0}}{\rho_W(1-\varepsilon_V)}\left[\frac{(1-f_c)}{G_S} - \frac{(1-f_m)f_c}{G_n}\right]\right\}} \tag{D.4}$$

where G_s is equal to G_n.

$$EMDD = \frac{f_m f_c \rho_{d0}}{\left[1-(1-f_m f_c)\frac{\rho_{d0}}{\rho_W G}\right] - \varepsilon_V} \tag{D.5}$$

$$EMDD = \frac{A}{B-\varepsilon_V} \tag{D.6}$$

where A and B are constants dependent upon material compositions and initial dry densities:

A=0.544 (Mg/m^3) and B=0.692 (dimensionless) for LBF in this research.

$$\sigma_m = 0.013 \exp\left[\frac{4.29A}{B-\varepsilon_V}\right]$$ Distilled Water, compression (D.7a)

$$\sigma_m = 0.002 \exp\left[\frac{5.18A}{B-\varepsilon_V}\right]$$ Distilled Water, swelling (D.7b)

$$\sigma_m = 0.003 \exp\left[\frac{4.68A}{B-\varepsilon_V}\right]$$ 100 g/l $CaCl_2$, compression (D.7c)

$$\sigma_m = 3\times10^{-8} \exp\left[\frac{11.74A}{B-\varepsilon_V}\right]$$ 100 g/l $CaCl_2$, swelling (D.7d)

$$\sigma_m = 0.001 \exp\left[\frac{5.53A}{B-\varepsilon_V}\right]$$ 100 g/l $CaCl_2$ – soil mixed, compression (D.7e)

$$\sigma_m = 4\times10^{-7} \exp\left[\frac{10.76A}{B-\varepsilon_V}\right]$$ 100 g/l $CaCl_2$ – soil mixed, swelling (D.7f)

$$\sigma_m = 0.003 \exp\left[\frac{4.53A}{B-\varepsilon_V}\right]$$ 200 g/l $CaCl_2$, compression (D.7g)

$$\sigma_m = 3\times10^{-8} \exp\left[\frac{11.63A}{B-\varepsilon_V}\right]$$ 200 g/l $CaCl_2$, swelling (D.7h)

$$\sigma_m = 0.005 \exp\left[\frac{3.78A}{B-\varepsilon_V}\right]$$ 100 g/l $CaCl_2$ Constrained, compression (D.7i)

$$\sigma_m = 2\times10^{-7} \exp\left[\frac{9.45A}{B-\varepsilon_V}\right]$$ 100 g/l $CaCl_2$ Constrained, swelling (D.7j)

where σ_m = mean stress (assumed to be equal to swelling pressure, P_s)

Bulk modulus (K) is the slope of the mean stress versus vertical strain.

$$K = 0.013\exp\left[\frac{4.29A}{B-\varepsilon_V}\right]\frac{4.29A}{(B-\varepsilon_V)^2}$$ Distilled Water, compression (D.8a)

$$K = 0.002\exp\left[\frac{5.18A}{B-\varepsilon_V}\right]\frac{5.18A}{(B-\varepsilon_V)^2}$$ Distilled Water, swelling (D.8b)

$$K = 0.003\exp\left[\frac{4.68A}{B-\varepsilon_V}\right]\frac{4.68A}{(B-\varepsilon_V)^2}$$ 100 g/l $CaCl_2$, compression (D.8c)

$$K = 3\times10^{-8}\exp\left[\frac{11.74A}{B-\varepsilon_V}\right]\frac{11.74A}{(B-\varepsilon_V)^2}$$ 100 g/l $CaCl_2$, swelling (D.8d)

$$K = 0.001\exp\left[\frac{5.53A}{B-\varepsilon_V}\right]\frac{5.53A}{(B-\varepsilon_V)^2}$$ 100 g/l $CaCl_2$ – soil mixed, compression (D.8e)

$$K = 4\times10^{-7}\exp\left[\frac{10.76A}{B-\varepsilon_V}\right]\frac{10.76A}{(B-\varepsilon_V)^2}$$ 100 g/l $CaCl_2$ – soil mixed, swelling (D.8f)

$$K = 0.003\exp\left[\frac{4.53A}{B-\varepsilon_V}\right]\frac{4.53A}{(B-\varepsilon_V)^2}$$ 200 g/l $CaCl_2$, compression (D.8g)

$$K = 3\times10^{-8}\exp\left[\frac{11.63A}{B-\varepsilon_V}\right]\frac{11.63A}{(B-\varepsilon_V)^2}$$ 200 g/l $CaCl_2$, swelling (D.8h)

$$K = 0.005\exp\left[\frac{3.78A}{B-\varepsilon_V}\right]\frac{3.78A}{(B-\varepsilon_V)^2}$$ 100 g/l $CaCl_2$ Constrained, compression (D.8i)

$$K = 2\times10^{-7}\exp\left[\frac{9.45A}{B-\varepsilon_V}\right]\frac{9.45A}{(B-\varepsilon_V)^2}$$ 100 g/l $CaCl_2$ Constrained, swelling (D.8j)

$$a_W = exp\left[-\frac{V_W}{RT}\times 0.013\times exp(4.29\,EMDD)\right]$$ Distilled Water, compression (D.9a)

$$a_W = exp\left[-\frac{V_W}{RT}\times 0.002\times exp(5.18\,EMDD)\right]$$ Distilled Water, swelling (D.9b)

$$a_W = exp\left[-\frac{V_W}{RT}\times 0.003\times exp(4.68\,EMDD)\right]$$ 100 g/l $CaCl_2$, compression (D.9c)

$$a_W = exp\left[-\frac{V_W}{RT}\times\left(3\times 10^{-8}\right)\times exp(11.74\,EMDD)\right]$$ 100 g/l $CaCl_2$, swelling (D.9d)

$$a_W = exp\left[-\frac{V_W}{RT}\times 0.001\times exp(5.53\,EMDD)\right]$$ 100 g/l $CaCl_2$–soil mixed, compression

(D.9e)

$$a_W = exp\left[-\frac{V_W}{RT}\times\left(4\times 10^{-7}\right)\times exp(10.74\,EMDD)\right]$$ 100 g/l $CaCl_2$ – soil mixed, swelling (D.9f)

$$a_W = exp\left[-\frac{V_W}{RT}\times 0.003\times exp(4.53EMDD)\right]$$ 200 g/l $CaCl_2$, compression (D.9g)

$$a_W = exp\left[-\frac{V_W}{RT}\times\left(3\times 10^{-8}\right)\times exp(11.63\,EMDD)\right]$$ 200 g/l $CaCl_2$, swelling (D.9h)

$$a_W = exp\left[-\frac{V_W}{RT}\times 0.005\times exp(3.78\,EMDD)\right]$$ 100 g/l $CaCl_2$ Constrained, compression

(D.9i)

$$a_W = exp\left[-\frac{V_W}{RT}\times\left(2\times 10^{-7}\right)\times exp(9.45\,EMDD)\right]$$ 100 g/l $CaCl_2$ Constrained, swelling

(D.9j)

where a_w = water activity

V_w = partial molal volume of water (1.8×10^{-5} m^3/mol)

R = universal gas constant (8.3143×10^{-6} m^3.MPa/mol.K)

T = absolute temperature (a value of 298 K is used in this research)

Appendix E: Equations for Linear-Elastic, Two-Material Axisymmetric Model

This appendix provides the equations for the solution of a Two-material axisymmetric linear elastic model. These equations have been drawn from Chandler (2005), Appendix B, Numerical Modelling of the Stress and Displacement of Emplacement Room Swelling-Clay Material, Ontario Power Generation report.

The geometry of a two material concentric cylinder problem is illustrated in Figure E.1.

$$\begin{aligned} \sigma_r &= 2A + \frac{B}{r^2}, \\ \sigma_\theta &= 2A - \frac{B}{r^2}, \\ u_r &= \frac{1}{2G}\left[2A(1-2v)r - \frac{B}{r}\right] \end{aligned} \qquad \text{(E.1)}$$

where σ_r = Radial Stress

σ_θ = Tangential Stress

u_r = Radial Displacement

G = Shear Modulus

v = Poisson's Ratio

A and B are coefficients that satisfy the imposed boundary conditions

$$\sigma_m = \frac{1}{3}(\sigma_r + \sigma_\theta)(1+v) \qquad \text{(E.2)}$$

where σ_m = mean stress

$$G = \frac{3K(1-2v)}{2(1+v)} \qquad \text{(E.3)}$$

where K = Bulk Modulus

$$a_{u1} + u_r \text{ (at } r = a_{u1}) = a$$

$$c_{u2} + u_r \text{ (at } r = c_{u2}) = c \qquad \text{(E.4)}$$

$$\sigma_{r1} \text{ (at } r = b_{u1}) = \sigma_{r2} \text{ (at } r = b_{u2})$$

$$b_{u1} + u_r \text{ (at } r = b_{u1}) = b_{u2} + u_r \text{ (at } r = b_{u2})$$

where a_u, b_u and c_u = radial dimensions after saturation (expansion of inner material and compression of outer material). Subscripts show the difference between the inner material (material 1) and the outer material (material 2).

Examples of properties and dimensions that are specific to the two materials include a_{u1}, b_{u1}, b_{u2}, c_{u2}, A_1, A_2, B_1, B_2, G_1, G_2, K_1, K_2, Ps_1 and Ps_2 (Ps = Swelling Pressure).

$$
\begin{aligned}
a - a_{u1} &= \frac{Ps_1}{2K_1} a_{u1} \\
b - b_{u1} &= \frac{Ps_1}{2K_1} b_{u1} \\
b - b_{u2} &= \frac{Ps_2}{2K_2} b_{u2} \\
c - c_{u2} &= \frac{Ps_2}{2K_2} c_{u2}
\end{aligned}
\qquad \text{(E.5)}
$$

$$
\begin{aligned}
\frac{2A_1}{2G_1}(1-2v_1)a_{u1} - \frac{B_1}{2a_{u1}G_1} &= \frac{Ps_1}{2K_1} a_{u1} \\
\frac{2A_2}{2G_2}(1-2v_2)c_{u2} - \frac{B_2}{2c_{u2}G_2} &= \frac{Ps_2}{2K_2} c_{u2}
\end{aligned}
\qquad \text{(E.6)}
$$

$$
\begin{aligned}
B_1 &= f_1 A_1 + g_1 \\
B_2 &= f_2 A_2 + g_2
\end{aligned}
\qquad \text{(E.7)}
$$

where

$$
\begin{aligned}
f_1 &= 2(1-2v_1)a_{u1}^2 \\
g_1 &= Ps_1 a_{u1}^2 \frac{G_1}{K_1} \\
f_2 &= 2(1-2v_2)c_{u2}^2 \\
g_2 &= Ps_2 c_{u2}^2 \frac{G_2}{K_2}
\end{aligned}
$$

$$
2A_1 + \frac{B_1}{b_{u1}^2} = 2A_2 + \frac{B_2}{b_{u2}^2} \qquad \text{(E.8)}
$$

$$h_1 A_1 + j_1 = h_2 A_2 + j_2 \qquad \text{(E.9)}$$

where

$$h_1 = 2 + 2(1-2v_1)\frac{a_{u2}^2}{b_{u1}^2}$$

$$j_1 = P_{s1}\frac{G_1}{K_1}\frac{a_{u1}^2}{b_{u1}^2} \quad .$$

$$h_1 = 2 + 2(1-2v_2)\frac{c_{u2}^2}{b_{u2}^2}$$

$$j_1 = P_{s2}\frac{G_2}{K_2}\frac{c_{u2}^2}{b_{u2}^2}$$

$$b_{u1} + \frac{A_1}{G_1}(1-2v_1)b_{u1} - \frac{B_1}{2G_1 b_{u1}} = b_{u2} + \frac{A_2}{G_2}(1-2v_2)b_{u2} - \frac{B_2}{2G_2 b_{u2}} \qquad \text{(E.10)}$$

$$k_1 A_1 + m_1 = k_2 A_2 + m_2 \qquad \text{(E.11)}$$

where

$$k_1 = (1-2v_1)\frac{b_{u1}^2 - a_{u1}^2}{G_1 b_{u1}}$$

$$m_1 = b_{u1} - \frac{Ps_1}{2K_1}\frac{a_{u1}^2}{b_{u1}} \quad .$$

$$k_2 = (1-2v_2)\frac{b_{u2}^2 - c_{u2}^2}{G_2 b_{u2}}$$

$$m_2 = b_{u2} - \frac{Ps_2}{2K_2}\frac{c_{u2}^2}{b_{u2}}$$

$$A_1 = \frac{(m_1 - m_2)/k_2 - (j_1 - j_2)/h_2}{h_1/h_2 - k_1/k_2} \qquad \text{(E.12)}$$

$$A_2 = \frac{h_1}{h_2} A_1 + \frac{j_1 - j_2}{h_2}$$

The four parameters A_1, A_2, B_1 and B_2, as defined in E.12 and E.7, can be substituted into E.1 to obtain the solutions for stress and displacement in the two materials as a function of radial location.

$$a_w = \exp\left[-\frac{V_w}{RT}\sigma_m\right] \qquad \text{(E.13) (Chandler 2005, Appendix A2.)}$$

where a_w = water activity

V_w = partial molal volume of water (1.8×10^{-5} m^3/mol)

R = universal gas constant (8.3143×10^{-6} m^3.MPa/mol.K)

T = absolute temperature (a value of 298 K is used in this research)

σ_m = mean stress

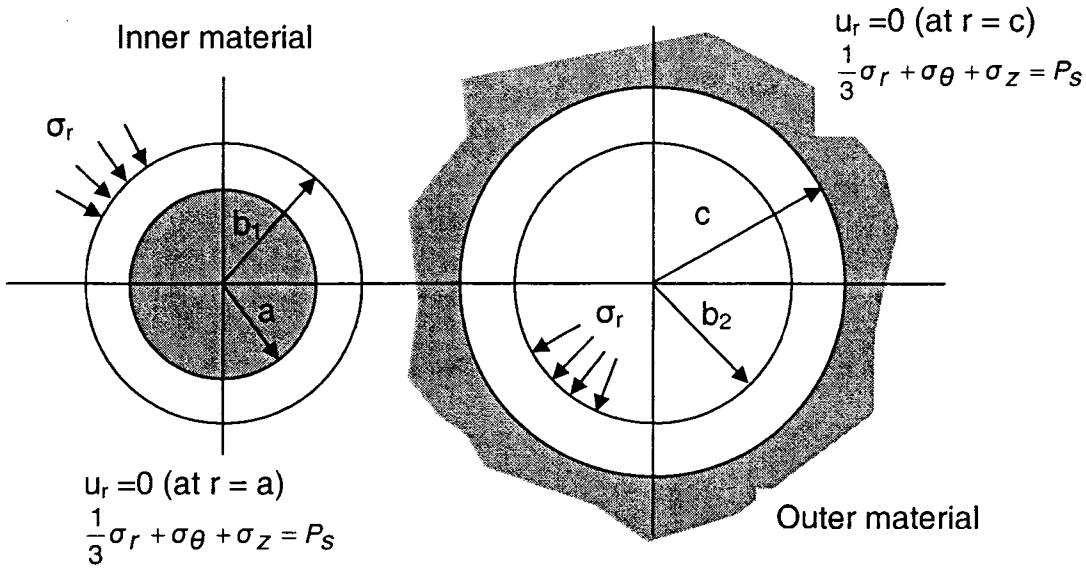

Figure E.1. Illustration of the geometry of a two material concentric cylinder (Chandler 2005)